VIBROMETRIC DETECTION OF BEAM DAMAGE DUE TO INCLUSIONS

THESIS

Aaron J. Reifsnyder, Captain, USAF

AFIT/GA/ENY/04-J01

DEPARTMENT OF THE AIR FORCE
AIR UNIVERSITY

AIR FORCE INSTITUTE OF TECHNOLOGY

Wright-Patterson Air Force Base, Ohio

APPROVED FOR PUBLIC RELEASE; DISTRIBUTION UNLIMITED.

The views expressed in this thesis are those of the author and do not reflect the official policy or position of the United States Air Force, Department of Defense, or the United States Government.

AFIT/GA/ENY/04-J01

VIBROMETRIC DETECTION OF BEAM DAMAGE DUE TO INCLUSIONS

THESIS

Presented to the Faculty

Department of Aeronautics and Astronautics

Graduate School of Engineering and Management

Air Force Institute of Technology

Air University

Air Education and Training Command

In Partial Fulfillment of the Requirements for the

Degree of Master of Science in Astronautical Engineering

Aaron J. Reifsnyder, BS, EIT

Captain, USAF

March 2004

APPROVED FOR PUBLIC RELEASE; DISTRIBUTION UNLIMITED

AFIT/GA/ENY/04-J01

VIBROMETRIC DETECTION OF BEAM DAMAGE DUE TO INCLUSIONS

Aaron J. Reifsnyder, BS, EIT
Captain, USAF

Approved:

//signed//	
Dr. Anthony N. Palazotto (Chairman)	date
//signed//	
Maj. Richard G. Cobb (Member)	date
//signed//	
Dr. Theodore Nicholas (Member)	date

Abstract

The Air Force Institute of Technology, in conjunction with the Structural Health Monitoring branch of the Air Force Research Laboratory, is researching methods of determining effects of notch location and size on beam structures using modal frequency analysis. This thesis explores the ability to detect included notches of varying magnitudes and locations within the frequency domain of an isotropic cantilever beam.

A series of experiments employing centerline-notched 2024 T3 and 2024 O aluminum beams was used to determine whether natural frequency measurement in beam structures is a valid mechanism for damage detection. Each specimen was excited by a strain actuator and the dynamic beam response measured using a laser Doppler vibrometer, thereby obtaining eigenvalues and eigenvectors for each case. Results are analyzed for frequency degradation trends based on location, notch length, and vibration mode. Correlation is made between experimentally observed values, ABAQUS modeling, and a series of MATLAB predictions utilizing a finite element solution approach developed by Perel and Palazotto (2002).

It is determined that modal frequency analysis is an adequate global indicator of damage presence and magnitude, which reduces global stiffness. Damage location is not easily identifiable from the data. It is also determined that ABAQUS and the MATLAB solution approach are accurate to within 10% of experimental resonant frequency values for short notch lengths and low vibration modes, but highly deviant from experiment for longer notch lengths and higher modes. Residual stresses contained in the 2024 T3 specimens from cold working are determined to have minimal effect on beam dynamics.

To My Wonderful Fiancée and Future Wife

Acknowledgments

I would like to express my sincerest thanks to my faculty advisor, Dr. Anthony Palazotto, for his guidance and patience with me through this thesis process. His insight and aid in analysis was always greatly appreciated. I also want to thank the fabrication experts at the AFIT machine shop for their expertise and ability to create accurate, usable test specimens for this project. Additionally, a special thank you to Mr. Mark Derriso for providing the funding to make this project actually happen.

I am also indebted to my fellow classmates for their humor and positive outlook as we all trudged through this sleep-depriving and sometimes frustrating program over the last year and a half. Thanks especially to Capt. Matt Kimsal for his motivating nature, because no matter how bad I had it, I could always count on him having it worse.

A final and ultimate thanks to God and the people He surrounds me with—their strength, prayers, and support will always be a blessing in my life, and will never be forgotten.

Aaron J. Reifsnyder

Table of Contents

Page

List of Figures

Page

Page

List of Tables

Page

VIBROMETRIC DETECTION OF BEAM DAMAGE DUE TO INCLUSIONS

I. Introduction

Structural Health Monitoring

The increasing complexity of modern aircraft and space structures brings a myriad of new challenges not only to design engineers and materials fabrication experts, but also to the post-production maintenance personnel who must thoroughly inspect each system for internal and external flaws to ensure failsafe operation. This inspection process is highly time-consuming and very costly: commercial airlines such as Delta and American typically reserve nearly 25% of their overall annual airline operating costs for maintenance and repair of the aircraft fleet, totaling over $711 million and $1.11 billion respectively in 2002 (Gage and McCormick, 2003). Massive institutions such as the commercial airline industry, NASA, and the Department of Defense would greatly benefit from a passive system-wide structural health monitoring (SHM) system on their fleets, not only to reduce aircraft and spacecraft downtime due to maintenance, but also to potentially avoid catastrophic failures such as the 2001 Airbus crash in New York City and the disintegration of the space shuttle Columbia over Texas in 2003.

Philosophy Behind SHM.

Structural health monitoring posits the concept of continual monitoring of a system's structural integrity via a series of sensor inputs analyzed automatically by a central computer validation system. The literature defines SHM as "a reliable system with the ability to detect and interpret adverse 'changes' in a structure due to damage or

normal operation" (Kessler *et. al.*, 2002:87). The "changes" mentioned in the definition can come from a variety of sources: manufacturing defects, impacts, fatigue cracks, thermal exposure, overstressing, etc. The central focus of SHM is to identify the presence of a change in structural integrity as early as possible using non-invasive technology, whether that change may occur at the surface of a structure or internal to the material.

Technological Approaches.

For SHM to be successful, the damage detection technique utilized must satisfy several key requirements, as adeptly outlined by Castellini and Revel (2000:1): "It must be non-destructive, easy to be used, rapid enough for online monitoring and with very reduced uncertainty in the response." Several approaches for non-invasive damage detection in structures have been studied with varying degrees of success, including X-ray photography, infrared thermography, ultrasonic scanning, dye penetration, and magnetic particle induction, among others. These approaches tend not to be easily used, particularly for large specimens or outside of a lab as they require extensive specialized optical imaging equipment or cumbersome detection devices.

The damage diagnostic methods most widely considered to be promising for SHM purposes involve vibration induction and the observation of modal frequency shifts in the presence of damage. Several factors make vibration-based damage detection a highly viable option: it is non-destructive, inexpensive, requires a minimal amount of equipment, and ultimately is global in nature—meaning that the natural frequencies w_n of a structural member depend upon the mass distribution and stiffness properties of the

entire member. This can be easily seen by considering the generalized governing differential equation of motion of a multi-degree-of-freedom system

$$[M]\{\ddot{x}\}+[C]\{\dot{x}\}+[K]\{x\}=\{F(t)\} \tag{1}$$

where $[M]$, $[C]$, and $[K]$ are the mass, damping, and stiffness matrices, respectively, $\{\ddot{x}\}$, $\{\dot{x}\}$, and $\{x\}$ are the acceleration, velocity, and displacement vectors, and $\{F(t)\}$ is the forcing function vector. Dividing through by the mass matrix and rewriting in classical form yields

$$\{\ddot{x}\}+2[z w_n]\{\dot{x}\}+[w_n^2]\{x\}=\frac{\{F(t)\}}{[M]} \tag{2}$$

where $[w_n^2]=\frac{[K]}{[M]}$. Therefore a change within either the mass or stiffness matrix of the structure (or both) will result in a shift in natural frequency.

Modal frequency determination is also low-cost and simple to conduct. One author concisely states the essence of frequency sensing when used in conjunction with structural health monitoring:

> Modal parameters can be easily and cheaply obtained from measured vibration responses. The responses are acquired by some form of transducer which monitors the structural response to artificially induced excitation forces or ambient forces in the service environment. Low input energy levels are sufficient to produce measurable responses since the input energy is dynamically amplified. (Salawu, 1995:718)

However, he also goes on to mention that a frequency change of greater than 5% would be necessary to detect the damage with confidence. This conjecture is based on the arguments that others in academia have put forth against natural frequency response as a method of damage detection, namely:

1) A frequency shift does not necessarily imply damage is present (i.e. ambient condition effects).
2) Damage at the modal nodes is not readily detected by this method.
3) Data analysis can be slow if a complete eigensolution is necessary for systems with large mass and stiffness matrices.
4) Initial data is necessary for the undamaged specimen (prior to damage induction) for comparison purposes to determine whether the mode has shifted.

Though all of these arguments are valid points, none make the approach as a whole invalid. It is important to consider that this research is still relatively young, and though semi-ideal conditions are utilized in the laboratory for theoretical verification, this does not mean that the approach only works under these conditions. For instance, ambient conditions do indeed cause slight changes in system parameters (such as thermal material expansion/contraction, air density damping, etc.), however these discrete offsets may be accounted for in aggressive frequency modeling methods beyond fundamental theory. Damage at modal nodes is difficult to detect since the nodes are inflection points for both surface velocity and acceleration, however considering multiple modes alleviates this problem by shifting the nodes with each successive mode. The data analysis considerations, though currently hefty, will become less of an issue as computer technology continues to progress and processor speeds get faster.

The arguments supporting modal analysis for damage detection are certainly more substantive, a few of which are listed below:

1) Changes in material stiffness due to internal damage must affect the modes (according to Eqs. (1) and (2)), and therefore should be able to be measured.
2) Natural frequencies are global in nature, and therefore damage in any area of the structure will affect the modes and can thereby be detected.
3) No one method of actuation is required to instigate dynamic modal response, and "low input energy levels are sufficient to produce measurable responses since the input energy is dynamically amplified" (Salawu, 1997:718).

4) Under actuation, the modal frequencies can be continuously monitored, triggering automated response when a damage-induced shift is detected.
5) The method can be used on practically any specimen (beams, plates, trusses, rods, etc.) since every object has a unique set of modal frequencies.

Therefore, despite the previously stated arguments against the methodology, many researchers and theorists on the subject accept modal frequency analysis as a valid approach deserving of further study, and have therefore intensively studied multiple simple structures in an attempt to create physically realistic models of induced-damage dynamic response.

Published Analytical Approaches

Though slow but steady progress has been made in the field of modal vibration response for damage detection, the idea behind the theory has been around for over 30 years. The initial concept of vibration monitoring for damage presence began with rotor cracking in machinery and railroad equipment, as presented by Dimaroganas (1970) and Nagy, Dousis, and Finch (1978). The latter work has been noted to explain that "the presence of cracks [in railroad wheels] causes some resonance frequencies to shift and others to split" (Man *et. al.*, 1993:2030). Cawley and Adams (1979) published a monumental work in this area, extending the concept of modal frequency shifts due to damage to a study of damage in plates, eventually leading to follow-on studies in trusses and beams as well.

Plate Analysis.

Cawley and Adams studied the effects of damage on the modal frequencies of a 450 x 350 x 6 mm aluminum plate and a similar-sized trapezoidal carbon-fiber-reinforced plastic plate (1979:53). They postulated that "if one set of frequencies were measured

before the structure was put into service, subsequent frequency measurements could be used to test whether the structure was still sound" (Cawley and Adams, 1979:49). Saw cuts, crushing, and holes were introduced into the free-edge plate specimens at various intervals and modal frequencies observed. They found that it was "possible to detect damage equivalent to the removal of one-percent of the cross-sectional area of the structure at a single location" (Cawley and Adams, 1979:49), and therefore reported the related frequency reductions as shown in Tables 1 and 2.

Table 1. Results From Rectangular Aluminum Plate

Damage	Undamaged frequencies (Hz)						Area removed (percentage of total)	
	125.05	158.94	278.29	301.52	361.44	466.98		
	Frequency reductions (Hz)						Actual	Predicted
Rectangular hole	0.41	0.77	1.18	0.37	0.72	0.81	0.31	0.47

Table 2. Results From Trapezoidal, Cross-Ply, CFRP Plate

Damage	Undamaged frequencies (Hz)										Predicted area removed with respect to virgin condition (percentage of total)
	125.05	158.94	278.29	301.52	361.44	466.98	361.44	361.44	361.44	361.44	
	Frequency reductions from virgin condition (Hz)										
First saw cut	0.06	0.39	0.29	0.14	-0.07	0.14	2.70	0.62	0.20	0.28	0.19
Second saw cut	0.85	5.46	4.50	2.08	1.78	4.32	5.29	3.70	1.20	1.68	2.17
Third saw cut	1.24	5.66	5.91	3.44	3.93	4.38	9.02	6.90	10.41	6.51	3.65

(Cawley and Adams, 1979:54)

Cawley and Adams were not the only researchers to test frequency reductions in plates due to damage. Jian, Tzou, Lissenden, and Penn (1997) embedded piezoelectric patches in the lamina of a series of glass fiber/epoxy prepreg plates and measured impulse-frequency response due to increasing internal delamination damage. They noted that "both low and high modes are affected by the delamination," however the lower modes required a much more significant damage inclusion to shift the modal frequency

than the higher modes (1997:355). Kessler *et. al.* (2002) took this experiment several steps further, examining graphite/epoxy plates with several different kinds of damages—holes, impacts, delaminations, fatigue areas, and bent areas. Using a Polytec scanning laser vibrometer (similar to the vibrometer used for experimentation in this thesis), they noted that "the frequency response method was found to be reliable for detecting even small amounts of damage in simple composite structures" (Kessler *et. al.*, 2002:87). They also verified that all of the aforementioned damage types were detectable using frequency analysis over the first four bending modes and first two torsion modes.

Truss Analysis.

For a structure comprised of multiple basic elements (plates, beams, rods, etc.), a change in the mass or stiffness matrix of any one individual element will result in not only a change in the eigenvalues of that element, but also a change in the eigenvalues of the structure as a whole. Assuming that the stiffness and mass matrices of a structure can be written as

$$[K] = \sum_{i=0}^{n} a_i [K_i] \tag{3}$$

$$[M] = \sum_{i=0}^{n} a_i [M_i] \tag{4}$$

where a_i are constants and K_i, M_i are the stiffness and mass matrices of the ith element, Chondros and Dimarogonas set up a simple 3-element truss using prismatic elements and actuated the truss to induce the first and second global vibration modes (1989:251). A crack was then introduced in one of the members and the associated frequency shifts recorded. They found that a structural stiffness reduction of 10% resulted in a 5%

decrease in the first eigenvalue and a 0.5% decrease in the second eigenvalue, thereby validating frequency shift as a detection method for the presence of damage in simple structures. Similarly, Thyagarajan, Schulz, and Pai (1998) studied the frequency response of an 18-element bridge truss with a 50% stiffness damage introduced into one of the members, resulting in an 8% reduction in the first natural frequency of the structure. The test was repeated several times with damage being introduced into different structural members each time, yielding an associated downward frequency trend with each case.

A series of cantilevered truss experiments were performed by Cobb (1996) to develop an algorithm for structural member damage identification in space applications using limited measurement data. A 96-member and a 104-member truss structure were considered over the first eight and first five flexible modes, respectively. Minimization of a cost function relating measured values and the analytical approach was accomplished via eigensystem sensitivities, and damage location was then pinpointed using the partial eigenstructure method developed. In all cases, "it was shown that the resulting natural frequencies from damage can only decrease" (Cobb 1996:9-1).

Beam Analysis.

The most extensive research for modal frequency analysis of damaged specimens has been in the area of beams, both composite and isotropic. The vast concentration of work has been focused on the study of surface inclusions, i.e. cracks, surface notches, impacts, etc. Though this thesis emphasizes internal damage in the form of a slot to model through-thickness delamination, the considerations of surface damage are certainly

applicable to establish frequency trends and an awareness of alternative modeling approaches.

Cawley and Ray (1988) utilized a free-free beam to test the frequency characteristics of area reduction in a specimen. They removed slices of material near the midpoint of several isotropic steel bars in depth increments of approximately 0.5mm, gradually reducing the second moment of area by about 50-60% over the course of the experimental set. The conclusion drawn from their experiment was that "the natural frequency changes produced by a defect of a given depth increase as the width of the defect is increased," and in fact the frequency reductions follow a more exponential rather than linear relation as crack depth increases (Cawley and Ray, 1988:366). Pandey, Biswas, and Samman (1991) looked not only at changes in the eigenfrequencies of cantilevered and simply supported beams with damage inclusions, but also at shifts in the "curvature mode shapes" given by the equation

$$v'' = \frac{M}{EI} \tag{5}$$

where v'' is the curvature at a given section, M is the bending moment at that section, E is the Young's Modulus and I is the second moment of inertia (Pandey *et. al.* 1991:322). This relation was applied to 20 continuous segments across the flexural profile of both a damaged and undamaged cantilever beam. The absolute difference between the curvature mode shapes for all segments of both beams was calculated and the results plotted, identifying a spike in the region where damage was present. They concluded that "from changes in frequency one can easily determine the presence of a crack or damage in a structure," however locating that damage was a "completely different question" as

cracks at different locations could potential yield the same frequency signature, hence consideration of the displacement field was necessary (Pandey *et. al.*, 1991:322).

Kam and Lee (1992) attempted to answer that "completely different question" posed by Pandey and his team with a strain energy approach for cantilevered beams under modal excitation. Using the strain energy relation for the ideal case:

$$W_0 = \tfrac{1}{2}\bar{r}_0^T \bar{K}_0 \bar{r}_0 \tag{6}$$

with

$$\bar{r}_0 = \bar{K}_0^{-1}\bar{F} \tag{7}$$

where W_0 is the strain energy, $\bar{K}_0$ is the stiffness matrix, $\bar{F}$ is a matrix of applied forces and $\bar{r}_0$ represents the nodal displacements, the authors compared the uncracked strain energy W_0 to the modified strain energy due to crack damage given by

$$W_1 = b\int_0^a \left[\frac{\left(K_I^2 + K_{II}^2\right)}{E'} + (1+n)\frac{K_{III}^2}{E}\right]da \tag{8}$$

where a is the crack depth, b is the element width, K_i are stress intensity factors (respectively for opening, sliding, and tearing type cracks), E is the elastic modulus, n is the Poissan's ratio, and $E' = E/(1-n^2)$ for plane strain (Kam and Lee, 1992:383-384). After applying a series of constraints, a minimization routine, and a Newton-Raphson solution approach, the authors backed out an approximate crack location with an error of approximately $\pm 5\%$ after studying the first 10 natural frequencies and mode shapes. They thereby further verified that frequency reduction of the natural modes is a viable method for identifying damage presence.

Beam Analysis—Torsional Spring Model.

Several authors attempted to model local stiffness reductions due to surface inclusions as a localized torsional spring connecting the neighboring two isotropic elements, with the torsional spring constant K_T proportional to the ratio of crack depth to beam depth, the Young's Modulus of the material, and the second moment of inertia. Doyle (1995) took this approach in developing a damage detection scheme that studied the generation and reflection of axial waves after transverse vibration is initiated. He compared observed experimental responses to a set of theoretical finite element (FE) predictions characterizing cracks at differing locations and magnitudes, and then chose a "best fit" for the experimental result through the use of a genetic algorithm to match theory with experiment. Dado (1997) also used the torsional spring model but emphasized different end conditions. His results showed that the respective modes of pinned-pinned, clamped-free, pinned-free, and clamped-clamped specimens all demonstrated eigenvector and eigenvalue shifts in the presence of surface damage. Patil and Maiti (2002) further utilized the torsional spring method to characterize the frequency responses of beams with multiple cracks. An indexed torsional spring constant K_{Tn} was applied to each crack location on the beam and the beam segmented into appropriate lengths where only one damage location was present within the given segment. Frequency variations of the segments were examined over the first three natural modes via their derived MATLAB procedure, and the segments with the greatest variation in frequencies were determined to be the segments within which damage was present.

Beam Analysis—Graphical Methods.

Purely graphical methods have been researched as well to determine damage presence and location within a beam structure. Kim and Stubbs (2002) used a series of plotted error indices for the first four modal frequencies of a cracked beam to identify the presence of a crack. Their error index (the difference between the ratio of measured modal frequency changes and the ratio of modal sensitivities for a given element) is defined by

$$e_{ij} = \frac{Z_m}{\sum_{k=1}^{NM} Z_k} - \frac{F_{mq}}{\sum_{k=1}^{NM} F_{kq}} \tag{9}$$

where

e_{ij} = localization error for the *i*th mode and the *j*th location
Z_m = fractional change of the *m*th eigenvalue after damage
F_{mq} = modal sensitivity of the *m*th modal stiffness with respect to the *q*th element
NM = number of modes considered

will equal zero when damage is present in the *j*th location using the *i*th modal information (Kim and Stubbs, 2002:150). The error index is then plotted for each mode, and where all e_{ij} go to zero exist potential locations for damage presence (see Figures 1 and 2). Note that the symmetry of the functions produces two locations, only one of which is correct and in both cases shown the correct solution resides in the region where $\frac{x}{L} < 0.5$. It should be further noted that though the error-index method worked well for crack locations between $\frac{x}{L} = 0.25$ and $\frac{x}{L} = 0.5$, this method proved to be highly inaccurate as

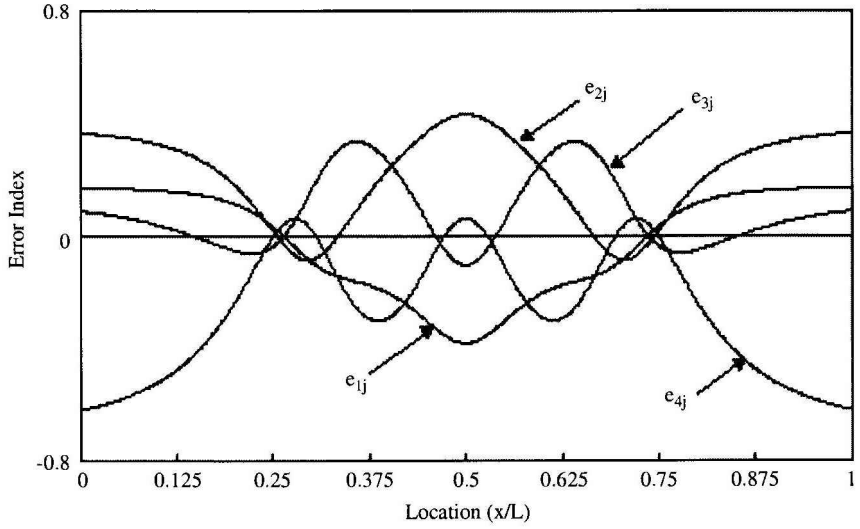

Figure 1. Localization Error Indices for Individual Modes for Crack Location x/L=0.25 (Kim and Stubbs, 2003:153)

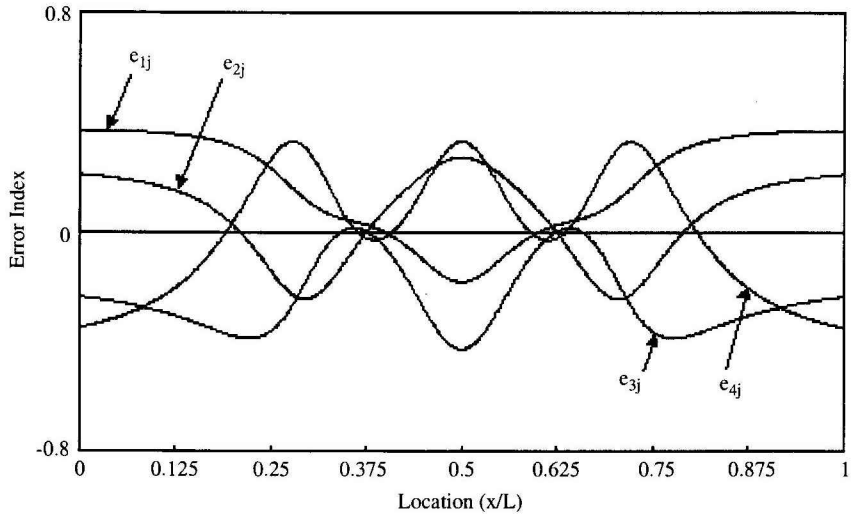

Figure 2. Localization Error Indices for Individual Modes for Crack Location x/L=0.375 (Kim and Stubbs, 2003:154)

$\frac{x}{L} \to 0$. Also, no cases were published where the crack was located beyond the midpoint of the beam.

A similar methodology was employed by Owolabi, Swamidas, and Seshadri (2002) to study the changes in modal frequencies and mode shapes due to thin saw cuts of various depths at several locations along the length of the beam. Quoting the earlier study by Cawley and Adams, the authors tested the postulate that "any localized damage would affect each mode differently, depending on the particular location of the damage" (Owolabi *et. al.*, 2002:2). For this they measured the natural frequencies of uncracked aluminum beams and compared these results to the frequencies of beams with a saw cut included at several locations. The authors then generated plots of the ratio of cracked-frequency and uncracked frequency (w_c/w) vs. the ratio of notch depth to beam width (a/h) for various crack location ratios along the length of the beam (c/L) as Figure 3 indicates. This experiment was run on both fixed-fixed beams and simply supported beams, and as Figure 3 shows, each mode was affected in a different manner depending on whether the crack was located near a modal node or not. The authors also created similar plots of eigenvectors for each mode and noted related displacement magnitude shifts.

Several other researchers took similar but slightly different graphical approaches to the frequency-shift characterization problem due to the onset of damage. Waldron *et. al.* (2002) utilized a scanning laser vibrometer to measure the surface velocity at points along the broad edge of an actuated beam after surface notches were introduced. They

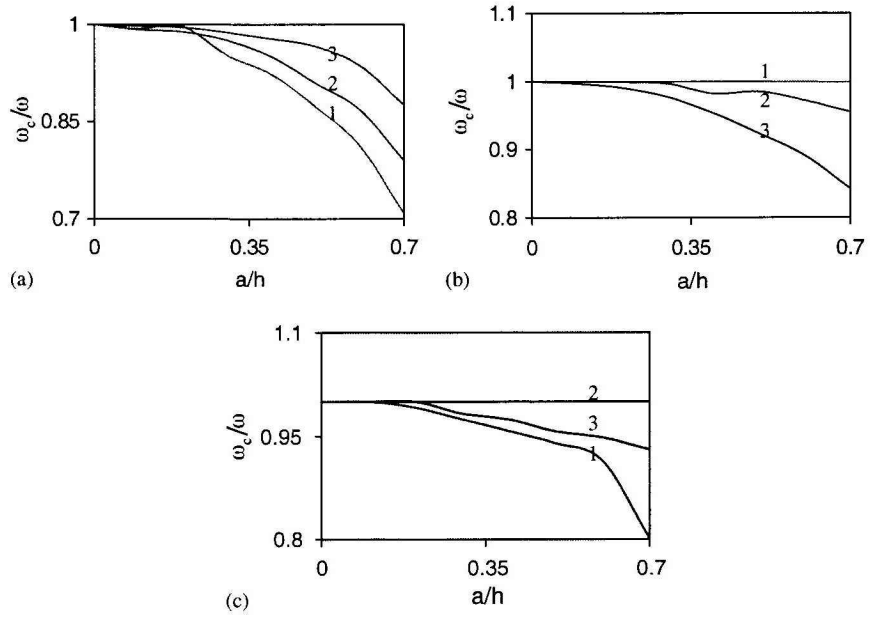

Figure 3. Natural frequencies (of various modes) in terms of crack depth for a simply supported beam for various crack location ratios c/l (1--8/16; 2--5/16; 3--3/16): (a) mode 1; (b) mode 2; (c) mode 3. (Owolabi et. al., 2003:8)

concluded that "at higher natural modes, damage is easier to detect" and that "there is a much higher probability of detecting damage when the damage is near the anti-nodal point" (Waldron *et. al.*, 2002:224), supporting conclusions previously reached by other authors. Ismail, Ibrahim, and Martin in a previous study (1989) directly examined frequency response scans over the actuation range 60-2000 Hz and recognized noticeable reductions in resonant peaks over that range. The data were then extrapolated and the frequency ratios (w_c/w_n) were plotted against crack size (a/h), as was later done by Owolabi *et. al.* Again, it was noted that natural frequencies in all modes, but particularly the higher modes, decreased as damage magnitude increased. Damage location played a significant part in which modes were most affected.

Beam Analysis—Internal Notches.

Since most of the literature has focused on surface damage (as this is the most common due to external impacts and operating environment considerations), comparatively little research has been conducted on internal delaminations in composite beams. These internal delaminations are actually a relatively common occurrence due to imperfect manufacturing methods, thermal debonding, impact/compression damage, etc., with the added problem that the damaged areas may not be able to be seen externally. Hence, researchers have attempted to use similar vibration analysis methods as those mentioned previously to detect internal damages versus those seen readily from the outside.

In 1982, Wang, Liu, and Gibby published a paper where free vibrations of split beams were investigated. They considered discrete portions of a beam where a split (simulated delamination) was either present or not present and developed corresponding non-dimensionalized equations of motion for each. For the regions where no split was present, only flexural vibration was assumed and thus the non-dimensionalized equation of motion for transverse displacement became

$$\frac{d^4W}{dx^4} - K^4W = 0 \tag{10}$$

where $W = w/L$ with w as transverse displacement amplitude and L as the beam length, $x = x/L$ with x as longitudinal coordinate of the notch centerpoint, and

$$K^4 = \left(\frac{\rho A}{EI}\right) L^4 \omega^2 \tag{11}$$

where

w = radian frequency of harmonic motion
r = material density
A = cross-sectional area
E = elastic modulus (Young's modulus)
I = second moment of area

(Wang *et. al.*, 1982:492). For the region where the split was encountered, both longitudinal and transverse vibration was considered for each sublaminate and each was treated as a separate beam. The governing differential equation for non-dimensionalized longitudinal displacement amplitude U was considered:

$$\frac{d^2U}{dx^2} + c^4K^4U = 0 \tag{12}$$

where $U = u/L$ with u as the longitudinal displacement, and $c^4 = I/AL^2$ (Wang *et. al.*, 1982:493). With these relations the authors developed a series of displacement matrices while ensuring continuity between the regions, and were then able to solve a set of simultaneous equations for the modal frequencies of interest. Though only the first, second, and third vibration modes of a fixed-fixed beam and the first and second modes of a cantilevered beam were considered, good results were obtained, demonstrating the expected decline in modal frequencies with increasing crack length or with more than one crack included.

Tracy and Pardoen (1988) also regionalized a centerline-notched beam into two homogeneous areas without a notch and two distinct sublaminates above and below the notch. A FORTRAN algorithm was then developed based on similar mathematical theory to that of Wang *et. al.*, and it was found that modes one through four experienced an increasing respective degradation in modal frequency due to a given notch length, supporting the idea that higher modes are affected by stiffness reductions more readily

than lower modes. The authors also stated that "as the delamination moves from regions of high shear force to regions of high curvature, the effect of the delamination is reduced" (Tracy and Pardoen, 1988:1207), meaning that crack propagation potential is minimized in the regions of high moment. However, as Salawu points out, "at modal nodes (points of zero modal displacements), the [axial] stress is minimum for the particular mode of vibration. Hence, a minimal change in a particular modal frequency could mean that the defect may be close to the modal node" (1997:718-719).

Also in 1988, Mujumdar and Suryanarayan studied frequency reductions in debonded steel strips. Using a cantilever setup, the authors adhered multiple pieces of spring steel together with an instant-curing cynoacrylate while leaving discrete regions unglued, both along the centroidal axis and off-midplane, thereby simulating different delamination regions. Their results supported the Tracy/Pardoen hypothesis that for any given mode, nodal damage is of higher consequence, stating that "in the case of beams with symmetric boundary conditions vibrating in the symmetric modes, the curvature is a maximum and the shear force is a minimum at midspan, therefore the weakening effect is a minimum for centrally located delaminations" (Mujumdar and Suryanarayan, 1988:455). They noted the expected decline in eigenfrequencies and eigenvectors over the first two vibration modes, and published a series of experimental data tables which are later used in this thesis as a comparison for the finite element approach by Perel and Palazotto (2002).

Using modal frequency analysis as an established and accepted method for damage detection in simple structures, Perel and Palazotto (2002) developed a MATLAB-based FE program to calculate the natural frequencies of an isotropic,

cantilevered beam with a notch inclusion to simulate delamination, having the ultimate goal of extending the proposed theory to composite members. The usefulness of their program is that, contrary to previous FE approaches in the literature, the user need not re-mesh the specimen for each crack condition, thereby saving valuable analysis and modeling time. The purpose of this thesis is to validate the use of modal frequency response as a damage detection method for internally-notched cantilevered aluminum beams, and analyze the resulting modal frequencies for degradation trends based on inclusion location, inclusion length, and vibration mode. Comparison of experimental results with the MATLAB FE program and the commercial FE analyzer ABAQUS is also carried out.

II. Theoretical Development

A brief theoretical synopsis of three major topics in this thesis is presented in this chapter for background understanding. First, cantilever beam theory is reviewed and the differential boundary-value problem solved from balance-of-force equations to produce the theoretical modal frequencies. These results are later used in Chapter IV to verify the experimental outcome of the first eight vibration modes of the control specimen. Then, the theory behind the MATLAB-based FE program developed by Perel and Palazotto (2003) is summarized. Their program is an object of analysis for this thesis and is constructed using the cantilever arrangement. Finally, an overview of Laser Doppler Vibrometry (LDV) is presented as LDV is the primary method of experimentation for this work.

Natural Frequency Derivation for Clamped-Free (Cantilevered) Beam

The natural frequencies for a simple cantilevered isotropic beam can be developed from a differential boundary-value problem for a continuous clamped-free system. As outlined extensively by Meirovitch (1986:221-226) and summarized in the derivation that follows, a differential beam element under transverse flexure will be kept in equilibrium by a differential applied external load, internal shear, and reaction moments at the left and right ends of the element (all assumed to be functions of displacement and time). A free-body diagram of this element is indicated in Figure 4.

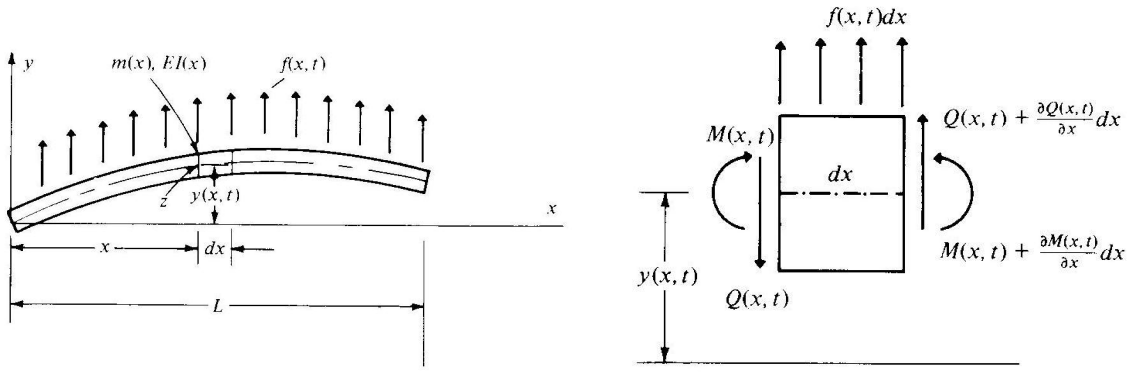

Figure 4. Differential Beam Element (Meirovitch 1986:221)

Setting an abscissa collinear with the at-rest neutral axis of the beam and an ordinate normal to the abscissa in the transverse direction (direction of displacement during vibration), balancing the force equation of motion $F = ma$ yields

$$\left[Q(x,t) + \frac{\partial Q(x,t)}{\partial x}dx\right] - Q(x,t) + f(x,t)dx = m(x)dx\frac{\partial^2 y(x,t)}{\partial t^2} \tag{13}$$

where $Q(x,t)$ is transverse shearing force, $f(x,t)$ is the applied external load, $m(x)$ is the mass per unit length, and $y(x,t)$ is the transverse displacement during vibration response. Similarly, the moment equation of motion has the form

$$\left[M(x,t) + \frac{\partial M(x,t)}{\partial x}dx\right] - M(x,t) + \left[Q(x,t) + \frac{\partial Q(x,t)}{\partial x}dx\right]dx + f(x,t)dx\frac{dx}{2} = 0 \tag{14}$$

where $M(x,t)$ is the reaction moment about the rotational axis and all other terms are as defined previously. If one cancels appropriately in Eq. (14) and eliminates dx^2 terms the results become

$$\frac{\partial M(x,t)}{\partial x} + Q(x,t) = 0 \tag{15}$$

which, when combined with Eq. (13), reduces to

$$-\frac{\partial^2 M(x,t)}{\partial x^2}+f(x,t)=m(x)\frac{\partial^2 y(x,t)}{\partial t^2} \tag{16}$$

From elementary mechanics of materials, bending deformation and bending moment are related by

$$M(x,t)=EI(x)\frac{\partial^2 y(x,t)}{\partial x^2} \tag{17}$$

where E is the modulus of elasticity of the material and $I(x)$ is the moment of inertia at the given distance from the origin. By combining Eqs. (16) and (17) and assuming no damping, one arrives at the fourth-order differential boundary-value equation of motion:

$$-\frac{\partial^2}{\partial x^2}\left[EI(x)\frac{\partial^2 y(x,t)}{\partial x^2}\right]+f(x,t)=m(x)\frac{\partial^2 y(x,t)}{\partial t^2} \qquad 0<x<L \tag{18}$$

For the solution of natural frequencies for a cantilevered beam, the distributed external forcing function $f(x,t)$ has zero magnitude. Boundary conditions for the beam at the clamped-end and free-end are respectively given by:

$$y(0,t)=0 \qquad \left.\frac{\partial y(x,t)}{\partial x}\right|_{x=0}=0 \tag{19}$$

$$\left.EI(x)\frac{\partial^2 y(x,t)}{\partial x^2}\right|_{x=L}=0 \qquad \left.\frac{\partial}{\partial x}\left[EI(x)\frac{\partial^2 y(x,t)}{\partial x^2}\right]\right|_{x=L}=0 \tag{20}$$

Using the method of separation of variables where

$$y(x,t)=Y(x)F(t) \tag{21}$$

and assuming that $F(t)$ represents bounded harmonic oscillation with a frequency w, then considering Eqs. (19), (20), and (21), Eq. (18) ultimately reduces to

$$\frac{d}{dx}\left[EI(x)\frac{d^2 Y(x)}{dx^2}\right]=w^2 m(x)Y(x) \qquad 0<x<L \tag{22}$$

For a uniform beam with constant E, I, and m over the range $0 < x < L$, the expression becomes

$$\frac{d^4Y(x)}{dx} - b^4Y(x) = 0 \tag{23}$$

where

$$b^4 = \frac{w^2 m}{EI} \tag{24}$$

The general solution to Eq. (23) is given by

$$Y(x) = C_1 \sin bx + C_2 \cos bx + C_3 \sinh bx + C_4 \cosh bx \tag{25}$$

where C_i are unknown coefficients for the harmonic terms. Since the clamped-end displacement and slope conditions are

$$Y(0) = 0 \qquad \left.\frac{dY(x)}{dx}\right|_{x=0} = 0, \tag{26}$$

the two resulting relations

$$C_1 + C_3 = 0 \qquad C_2 + C_4 = 0 \tag{27}$$

combine with Eq. (25) to form

$$Y(x) = C_1(\sin bx - \sinh bx) + C_2(\cos bx - \cosh bx) \tag{28}$$

Further invoking the boundary conditions for free-end moment and shear defined by

$$\left.\frac{d^2Y(x)}{dx^2}\right|_{x=L} = 0 \qquad \left.\frac{d^3Y(x)}{dx^3}\right|_{x=L} = 0, \tag{29}$$

two simultaneous equations are produced:

$$C_1(\sin bL + \sinh bL) + C_2(\cos bL + \cosh bL) = 0 \tag{30}$$

$$C_1(\cos bL + \cosh bL) - C_2(\sin bL - \sinh bL) = 0 \tag{31}$$

After solving for C_2 in terms of C_1 and realizing that $C_1 \neq 0$ must be true for the non-trivial solution to exist, the resulting characteristic equation is formed:

$$\cos bL \cosh bL = -1 \tag{32}$$

The resonant eigenvalues b_r found by numerically solving Eq. (32) are inserted into the displacement function of Eq. (28) to form the resonant natural modes (see Figure 5) in terms of only C_1, b_r, x, and L:

$$Y_r(x) = \frac{C_1}{\sin b_r L - \sinh b_r L}\left[(\sin b_r L - \sinh b_r L)(\sin b_r x - \sinh b_r x)\right.$$
$$\left. + (\cos b_r L + \cosh b_r L)(\cos b_r x - \cosh b_r x)\right] \qquad r = 1, 2, \ldots \tag{33}$$

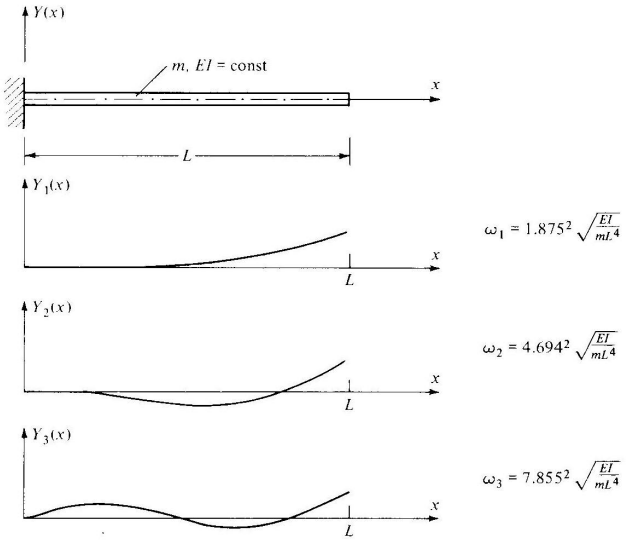

Figure 5. First Three Mode Shapes for a Cantilevered Beam (Meirovitch 1986:226)

A listing of the first ten b_r values is given in Table 3, taken from Gorman's text on free vibrations of beams and shafts (1975).

Table 3. Resonant Eigenvalues for Vibration Modes (Cantilevered Beam)

MODE	β_r
1	1.875
2	4.694
3	7.855
4	10.996
5	14.137
6	17.279
7	20.420
8	23.562
9	26.704
10	29.845

Therefore, considering the eigenvalue solution of Eq. (32) and the definition given by Eq. (24), the resonant (natural) frequencies w_r for the cantilevered beam are

$$w_r = b_r^2 \sqrt{\frac{EI}{mL^4}} \qquad r = 1, 2, ... \tag{34}$$

For the purposes of the experiments undertaken in this thesis, only the first eight resonant modes were considered.

Theoretical Development of the MATLAB Algorithm

The MATLAB-based finite element solution approach developed by Perel and Palazotto (2002, 2003) incorporates basic Euler-Bernoulli beam theory for element formulation to calculate the modal frequencies of a delaminated cantilevered beam under piezoelectric actuation. The program was written specifically for the cantilevered beam

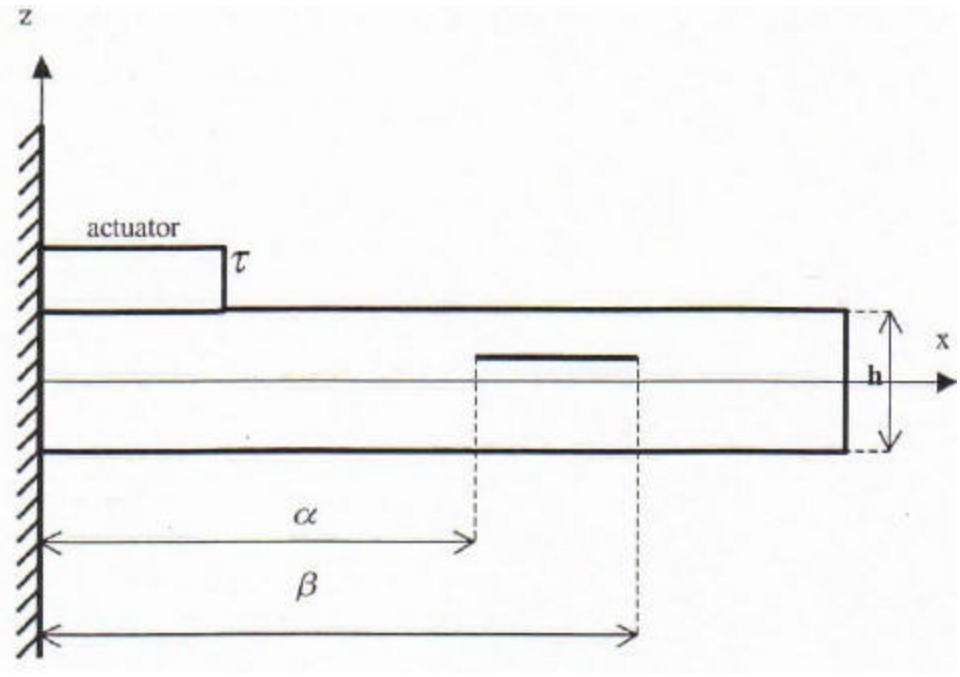

Figure 6. Zonal Definition of Cantilevered Beam with Attached Piezoelectric Actuator (Perel and Palazotto, 2002:4460)

case with a piezoelectric actuation source affixed to the surface of the beam, along its breadth, near the fixed base (shown in Figure 6). For the initial formulation, the delaminated region is assumed external to the beam portion covered by the piezoelectric actuator. The crack tip coordinates, indicated by the distances a and b, are parallel to the free longitudinal surfaces and centerline of the beam. The dimension h is the transverse thickness of the beam (the minor dimension), while the actuator thickness is represented by the dimension t. The notch extends completely through the width of the beam to create through-width homogeneity of the disbonded area.

As extensively explained by Perel and Palazotto and briefly summarized here, the Euler-Bernoulli development utilized within the MATLAB code assumes a transverse displacement function of the form

$$w(x,z,t) = W_0(x,t) + D_a^b(x) H_g(z)\left[W_1(x,t) - W_0(x,t)\right] \tag{35}$$

where a and ß are the longitudinal notch tip coordinates and ? is the z-coordinate of the notch centerline. Equation (35) also incorporates a double-sided unit step function of the form

$$D_a^b(x) \equiv \begin{cases} 1 & \text{for } a < x < b \\ 0 & \text{for } 0 \le \text{x} \le a \text{ and } b \le \text{x} \le \text{L} \end{cases} \tag{36}$$

and a Heaviside function defined by

$$H_g(z) \equiv \begin{cases} 0 & \text{for } -h/2 < z \le g \\ 1 & \text{for } g < z < h/2 \end{cases} \tag{37}$$

$W_0(x,t)$ is the transverse displacement of the central beam axis antecedent to, posterior to, and below the notch while $W_1(x,t)$ indicates the transverse displacement of the upper delaminated portion on the region $a < x < b$. The double-sided unit step and Heaviside functions mathematically restrict the sublaminates from overlapping during vibration response, which is physically impossible. Compatibility of displacement and slope between notched and notchless regions during dynamic response incorporates the extended Hamilton's Principle:

$$d\int_{t_1}^{t_2} J\,dt - \int_0^L q\,dw\Big|_{z=h/2}\,dx = 0 \tag{38}$$

where q represents the uniform load distributed across the upper surface of the beam and J is a modified Lagrangian function of the form

$$J = \iiint_V (\hat{U} - \hat{T} - lf)\,dV = b\int_0^a \int_{-h/2}^{h/2} (\hat{U} - \hat{T})\,dz\,dx + b\int_a^b \left[\int_{-h/2}^{g} (\hat{U} - \hat{T})\,dz + \int_g^{h/2} (\hat{U} - \hat{T})\,dz - lf \right] dx + b\int_b^L \int_{-h/2}^{h/2} (\hat{U} - \hat{T})\,dz\,dx \tag{39}$$

The kinetic energy density and strain energy density are respectively defined by

$$\hat{T} = \frac{1}{2} r (\dot{u}^2 + \dot{w}^2) \tag{40}$$

$$\hat{U} = \frac{1}{2} s_{xx} e_{xx} = \frac{1}{2} s_{xx} \left[\frac{\partial u}{\partial x} + \frac{1}{2} \left(\frac{\partial w}{\partial x} \right)^2 \right] \tag{41}$$

and $l = l(x,t)$ is the Lagrange multiplier of the contact forcing function within the delamination:

$$f(W_0^{(2)}, W_1^{(2)}) \equiv (W_1^{(2)} - W_0^{(2)}) \left[1 - H_0 (W_1^{(2)} - W_0^{(2)}) \right] = 0 . \tag{42}$$

For the finite element matrix formulation, the authors approximate the unknown functions $W_0(x,t)$ and $W_1(x,t)$ from Eq. (35) by third-degree Hermit polynomials, considering classical two-dimensional beam element shape functions and the respective nodal degrees of freedom:

$$W_0 = \begin{bmatrix} N_1 & N_2 & N_3 & N_4 \end{bmatrix} \begin{Bmatrix} W_0(0) \\ \frac{\partial W_0}{\partial x}(0) \\ W_0(L) \\ \frac{\partial W_0}{\partial x}(L) \end{Bmatrix} \tag{43}$$

$$W_1 = \begin{bmatrix} N_1 & N_2 & N_3 & N_4 \end{bmatrix} \begin{Bmatrix} W_1(0) \\ \dfrac{\partial W_1}{\partial x}(0) \\ W_1(L) \\ \dfrac{\partial W_1}{\partial x}(L) \end{Bmatrix} \tag{44}$$

where

$$N_1 = 1 - \frac{3x^2}{L^2} + \frac{2x^3}{L^3}, \quad N_2 = x - \frac{2x^2}{L} + \frac{x^3}{L^2}, \quad N_3 = \frac{3x^2}{L^2} - \frac{2x^3}{L^3}, \quad N_4 = -\frac{x^2}{L} + \frac{x^3}{L^2}, \tag{45}$$

which are taken from the finite element text written by Cook *et. al.* (1974:25). The finite beam element showing the active degrees of freedom considered in the MATLAB approach is shown in Figure 7.

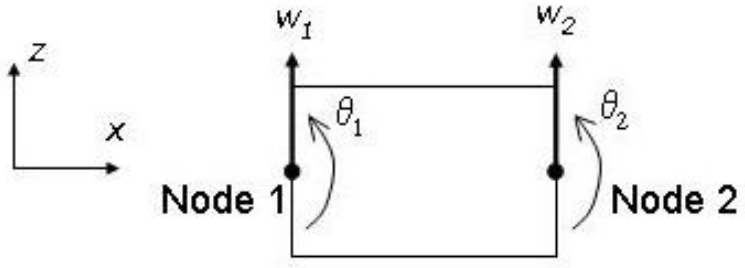

Figure 7. Finite Beam Element Showing Active Degrees of Freedom Utilized in the MATLAB Formulation.

After utilizing the eight given nodal parameters and the respective strain-displacement matrices $[B_w]$ and $[B_u]$ (derivation not shown for brevity) to produce expressions for the transverse and longitudinal displacements, the authors compiled the element stiffness matrix defined by

$$\underset{(8x8)}{[k]} = b\int_{0}^{L}\int_{-h/2}^{h/2} \underset{(8x1)}{[B_e]^T} \frac{1}{S_{11}} z^2 \underset{(1x8)}{[B_e]} dz\, dx \tag{46}$$

where b is the width of the beam, S_{11} is the elastic compliance coefficient of the material $\left(S_{11} = \frac{1}{E_{11}}\right)$, and $\underset{(1x8)}{[B_e]}$ comes from the strain energy approach where

$$\underset{(1x8)}{[B_e]} = -\frac{\partial^2 [B_w]}{\partial x^2} \tag{47}$$

The strain energy for the finite element in terms of the nodal parameters then becomes

$$U = \frac{1}{2} \underset{(1x8)}{\{q\}^T} \underset{(8x8)}{[k]} \underset{(8x1)}{\{q\}} + U_{nq} \tag{48}$$

where the nodal parameters $\{q\}$ are a column matrix of the terms on the extreme right-hand side of Eqs. (43) and (44), and U_{nq} is an additional strain energy term that depends non-quadratically on the nodal parameters and $[B_u]$.

The same basic approach is followed to characterize the stiffness properties of all finite elements within the undamaged region overlaid by the piezoelectric actuator, the undamaged regions of the free cantilever, and the cracked region within the beam. Appropriate constraints accounting for continuity of displacements and slopes at zonal interfaces are applied through the functional continuity of the interpolation polynomials given in Eqs. (43) and (44) and their derivatives, as well as through the penalty function method incorporating the global nodal parameters q_i (Perel and Palazotto, 2002).

The actuation force produced by the affixed piezoelectric patch is integrated through the virtual work principle and through the constitutive equations of an

orthotropic piezoelectric layer, thereby yielding the modified virtual work principle defined by

$$b\int_0^L\int_{-h/2}^{h/2}\frac{1}{S_{11}^{(c)}(z)}e_{xx}de_{xx}dz\,dx+b\int_0^L\int_{h/2}^{h/2+t}\frac{1}{S_{11}^{(p)}(z)}\left(e_{xx}-d_{31}\frac{V}{t}\right)de_{xx}\,dz\,dx$$
$$+b\int_0^L\int_{-h/2}^{h/2}r^{(c)}(g+\ddot{w})dw\,dz\,dx+b\int_0^L\int_{h/2}^{h/2+t}r^{(p)}(g+\ddot{w})dw\,dz\,dx \qquad (49)$$
$$+b\int_0^L\int_{-h/2}^{h/2}r^{(c)}\ddot{u}du\,dz\,dx+b\int_0^L\int_{h/2}^{h/2+t}r^{(p)}\ddot{u}du\,dz\,dx-\int_0^L q\,dw\,dx=0.$$

where

V = applied voltage across the piezoelectric patch
t = thickness of piezoelectric patch
d_{31} = a matrix element characterizing the material properties of the PZT patch
$r^{(c)}$ = density of beam material ("c" denotes "composite")
$r^{(p)}$ = density of piezoelectric patch material
g = Gravitational constant ($9.81\,\frac{m}{s^2}$)
q = unit surface electric charge
(*u is defined below)*

Ultimately, incorporating the modified virtual work principle from Eq. (49) with the Euler-Bernoulli assumptions for transverse and longitudinal displacement

$$w(x,z,t)=W_0(x,t) \qquad (50)$$

$$u(x,z,t)=-\frac{\partial W_0(x,t)}{\partial x}z \qquad (51)$$

the authors produced the following differential equations of motion as the basis of the MATLAB program development:

$$I_2\frac{\partial^4 W_0}{\partial x^4}+J_0\frac{\partial^2 W_0}{\partial t^2}-J_2\frac{\partial^4 W_0}{\partial t^2\partial x^2}=q-I_1\frac{\partial^2 V}{\partial x^2}-J_0 g \quad \text{for } 0\le x\le L \qquad (52)$$

$$I_2 \frac{\partial^2 W_0}{\partial x^2} + I_1 V = 0 \text{ or } I_2 \frac{\partial^2 W_0}{\partial x^2} + I_1 V = \frac{\partial W_0}{\partial x} \text{ constrained at } x = 0 \text{ and } x = L \quad (53)$$

$$I_2 \frac{\partial^3 W_0}{\partial x^3} - J_2 \frac{\partial^3 W_0}{\partial t^2 \partial x} + I_1 \frac{\partial V}{\partial x} = 0 \text{ or}$$

$$I_2 \frac{\partial^3 W_0}{\partial x^3} - J_2 \frac{\partial^3 W_0}{\partial t^2 \partial x} + I_1 \frac{\partial V}{\partial x} = W_0 \text{ constrained at } x = 0 \text{ and } x = L \quad (54)$$

where

$$I_2 = b\left(\int_{-h/2}^{h/2} \frac{1}{S_{11}^{(c)}(z)} z^2 dz + \int_{h/2}^{h/2+t} \frac{1}{S_{11}^{(p)}(z)} z^2 dz \right) \quad (55)$$

$$I_1 = \frac{1}{t} b \int_{h/2}^{h/2+t} \frac{d_{31}}{S_{11}^{(p)}(z)} z \, dz \quad (56)$$

$$J_0 = b\left(\int_{-h/2}^{h/2} r^{(c)} dz + \int_{h/2}^{h/2+t} r^{(p)} dz \right) \quad (57)$$

$$J_2 = b\left(\int_{-h/2}^{h/2} r^{(c)} z^2 dz + \int_{h/2}^{h/2+t} r^{(p)} z^2 dz \right) \quad (58)$$

Laser Doppler Vibrometry (LDV)

The essence of LDV is based on the principle that incident laser light to a test object will induce a Doppler shift in the reflected laser beam if the object is in motion. This reflected beam can then be detected and compared with the original beam to judge the wavelength difference and therefore the object surface velocity along the axis of the incident laser beam. Since laser light has an extremely high frequency (~ 4.74×10^{14} Hz), light intensity must be measured instead of direct wavelength shift.

An interferometer is therefore used to measure intensity differences of light beams. A laser beam enters a beam splitter and is divided into a measurement beam (the

beam that reflects off of the object being measured) and a reference beam that stays internal to the vibrometry system (see Figure 8) . The reflected beam is then mixed with the reference beam and the resultant light is measured by a photodetector. The beat frequency of the resultant light generates a time-dependent intensity I at the points where the measurement and reference beams interfere (Polytec, 2003). This intensity can be characterized by the equation

$$I(t) = I_R I_M R + 2K\sqrt{I_R I_S R}\cos(2pf_D + \Phi) \tag{59}$$

where

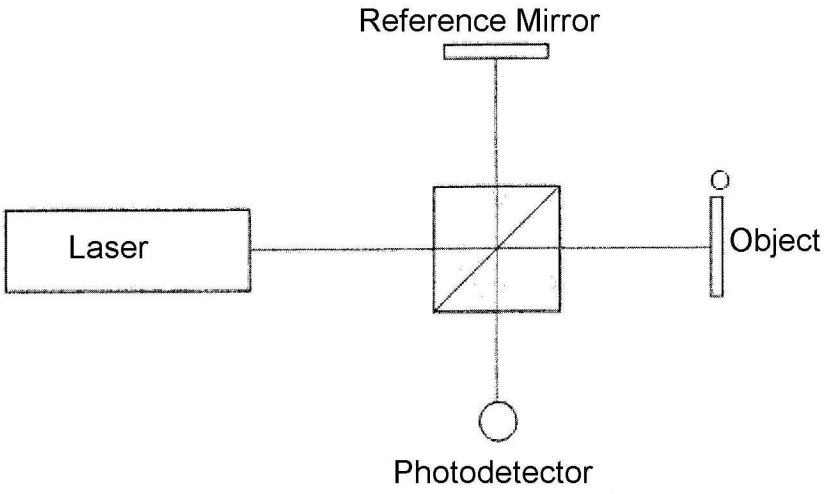

Figure 8. Diagram of Laser Vibrometer Setup (Polytec, 2003:1)

I_R = intensity of the reference beam
I_M = intensity of the measurement beam
R = effective reflectivity of the measured surface
K = a mixing efficiency coefficient
I_S = intensity of the shifted beam

f_D = $2v/l$ = Doppler frequency of the shifted beam where v is the velocity of the incident surface and l is light wavelength

Φ = $4p\Delta L/l$ = phase angle shift with ΔL as the vibrational displacement of the incident surface

With the measured $I(t)$, Equation (59) can be solved for the velocity term in f_D and therefore the object surface velocity is known. Note that as the velocity vector moves toward the light source, the reflected light undergoes an increase in frequency. Conversely, as the velocity vector moves away from the light source, the reflected light decreases in frequency.

The velocity measurements can be integrated with respect to time to obtain displacements and differentiated with respect to time to obtain accelerations. Using multiple scan points on a given object, the three dynamic parameters from each point can be interpolated to produce an overall dynamic profile of the object excitation. This interpolation allows direct observation of the vibrational eigenvectors and therefore the associated eigenvalues can be calculated.

Using the principles mentioned above, an LDV system can be employed to measure any vibrating or moving object non-intrusively. Three methods of measurement are typically utilized: continuous scanning, point-by-point scanning, and a tracking mode in which the laser probe stays fixed on one particular point on a moving object (Halkon *et. al.*, 2003:773). For the particular purposes of this thesis, point-by-point scanning over a discrete area was used.

III. Experimental Method and Setup

For the experimental portion of this study, 15 aluminum specimens were initially designed (ultimately this number grew to 18) with centerline notches of varying lengths near the free end of the cantilever, the midpoint, and the clamped end. These specimens were piezoelectrically actuated using a Quick Pack strain actuator and the eigenmodes of each beam obtained through laser vibrometry. The experimental results were then analyzed for frequency response trends based on notch location and magnitude, as accomplished in Chapter IV. The acquired modal frequencies were also compared to the MATLAB FE output for the cases considered, as well as the ABAQUS CAE finite element program.

This chapter explains the experimental procedure and describes the equipment used for data acquisition.

Experimental Test Equipment

The experimental validation was conducted in the Vibration Laboratory on the campus of the Air Force Institute of Technology. In this laboratory, two laser vibrometers were used during the experimental process:

Laser Vibrometer 1: Polytec OFV-056 scanning head with OFV-5000 controller and PSV-Z-040 junction box

Laser Vibrometer 2: Polytec PSV-400 scanning head with OFV-5000 controller and PSV-400 junction box

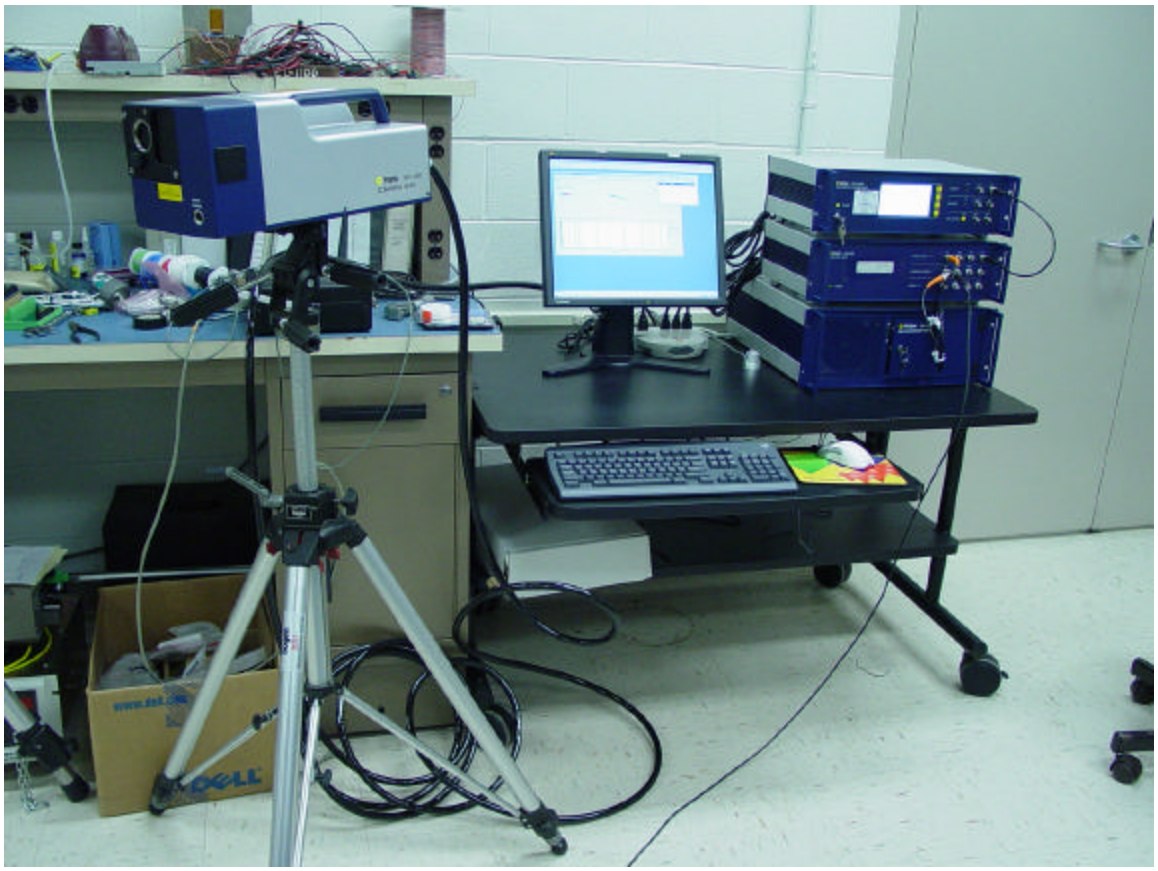

Figure 9. Polytec Laser Vibrometer with Associated Computer Hardware.

The second vibrometer was used as an upgrade provided by Polytec, Inc. to the original equipment, received partway through the experimental process. A picture of this vibrometer with the associated hardware is shown in Figure 9. Each vibrometer was connected to an associated desktop computer (powered by an AMD Athlon XP 3000 chip) supplied by Polytec, Inc. with Polytec Scanning Vibrometer Version 8.0 software loaded for scan analysis. Other test hardware included the following (see Figures 10 and 11):

Clamp: Newport Research Corp. (NRC) Model B-1

Stand: NRC Model 45

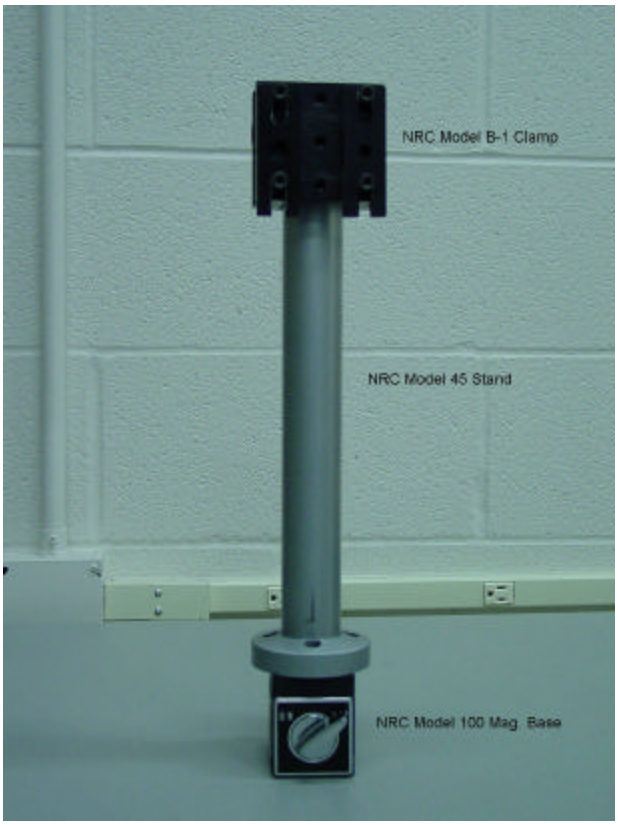

Figure 10. Front View of NRC Clamp, Stand, and Magnetic Base.

Figure 11. ACX Quick Pack Power Amplifier Model EL 1224

Magnetic Base: NRC Model 100 Magnetic Base

Amplifier: Active Control eXperts (ACX) Quick Pack Power Amplifier Model EL 1224

The magnetic base was placed on the steel surface of a pneumatic shaker table in the at-rest position to eliminate base motion. The cylindrical test stand was then affixed to the magnetic base through four socket head cap screws, and the clamp slipped onto the top of the test stand and tightened via a locking screw. This clamping stand was used to establish the cantilevered end condition for the test specimens.

Experimental Specimen Design

Though the frequency analysis accomplished in this thesis (as well as the MATLAB development proposed by Perel and Palazotto) will ultimately serve as a foundation for the characterization of delaminations in composite structural cross-sections, it was important for the initial verification experiments to avoid cross-ply and off-angle stresses (which may affect dynamic output) to ensure purity of the experimental results. To this end, isotropic aluminum beams were chosen as the desired test specimens because they can be inexpensively manufactured, aluminum was readily available at the machine shop, and the lack of lamination layers allowed for a pure dynamic response with much less potential for previously existing manufacturing defects (as would be the case with composites). Since 2024-T3 aluminum was most abundant in the machine shop, this material was selected (initially) for specimen fabrication.

The overall dimensions of the beams were chosen essentially for machining convenience since the beam characteristics are part of the input field for the MATLAB analysis (see Appendix A), and could therefore be of any value. A dynamically

measurable length of approximately 12 inches was desired, so the beams were cut to a length of 15 inches to allow for the 3-inch clamped area (the width of the NRC clamp) for establishment of the cantilever. The width of the beam was chosen to be 1 ½ inches to fit between the four cap screws of the clamping block while also minimizing the depth of cut necessary to create the included notch. The depth of the beam was selected to be ? -inch to allow for drilling of a $\frac{1}{16}$-inch starter hole for the electrical discharge machining (EDM) cutting wire (explained later in this section), since a smaller hole greatly increased the likelihood of snapping the drill bit off inside the specimen. Figure 12 shows a typical specimen profile.

For a complete frequency evaluation test set, three distinct locations for notch inclusions were required: notches near the clamped end of the beam (but outside of the

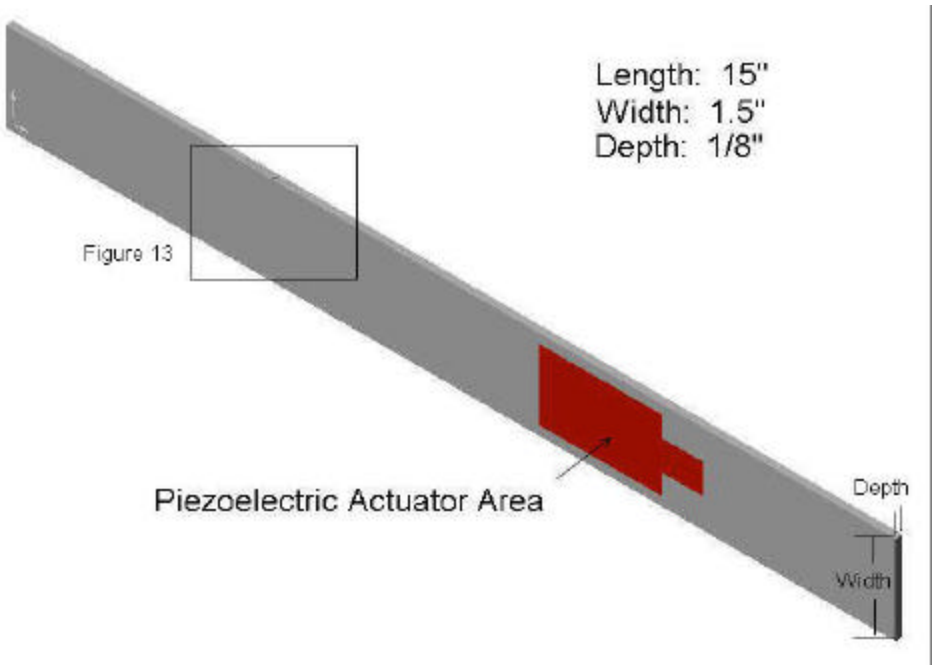

Figure 12. General Aluminum Test Specimen Profile.

2 1/16-inch PZT area), notches near the center of the testable area, and notches near the free end of the cantilever. All three locations were considered in both the MATLAB analysis and experimentally.

For the experimental portion of the analysis, 15 aluminum beams of the type shown in Figure 12 were manufactured. The first was a control specimen in which no notch was included. This piece served as a basis for vibrational trend comparison versus the beams including centerline notches, as well as a verification of the cantilever beam theory and the coefficients presented in Table 3 in Chapter II. The next 12 beams consisted of 3 sets having 4 notched beams each. Since the MATLAB program required all values to be entered in metric (SI) units, the notches were cut in units of centimeters. The first set included 4 beams with centerline notches near the clamped end of each beam, but forward of the PZT location, in lengths of 4cm, 8cm, 12cm, and 16cm. The two remaining four-beam sets contained notches having the same lengths as the first, with one set having the notches at the center of the active region of the beams, and the other set having the notches at the free end of the beams. Two additional beams were created: one with a 20-cm notch and one with a 24-cm notch. Both of these notches were centrally located in the cantilever portion of the beam. Appendix B contains example drawings of the free-end notched beams—all other beams were drawn similarly. A $\frac{1}{16}$-inch starter hole was specified near the center of each notch (shown in Figure **13**) to allow for the EDM cutting wire. Unfortunately, the specimen having the 8-cm notch near the cantilevered end was incorrectly fabricated and due to other machining jobs at the time could not be remade. The entire set of original specimens (minus the mismanufactured piece) is depicted in Figure 14.

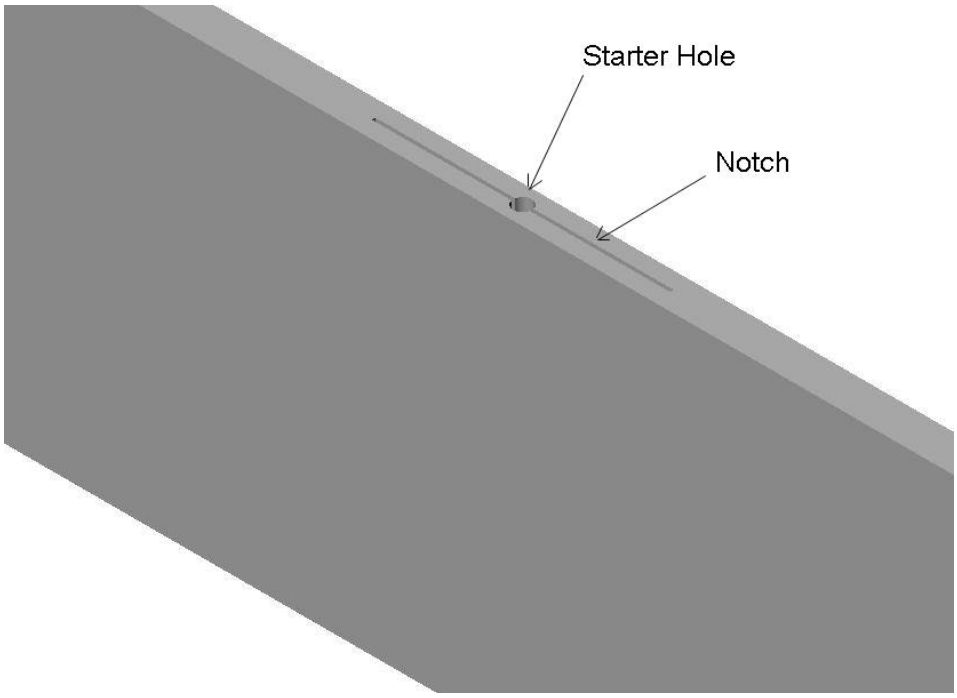

Figure 13. Close-up of Notched Area in a Typical Test Specimen.

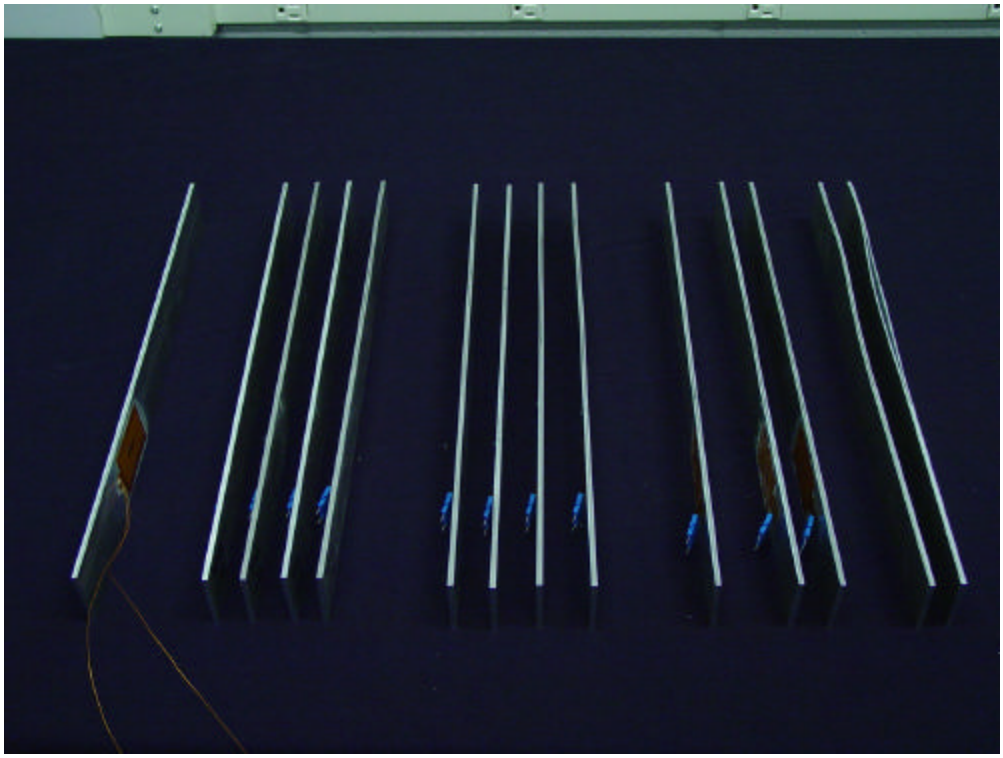

Figure 14. Set of Original 2024 T3 Specimens (minus 8-cm clamped-end specimen).

The notches in the beams were created using the EDM process. This approach utilizes an ultra-high current passing through a thin wire to burn away material, thereby creating a "cut" in the specimen. Throughout the process, the cutting area is constantly flooded by a liquid coolant (in this case water) to ensure thermal conduction from the wire to areas of material beyond the immediate cut is minimized. The EDM machine used for manufacturing the specimens for this project could create a notch with a smallest width of 0.012", which was therefore chosen as the appropriate notch width to simulate a delamination as closely as possible.

Residual Stresses.

Upon receipt of the specimen set from the machine shop technicians, it was noted that, in the beams with long notch lengths, warping had occurred in the sublamina. Initial conjecture suggested that high temperature inductions from the EDM process had thermally stressed the material, however this proved incorrect after further understanding of the extensive cooling methods used during the procedure. Attention then turned to the material itself, particularly the temper designation of the aluminum—T3. According to www.efunda.com, a website dedicated to engineering fundamentals, the T3 temper indicates that the aluminum has been "solution heat treated and then cold worked," which is done to improve material strength and decrease thermal sensitivity. However, a byproduct of the cold working process (in this case, cold rolling) is plastic deformation along the surface boundary and the introduction of latent compressive stresses into the final material. Figure 15 shows a simple diagram of the stress/strain results of the cold rolling procedure.

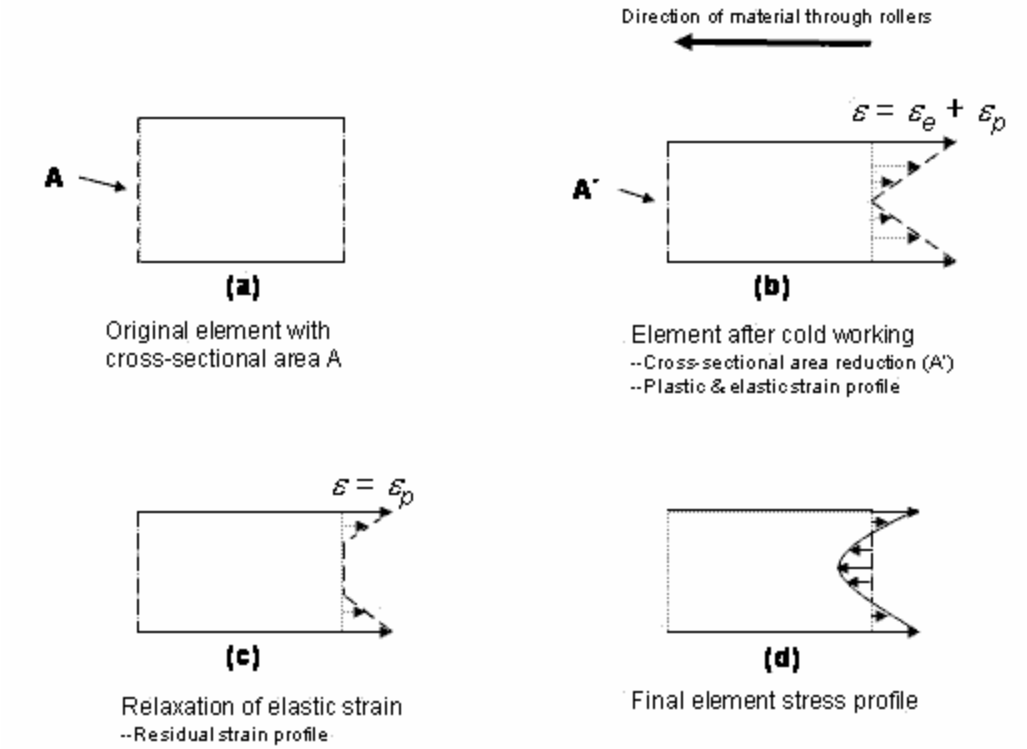

Figure 15. (a) Small Beam Element Prior to Cold Rolling; (b) Small Beam Element After Cold Rolling with Strain Profile

The presence of these stresses caused the internal notch faces to come together, and in the cases of the longer notch lengths, the beams to deform (such as the 20-cm and 24-cm beams at the extreme right of Figure 14). The effects of residual stresses on the four-beam set with notches at the free end are shown in Figure 16. The other two sets of beams were likewise affected.

Though most of the beam specimens were still usable for comparative frequency testing (see Chapter IV—*2024 T3 vs. 2024 O Frequency Comparison*), the 20-cm and 24-cm notch lengths were highly deformed and therefore rendered unusable. It was desired to relieve the residual stresses in the specimens to allow the notches to open and

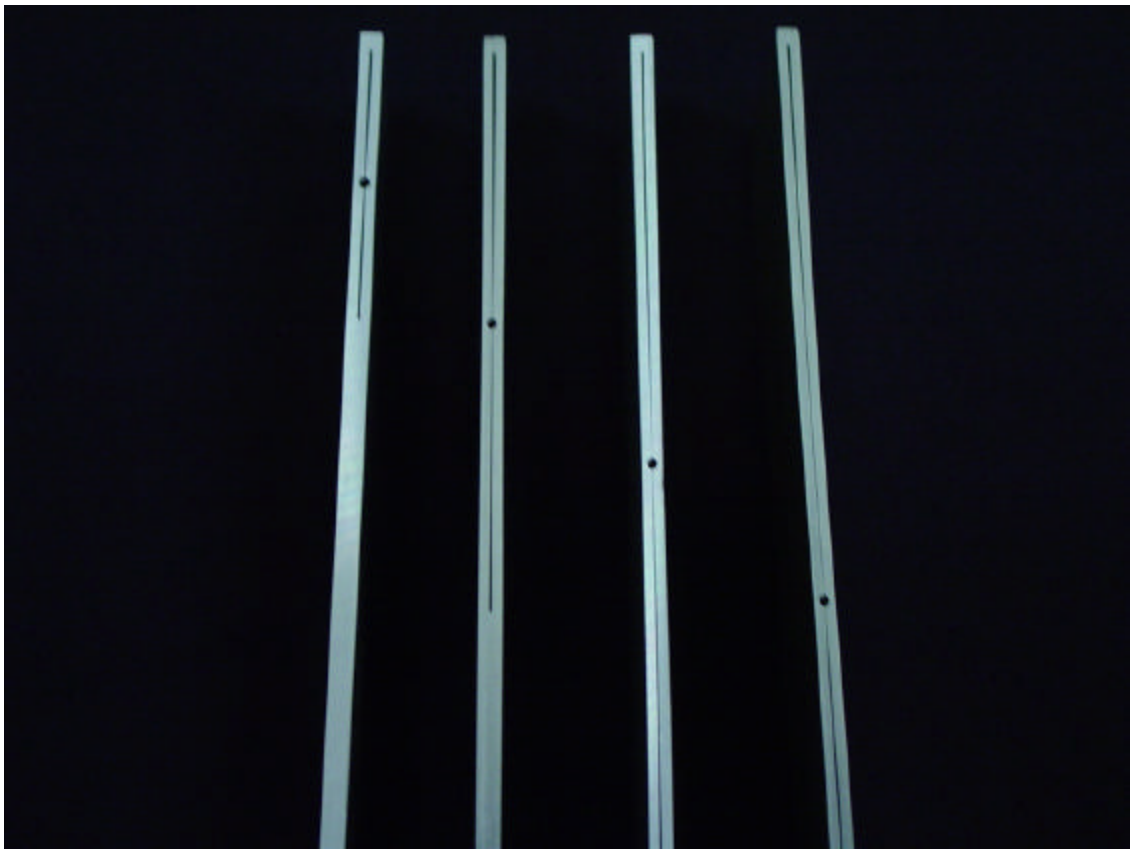

Figure 16. Residual Stress Effects of Cold Working on Beams with Notches at the Free End.

eliminate the beam warping if possible. Initial consideration was given to thermally de-stressing the beams, as is typically done with titanium and steel. However, the temperatures required to stress-relieve aluminum, typically greater than 650° F, exceed the threshold where mechanical properties remain unchanged (Armao, 1999:6). Another method considered for stress alleviation in the aluminum beams was stretch-strain relieving. In this process, the aluminum is strained by approximately 0.75% in an effort to reduce the inhomogeneous plastic deformation throughout the cross-section (Nicholas, 2003). From basic material mechanics, the strain e of a material satisfies the relation

$$e = \frac{s}{E} \tag{60}$$

where E is the modulus of elasticity and s is the axial tensile stress. Since the strain percentage is desired to be 0.75, meaning $e = 0.0075$, and using the 2024 T3 aluminum modulus of E=10.6 x 10^6 psi in Eq. (60), the required applied stress to strain-relieve the specimens is $s = 79{,}500$ psi. This value far exceeded the 20,000 psi limit of the AFIT machine shop stress equipment. A final approach to relieving the test beam stresses was to choose a different temper of aluminum and remanufacture some of the pieces.

Since the considered MATLAB algorithm is written such that the constitutive properties and mass density of the material need only be considered during analysis, an alternative 2024 aluminum temper could be utilized for additional specimen fabrication. Aluminum 2024 O was therefore chosen as the suitable substitute to 2024 T3. The 2024 designation means that the copper alloy percentages are the same in each alloy grade and hence the constitutive properties (which are alloy dependent) remain unchanged. The "O" temper designation indicates the aluminum was post-processed by annealing and recrystallization only, meaning post-fabrication work had not been done on the aluminum and therefore residual stresses were absent.

The aluminum 2024 O was used to remanufacture the 20-cm and 24-cm notched specimens, as well as to recreate the 4-beam test set with notches at the cantilevered end (both for comparative purposes with the 2024 T3 as well as to obtain the 8-cm specimen mismanufactured in the initial test series). The resulting specimens were stress-free, as can be seen from Figure 17 and particularly evident in Figure 18, which is a comparison of the 24-cm notched specimens manufactured from 2024 T3 and 2024 O. An

enlargement of the notched regions of the two specimens in Figure 18 is shown in Figure 19. With the addition of the six 2024 O test beams to the original set of 12 usable 2024 T3 beams, the total test array grew to 18 specimens. These aluminum beams served as the basis for studying damage identification through modal vibration analysis and for evaluation of the MATLAB and ABAQUS natural frequency prediction accuracies.

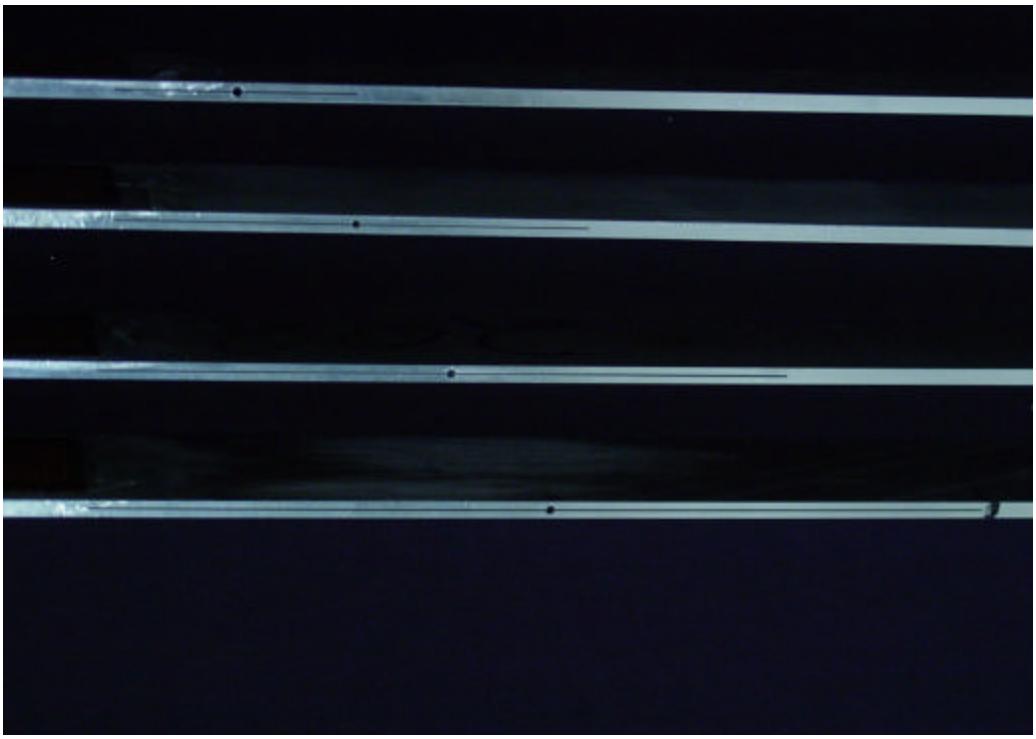

Figure 17. Aluminum 2024 O Specimens with Notches at the Clamped End.

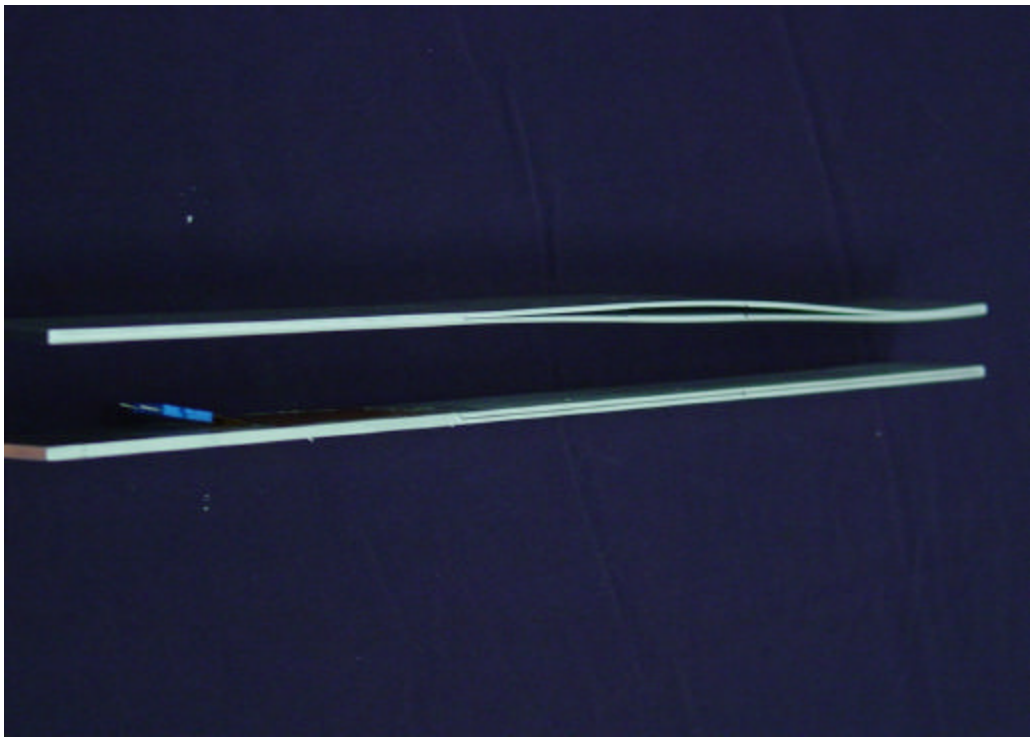

Figure 18. Comparison of 24-cm Notched Specimens (2024 T3 above; 2024 O below).

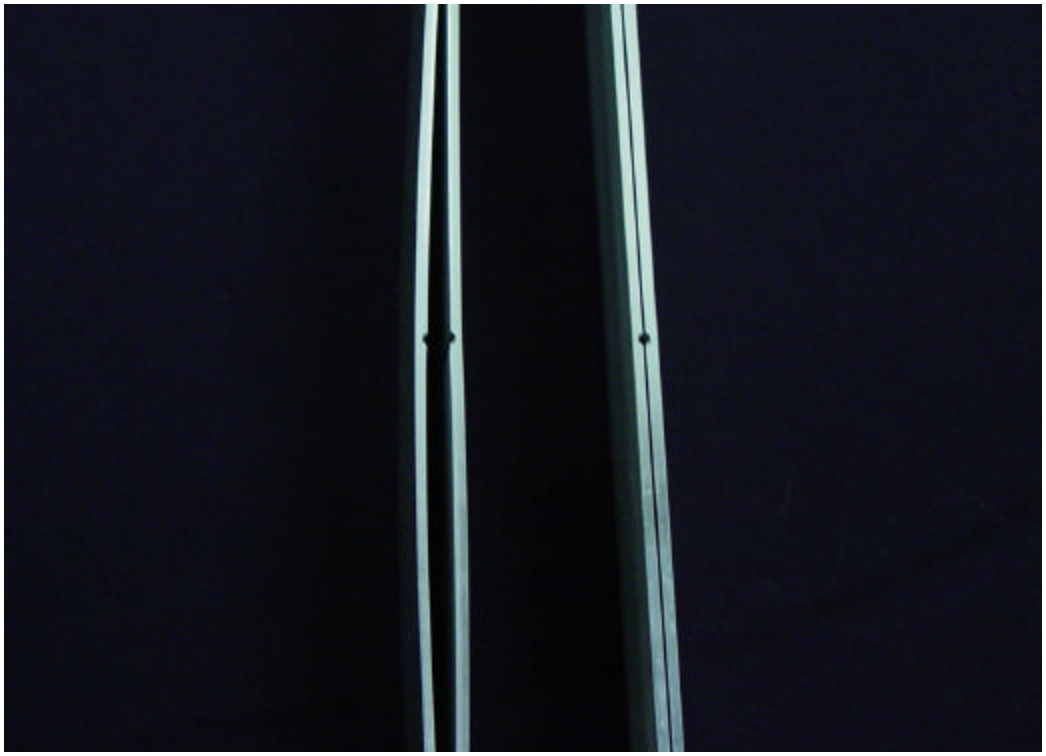

Figure 19. Enlargement of Notched Regions of 24-cm Notched Beams (2024 T3 left; 2024 O right).

Piezoelectric Transducer (PZT) Application

The vibrational excitation of the test specimens was accomplished via a piezoelectric strain actuator (see Figure 20) mounted on the surface of the beam near the cantilever base, as prescribed by Perel and Palazotto (2002) and diagrammatically shown in Figure 6. The proper application of the actuator was of highest importance for accurate excitation results and modal values. Figures 21-a through 21-l depict the PZT application process. The procedures were outlined in similar fashion in the accompanying documentation provided with the M-Line M-Bond Application Kit.

Piezoelectric actuators were affixed to all 18 test specimens in the prescribed way. Special care was taken to ensure that the long PZT edge remained parallel to the beam edge, as tilted application could result in decreased resonant signatures.

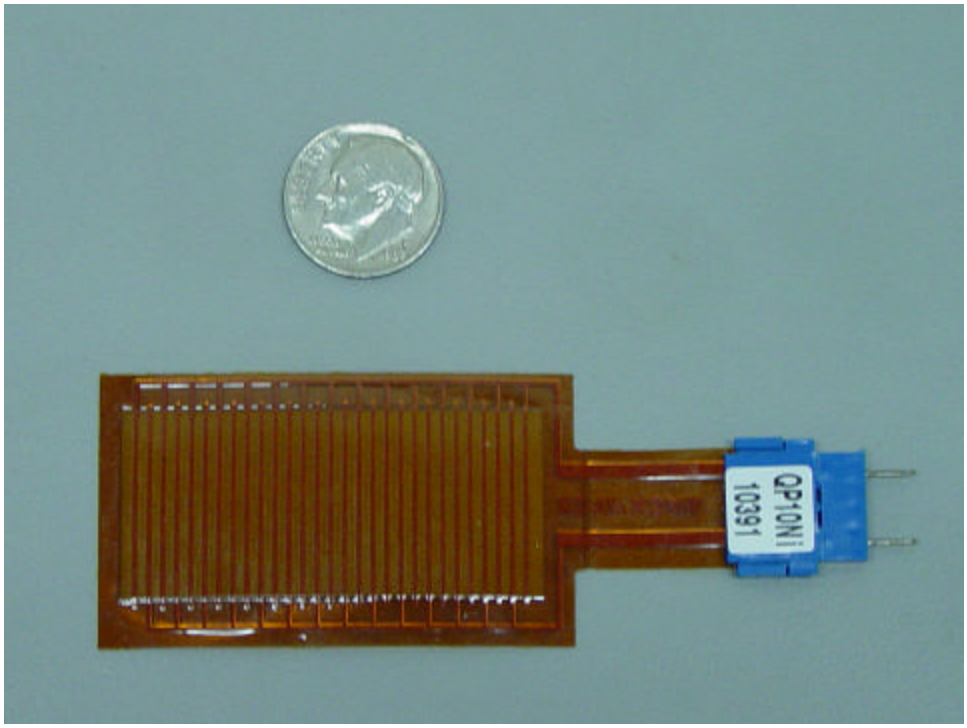

Figure 20. Quick Pack QP10Ni Strain Actuator Used for Vibrational Excitation.

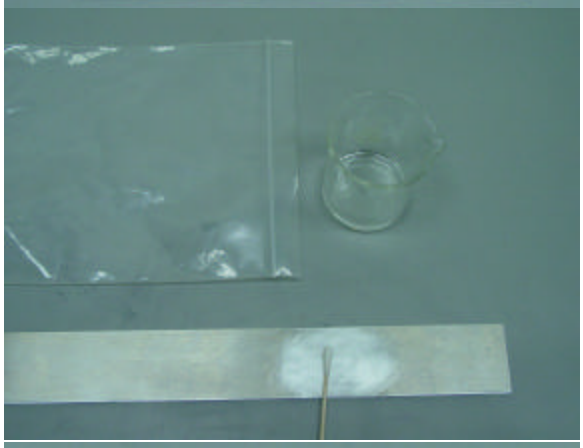

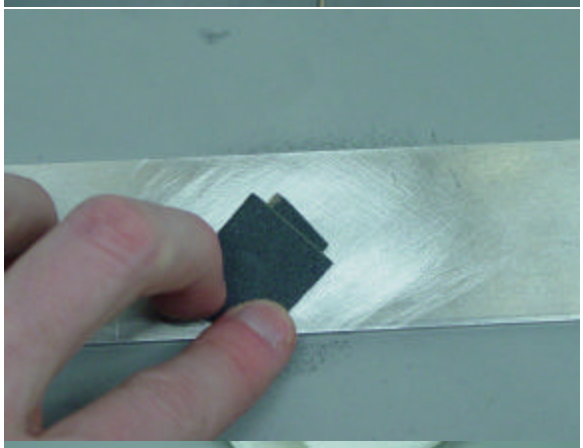

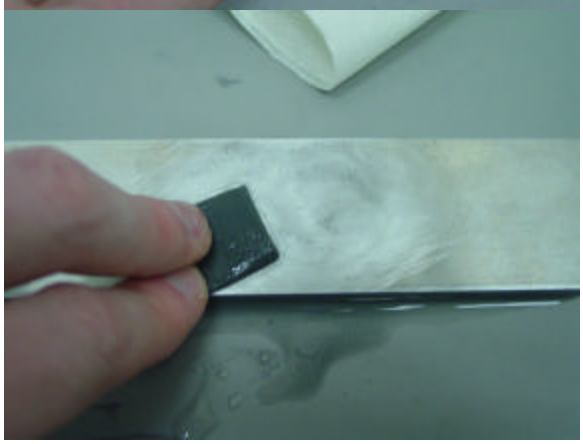

Figures 21-a through 21-l. PZT Application Process.

Figure 21-a. Equipment Required for PZT Application. From top-left to bottom right: 220-grit sandpaper, 400-grit sandpaper, ethyl alcohol, scotch tape, hand clamp, clamping block, cotton swabs, PZT actuator, M-Bond 200 adhesive, M-Prep Conditioner A, M-Prep Neutralizer 5A, Catalyst C, test specimen.

Figure 21-b. Degreasing. Application area thoroughly degreased using a cotton swab and ethyl alcohol.

Figure 21-c. Dry Abrasion. Area dry-abraded twice using 220-grit sand paper. Residue wiped away with clean cloth.

Figure 21-d. Wet Abrasion. Area wet-abraded twice using M-Prep Conditioner A. Liquid and residue wiped away in one motion and in one direction using clean cloth (to avoid redeposit of abraded material).

Figure 21-e. Clean with Conditioner A. M-Prep Condition A applied to area and wiped with cotton swabs repeatedly until swab comes out clean. Area wiped once with clean cloth.

Figure 21-f. Neutralize. M-Prep Neutralizer 5A thoroughly applied to area with cotton swab. Area wiped once with clean cloth.

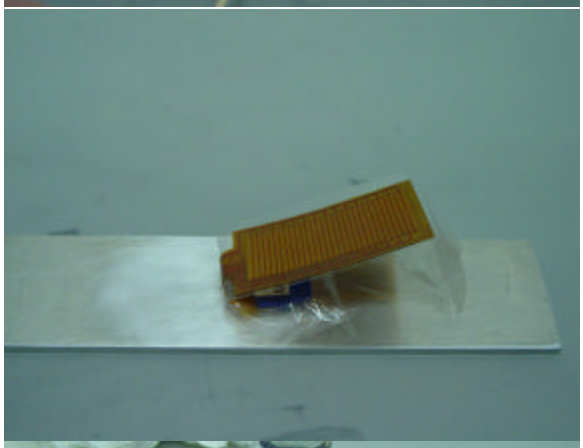

Figure 21-g. PZT Placement. PZT picked up using scotch tape (to avoid finger prints on application side) and positioned as desired on freshly abraded area. Tape folded back to reveal underside of patch. Underside cleaned with ethyl alcohol using a cotton swab.

Figure 21-h. Catalyst Applied. To underside of PZT, Catalyst C applied to accelerate bonding process.

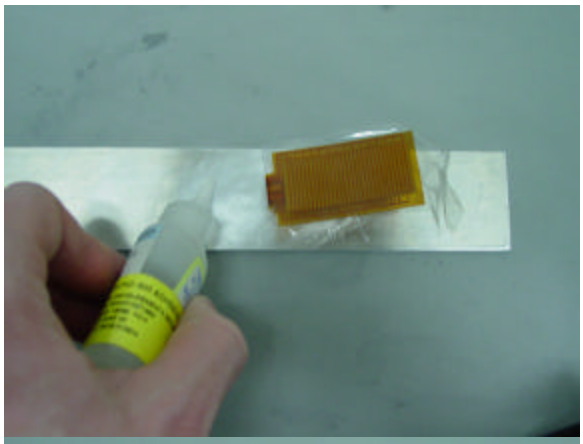

Figure 21-i. Application of Bonding Agent. M-Bond 200 squeezed onto specimen surface in thin, parallel lines to ensure complete coverage of the underside of PZT.

Figure 21-j. PZT Placement and Clamping. PZT immediately folded over and visually checked for complete coverage of M-Bond 200 on bottom surface. Excess bonding agent is squeezed out from under PZT and wiped away. Clamp used to ensure constant pressure throughout drying time. Aluminum block diffuses pressure over entire PZT and alleviates direct contact between clamp teeth and actuator. Allowed to set for 15 minutes.

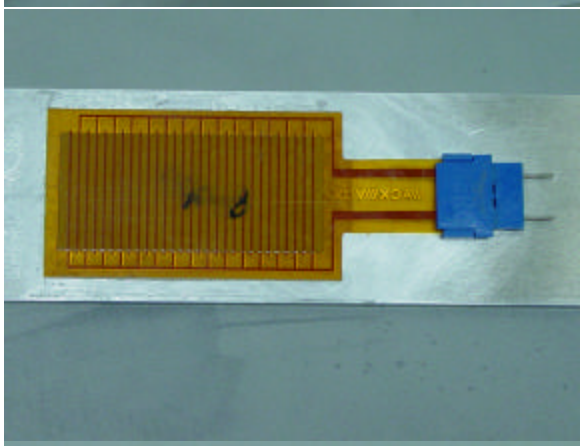

Figure 21-k. Final Product. Final view of test specimen with attached PZT after scotch tape removed.

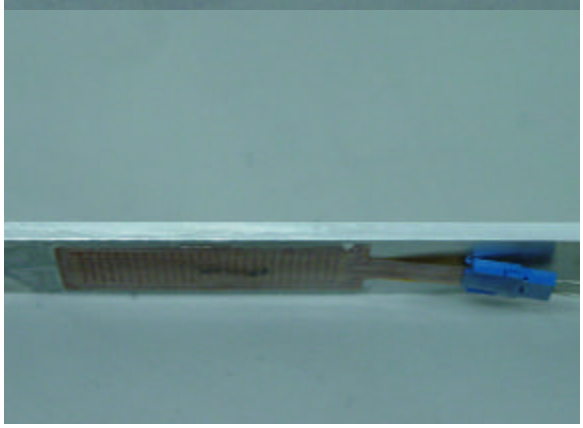

Figure 21-l. Final Product—Side View. Side view of final product. Ensured universal adhesion of all areas of actuator.

Laser Vibrometry Setup and Procedure

Once all aluminum test specimens were fabricated and PZT actuators attached, the experimental analysis could begin. Originally it was desired to measure the modal response of each beam 3 times to obtain an average driving frequency for each of the 8 tested modes—thereby yielding a total of 54 separate vibration tests for the 18 test specimens. However, it was later found that better results were obtained if the first four modes were tested followed by a test for modes five through eight. Therefore, each beam was tested six times: three times for modes 1-4 and three times for modes 5-8, then the average modal frequency of the three tests for each given mode was calculated and considered to be the excitation frequency for that respective mode. In all cases, the three experimentally-obtained resonant frequency values for a given vibration mode deviated from the calculated mean by no more than 1%, and in most cases the deviation was less than 0.5%. In all, a total of 108 separate tests were run. All tests followed the same test procedure as outlined in this section.

Hardware Arrangement.

A clear test area was chosen in the lab where no foreign objects could impact the laser line-of-sight from the scanning laser head. All connections were ensured proper on the computer hardware as well as the scanning head, and the scanning head positioned normal to shaker table area where specimen actuation would take place. A signal cable was run from the signal output node on Generator 1 of the junction box to the input jack of the ACX amplifier. Switches on the amplifier were set to a voltage limit of 200V and a current limit of 200mA. Another signal cable was connected from the output jack of

the amplifier to a set of alligator clips that would later attach to the prongs of the piezoelectric actuator.

The clamping end of the test specimen was placed behind the mounting brackets of the NRC clamp (taking care not to crush the tab of the PZT) and the cap screws finger tightened. As mentioned by several authors in the literature, proper end conditions are of primary importance for accurate results, therefore special care was taken to ensure constant clamping pressure across the brackets. Each bracket was visually inspected for an improper clamping arrangement (Figure 22), and if found, was corrected for good contact, as shown in Figure 23. All cap screws were then tightened evenly using an allen wrench. The final assembly, including the specimen, clamp, stand, and magnetic base is shown in Figure 24.

The assembly was then placed on the appropriate area of the shaker table and the magnetic base switch turned to the "on" position. The ACX amplifier was placed near the assembly on a foam pad (to attenuate vibrations from its internal cooling fan to the table) and the alligator clips leading from the signal output jack connected to the prongs of the PZT. The alligator clip wires were rested on the clamp in such a way so as to not dangle from the PZT tab, which could sway and induce vibrations into the beam. The laser vibrometer scanning head was then turned on and centered on the aluminum beam, ensuring that the reference position of the laser coincided with the centerpoint of the active area of the specimen. Through the PSV software, a visual verification of the perpendicularity of the aluminum beam with the scanning head was accomplished using the viewport of the image receiver. Once all adjustments were made, the final setup resembled Figure 25. A dark cloth was added as a backdrop to the test area for contrast

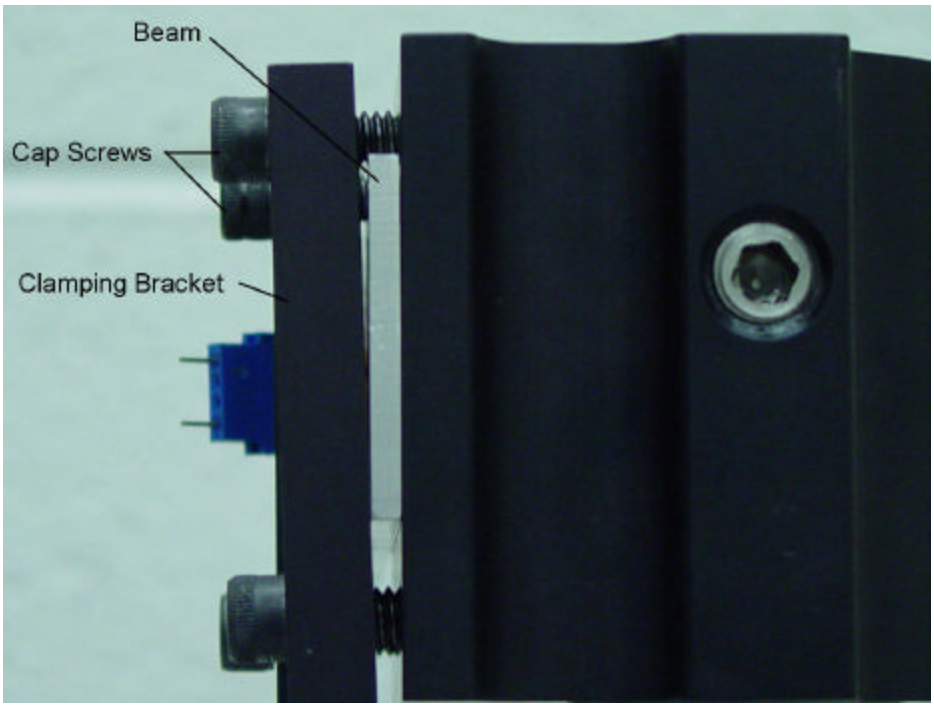

Figure 22. Improper Clamping of Test Specimen. Note Skewed Bracket in Foreground (viewed from cantilevered end).

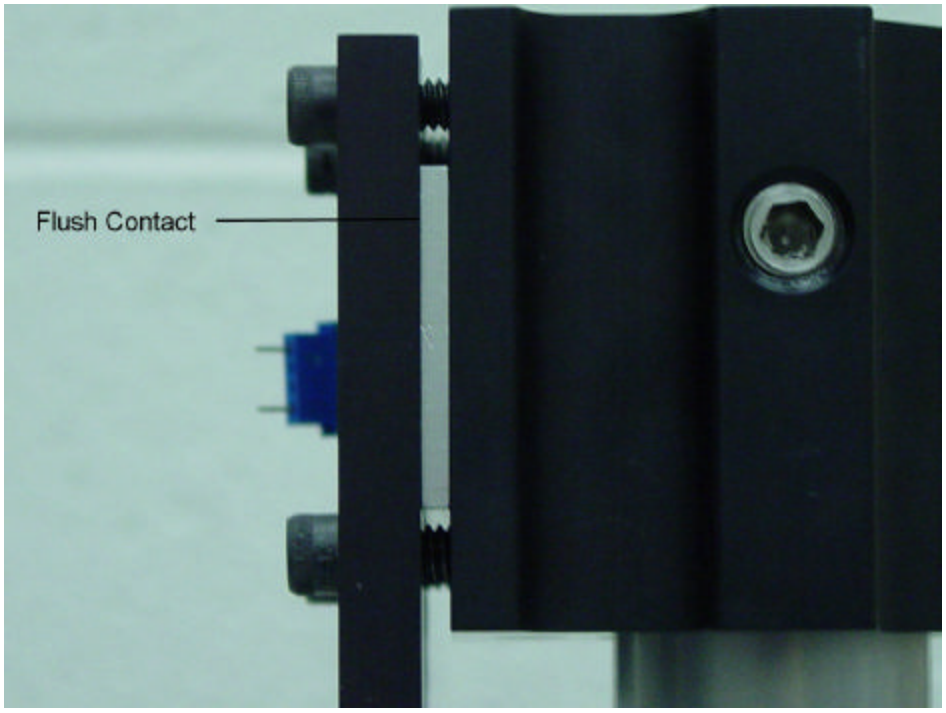

Figure 23. Proper Clamping of Test Specimen (viewed from cantilevered end).

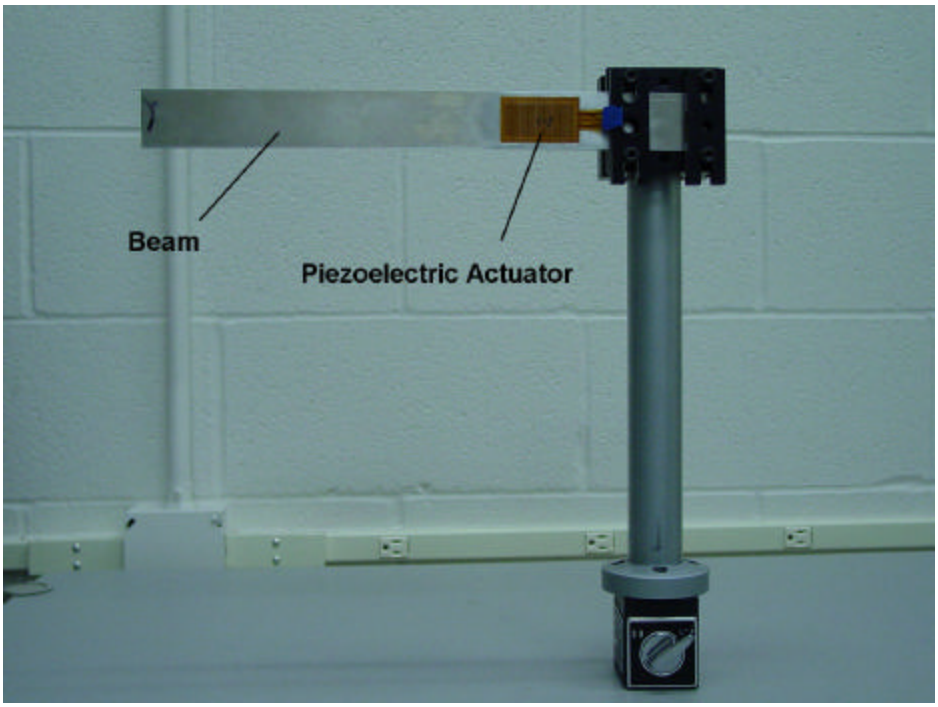

Figure 24. Final Assembly Including Test Specimen.

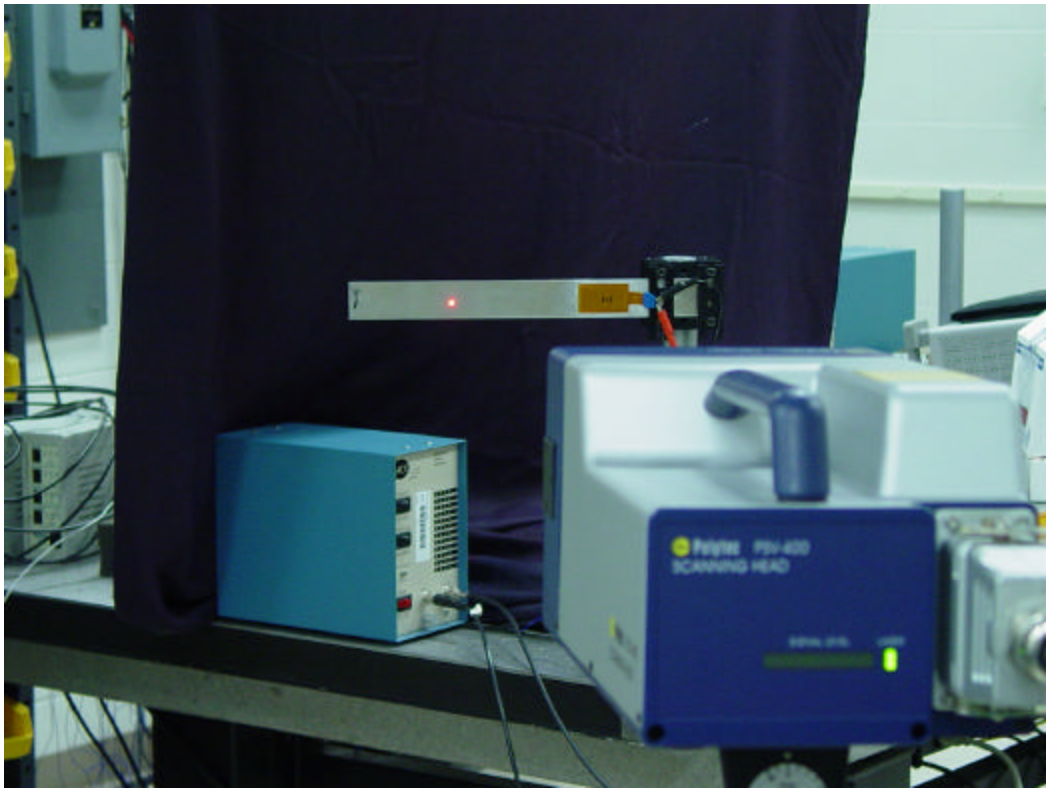

Figure 25. Laser Vibrometer Scanning Head Positioned Perpendicular to Test Beam Apparatus.

enhancement, and during actual testing the laboratory lights were dimmed to reduce luminous noise.

Software Preparation.

Using the scan point centered on the test beam, an alignment plane was fashioned by taking reflective intensity readings at various points along the test surface, thereby informing the software of the location of the test surface in 3-D space. A scanning grid was then superimposed over the digital image of the beam to include all active regions of the cantilever (minus the area covered by the actuator). For adequate measurement of eigenvalues and eigenvectors, this grid was chosen to have a density of 6 scan points across the width of the beam and 14 scan points along the length, for a total of 84 scan points on the beam surface (see Figure 26).

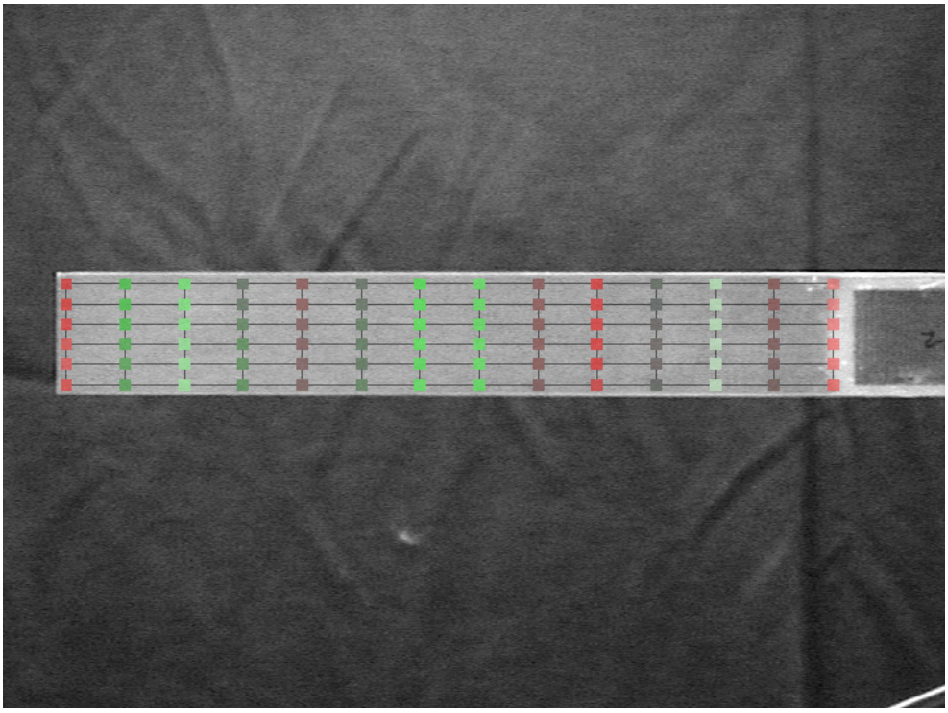

Figure 26. 6x14 Scanning Point Grid Density on Cantilevered Test Specimen.

Other internal software options for data acquisition (chosen from the Acquisition tab) were set as follows:

General:
Acquisition Mode: FFT (Fast Fourier Transform)
Averaging: Complex
No Remeasure

Frequency: 1.25 kHz or 5 kHz
[1.25 kHz setting used for measuring modes 1-4; 5 kHz used for modes 5-8]

Window: Rectangle

Trigger: Source off

Vibrometer:
Velocity: 25 mm/s/V
Tracking Filter: slow

Generator: Pseudo-random
Amplitude: 2
Steady State: 5 sec.
Offset: 0

Once all settings were chosen, data acquisition could commence after selecting a file in which to store the data. Upon test onset, the computer sent a series of repeated actuation signals through the amplifier to the PZT and the surface velocity of the test beam was measured via the vibrometry theory explained in Chapter II. The Polytec software correlated the excitation frequencies with the associated velocity readings for each scan point over time, and from this information produced an average velocity response function over the tested frequency bandwidth from which eigenvalues could be extrapolated at the resonant peaks (see Figures 27 and 28). This process was repeated six times for each beam (as explained previously, three times at driving frequencies ranging from 0 to 1.25 kHz to obtain vibration modes 1-4, and three times at frequencies ranging

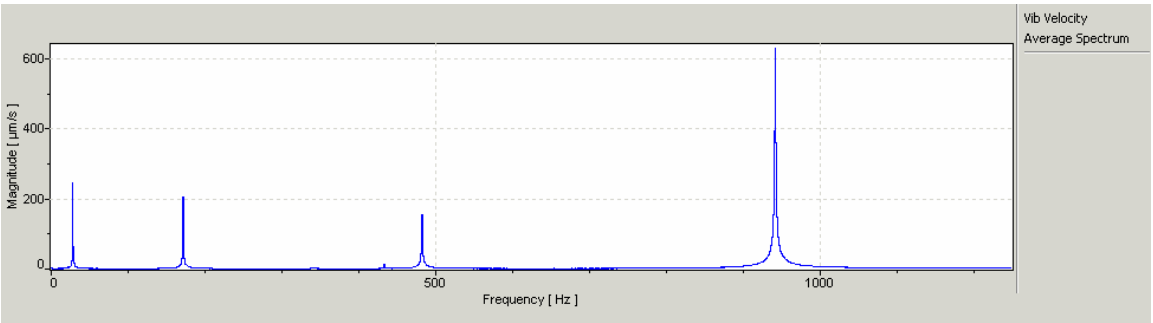

Figure 27. Resonant Peaks Indicating 1st Through 4th Modal Actuation Frequencies for the Notchless Beam Case (Bandwidth: 0 to 1.25 kHz)

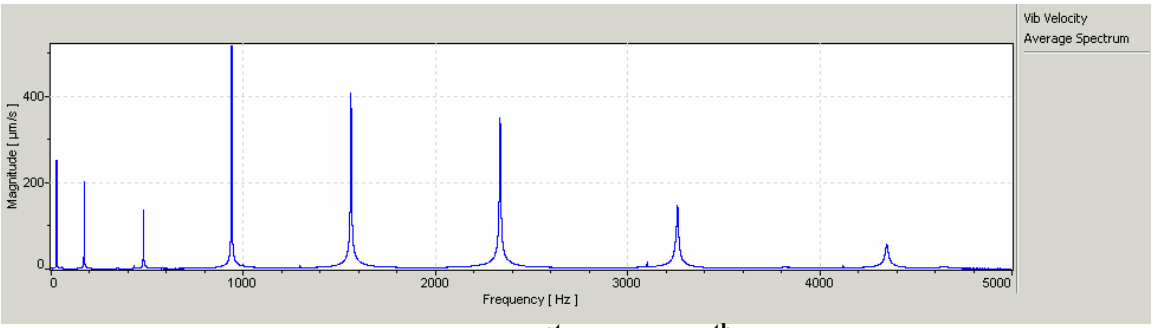

Figure 28. Resonant Peaks Indicating 1st Through 8th Modal Actuation Frequencies for the Notchless Beam Case (Bandwidth: 0 to 5 kHz)

from 0 to 5 kHz to obtain the remaining 4 modes). A 1.25 kHz reading and a 5 kHz reading were done sequentially, then the beam loosened and reclamped for the next pair of readings in an effort to average the effects of the end condition. All 18 beams were tested in this manner, and the resulting data used for comparison with the predictions generated by the MATLAB and ABAQUS FE programs.

IV. Experimental Results and Analysis

In this chapter, the experimental results obtained in the laboratory from all beam specimens are analyzed for frequency degradation trending based on notch location, notch size, and vibration mode, as well as compared to the frequency output predicted by the MATLAB FE program developed by Perel and Palazotto (2002), the frequencies predicted by the ABAQUS FE modeling program, and elementary beam theory (in the notchless case). Also, the vibrational test results for delaminated beams published by Mujumdar and Suryanarayan (1988) are compared to the MATLAB predictions for several scenarios. Ultimately, a determination is made as to whether notch locations, sizes, and effects on vibration modes are decidedly interrelated, and whether the MATLAB and ABAQUS FE programs accurately characterize experimental results for notched cantilevered beams.

Control Specimen—Notchless Beam Case

Following the cantilever beam theory outlined in Chapter II, the theoretical eigenvalues for a notchless 12"x 1½"x 1/8" aluminum specimen were calculated using Eq. (34) and the coefficients from Table 3. Setting $E = 10.6 \times 10^6$ psi = 73.084 GPa, $I = \frac{bh^3}{12} = \frac{(1.5")(1/8")^3}{12} = 2.44 \times 10^{-4}$ in^4 = 1.0×10^{-10} m^4, $m = 0.225\text{lb}_\text{m} = 0.102$ kg, and $L = 12$ in = 0.3048 m, the first eight natural frequencies were calculated. The obtained theoretical frequencies hold for both 2024 T3 and 2024 O aluminum since the Young's modulus changes negligibly and the mass, the second moment of inertia, and the length are constant.

Table 4. Comparison of Theoretical Modal Frequencies vs. Experimental Frequencies for 2024 T3 Notchless Specimen.

MODE	Theory (Hz)	Experiment (Hz)	? (%)
1	28.37	28.09	-0.99
2	177.78	172.43	-3.01
3	497.68	484.10	-2.73
4	975.53	944.80	-3.15
5	1612.45	1565.67	-2.90
6	2408.85	2342.00	-2.78
7	3364.22	3267.67	-2.87
8	4479.16	4359.33	-2.68

Experimentation compared well with theory. Using the laser vibrometer and cantilever setup outlined in Chapter III, the natural frequencies of the notchless 2024 T3 test specimen were obtained. Table 4 lists these results along with an error percentage from theory. Note the percentage difference of experiment from theory is approximately 3% in all but the first mode, thereby validating the experimental setup and clamped end condition as adequate for vibrational analysis for all modes. This percentage offset was later found to be essentially the same for the comparison of the notched specimens for both the T3 and O tempers (ref. Table 14 later in the chapter), where the notched beams containing residual stresses displayed modal frequencies consistently ~3% below the notched beams bereft of residual stresses.

Modal frequency results from ABAQUS also agreed well with theory for the notchless specimen case. Modeling a 12-inch aluminum beam specimen with a fixed end condition and meshing the part using 1,500 8-noded 3-D brick elements resulted in modal frequency values deviating only 1% from the theoretical values, as shown in Table 5.

Table 5. Comparison of Theoretical Modal Frequencies vs. ABAQUS Results for Notchless Aluminum Specimen.

MODE	Theory (Hz)	ABAQUS (Hz)	? (%)
1	28.37	28.63	0.92
2	177.78	179.24	0.82
3	497.68	501.93	0.85
4	975.53	984.31	0.90
5	1612.45	1628.50	1.00
6	2408.85	2434.00	1.04
7	3364.22	3399.50	1.05
8	4479.16	4522.60	0.97

Finally, the theoretical frequencies were evaluated against the MATLAB output for the notchless beam case. To characterize the notchless condition, the endpoint coordinates in the input field of the program were offset by an extremely small margin to avoid the zero condition (which causes singularities in the sub-file calculations as the program is executed). Four separate trials for the notchless case were considered, respectively having a 20-element mesh, a 40-element mesh, a 100-element mesh, and a 200-element mesh. Using the technique explained in Appendix A, the correct modal frequency values were isolated from the MATLAB results, yielding excellent agreement with theory and close agreement with experimentation (see Tables 6 and 7). The 200-element mesh required excessive memory usage and caused MATLAB to stop responding. The 200-element mesh was therefore not used.

Employing the 3% adjustment for residual stresses being present in the test beam brought the MATLAB results from Table 7 much closer to the experimental frequencies, as can be seen in Table 8. It is therefore evident that the MATLAB program developed

Table 6. MATLAB Frequency Results vs. Theory for 20-, 40-, and 100-Element Meshes.

MODE	Theory (Hz)	MATLAB (Hz)			Deviation from Theory		
		20-elem.	40-elem.	100-elem.	$?_{20}$ (%)	$?_{40}$ (%)	$?_{100}$ (%)
1	28.37	28.60	28.49	28.25	0.81	0.42	-0.42
2	177.78	177.56	177.72	177.11	-0.12	-0.03	-0.38
3	497.68	494.61	496.23	494.88	-0.62	-0.29	-0.56
4	975.53	966.74	970.55	969.60	-0.90	-0.51	-0.61
5	1612.45	1599.04	1603.29	1604.76	-0.83	-0.57	-0.48
6	2408.85	2395.31	2396.42	2395.12	-0.56	-0.52	-0.57
7	3364.22	3353.47	3350.19	3328.50	-0.32	-0.42	-1.06
8	4479.16	4465.63	4460.65	4419.84	-0.30	-0.41	-1.32

Table 7. MATLAB Frequency Results vs. Experimental Results for 20-, 40-, and 100-Element Meshes.

MODE	Exp. (Hz)	MATLAB (Hz)			Deviation from Exp.		
		20-elem.	40-elem.	100-elem.	$?_{20}$ (%)	$?_{40}$ (%)	$?_{100}$ (%)
1	28.09	28.60	28.49	28.25	1.82	1.42	0.57
2	172.43	177.56	177.72	177.11	2.98	3.07	2.71
3	484.10	494.61	496.23	494.88	2.17	2.51	2.23
4	944.80	966.74	970.55	969.60	2.32	2.73	2.62
5	1565.67	1599.04	1603.29	1604.76	2.13	2.40	2.50
6	2342.00	2395.31	2396.42	2395.12	2.28	2.32	2.27
7	3267.67	3353.47	3350.19	3328.50	2.63	2.53	1.86
8	4359.33	4465.63	4460.65	4419.84	2.44	2.32	1.39

Table 8. MATLAB Frequency Results vs. Experimental Results with 3% Adjustment for 20-, 40-, and 100-Element Meshes.

MODE	Exp. with 3% Adj. (Hz)	MATLAB (Hz)			Deviation from Exp.		
		20-elem.	40-elem.	100-elem.	$?_{20}$ (%)	$?_{40}$ (%)	$?_{100}$ (%)
1	28.93	28.60	28.49	28.25	-1.15	-1.53	-2.36
2	177.60	177.56	177.72	177.11	-0.02	0.07	-0.28
3	498.62	494.61	496.23	494.88	-0.80	-0.48	-0.75
4	973.14	966.74	970.55	969.60	-0.66	-0.27	-0.36
5	1612.64	1599.04	1603.29	1604.76	-0.84	-0.58	-0.49
6	2412.26	2395.31	2396.42	2395.12	-0.70	-0.66	-0.71
7	3365.70	3353.47	3350.19	3328.50	-0.36	-0.46	-1.11
8	4490.11	4465.63	4460.65	4419.84	-0.55	-0.66	-1.56

agrees fully with experimental results, theory, and ABAQUS for the notchless, isotropic beam case.

***Eigenvector Comparison*.**

When obtaining resonant frequencies, it was important to ensure the eigenvalues being considered corresponded to the correct eigenvector associated with the desired mode shape. This was particularly important when using the MATLAB program, which normalized the displacements for all degrees of freedom and therefore required a visual verification of the modal amplitude to obtain the correct eigenvalue for the mode. Figures 29-a through 29-h graphically display the eigenvector comparison between ABAQUS, experimental results, and the MATLAB output (cases shown are results from the notchless beam). For each test comparison across the spectrum of experimental cases, the eigenvalue outputs of the various predictive/experimental methods were matched to a particular eigenvector, and the eigenvectors analyzed to ensure cross-

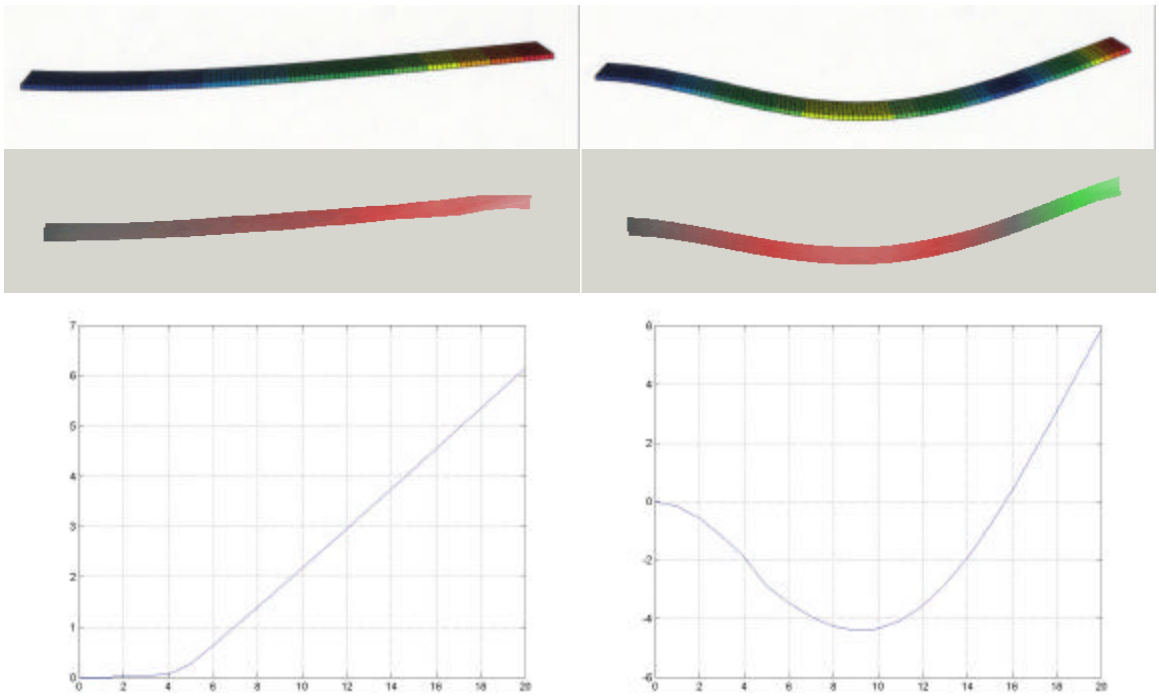

Figure 29-a. Mode 1 Eigenvector Comparison—ABAQUS, Experiment, MATLAB

Figure 29-b. Mode 2 Eigenvector Comparison—ABAQUS, Experiment, MATLAB

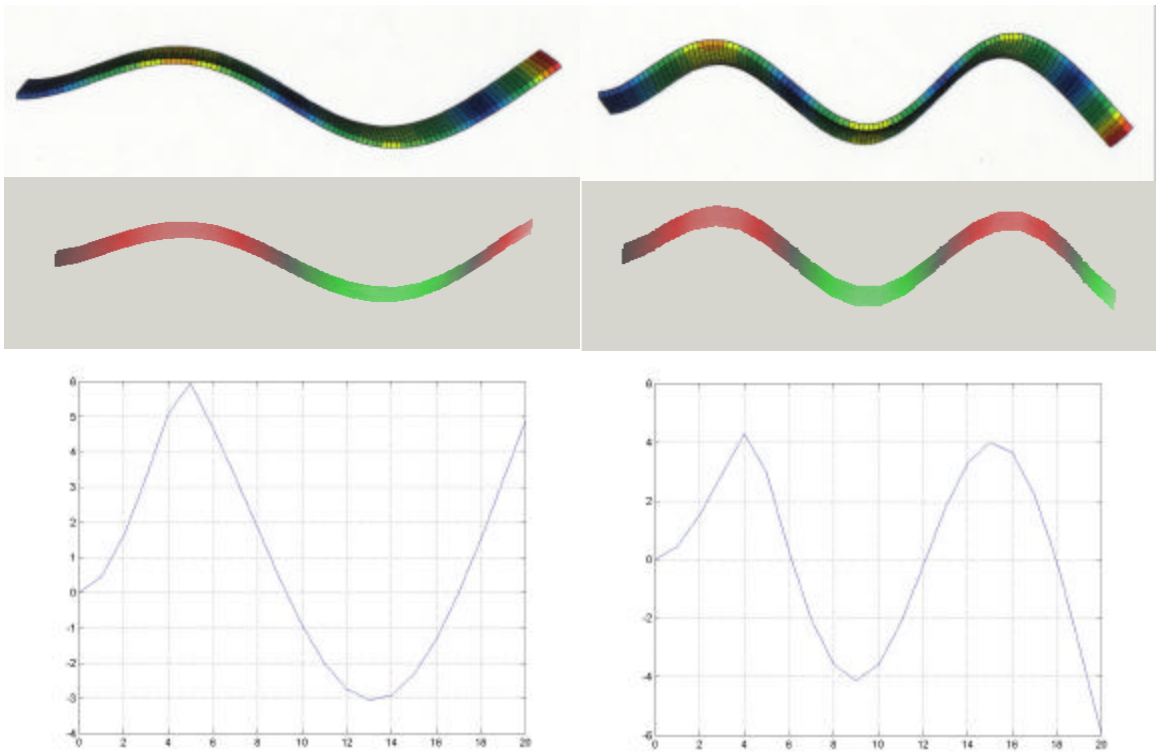

Figure 29-c. Mode 3 Eigenvector Comparison—ABAQUS, Experiment, MATLAB

Figure 29-d. Mode 4 Eigenvector Comparison—ABAQUS, Experiment, MATLAB

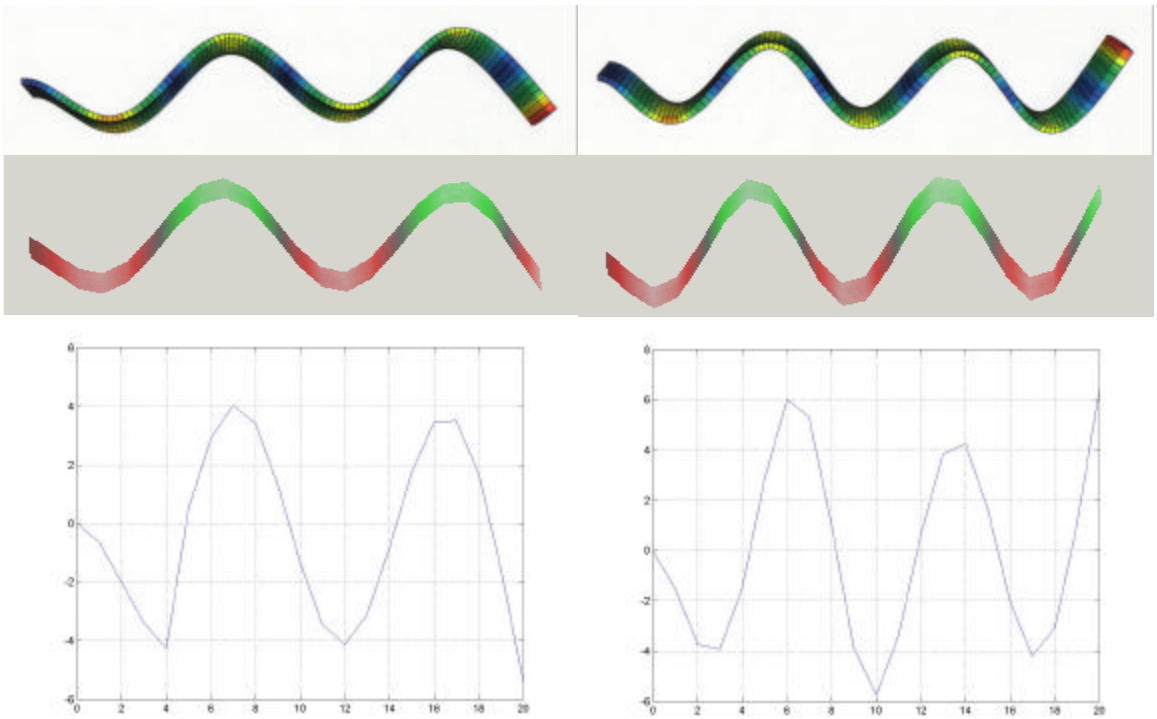

Figure 29-e. Mode 5 Eigenvector Comparison—ABAQUS, Experiment, MATLAB

Figure 29-f. Mode 6 Eigenvector Comparison—ABAQUS, Experiment, MATLAB

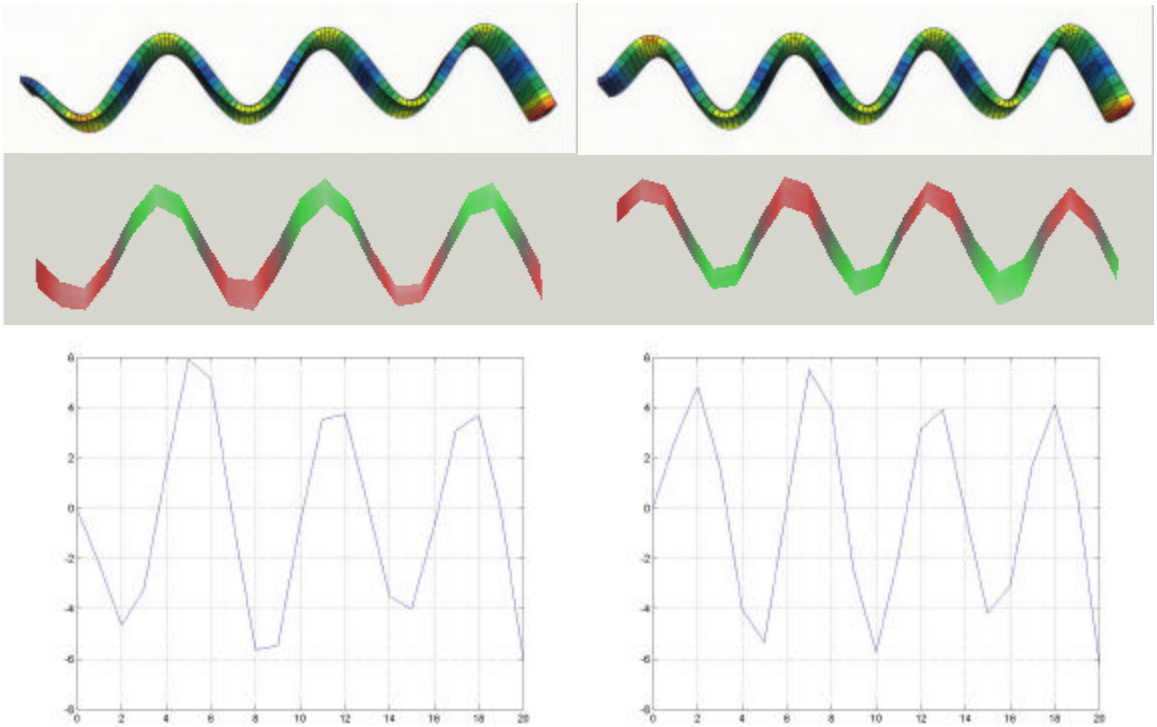

Figure 29-g. Mode 7 Eigenvector Comparison—ABAQUS, Experiment, MATLAB

Figure 29-h. Mode 8 Eigenvector Comparison—ABAQUS, Experiment, MATLAB

comparison of the same modal frequency as is done in the figures. This process confirmed that modal frequency comparison occurred between similar modes, and no spurious data sets were included for non-translational vibrations (such as torsional modes, longitudinal modes, etc.).

Notched Beam Cases—Experimental Results

The series of 2024 T3 aluminum specimens was likewise tested via laser Doppler vibrometry according to the methods previously outlined. This test set included the following, as described in Chapter III—Experimental Specimen Design:

1) Four beams with an included notch propagating from the free end of the cantilever—notch lengths of 4cm, 8cm, 12cm, and 16cm.
2) Four beams with an included notch propagating from the midpoint of the cantilever—notch lengths of 4cm, 8cm, 12cm, and 16cm.
3) Three beams with an included notch propagating from the fixed end of the cantilever—notch lengths of 4cm, 12cm, and 16cm (the 8cm specimen was mismanufactured).

Table 9 lists the modal frequencies obtained for the first eight vibration modes for all test beams, as well as a deviation percentage from the control specimen (notchless beam). Note that, with the exception of the first mode, the percentage deviation from the control specimen increases as the notch length increases. This trend is due to reductions in the flexural rigidity EI of the beam, where E is the elastic modulus and $I = \frac{bh^3}{12}$ for the notchless cross-section, while the centerline-notched cross-section contains

$$I = 2\frac{b\left(\frac{h}{2}\right)^3}{12} = \frac{bh^3}{48} \tag{61}$$

Table 9. Experimental Modal Frequencies and Percent Deviation from Control Specimen for 2024 T3 Notched Beams.

NOTCH SIZE (cm) AND LOCATION		MODAL FREQUENCIES (Hz) Deviation from control values (%)							
		1	2	3	4	5	6	7	8
	4 Free end	28.91 -0.08	175.27 -1.32	471.73 -5.39	931.77 -4.25	1485.00 -7.91	2213.33 -8.25	3116.00 -7.42	4151.00 -7.55
	8 Free End	29.30 1.27	166.93 -6.01	421.63 -15.44	774.33 -20.43	1359.67 -15.69	1779.33 -26.24	2533.33 -24.73	3476.67 -22.57
	12 Free End	29.04 0.36	154.30 -13.12	406.27 -18.52	658.20 -32.36	1090.33 -32.39	1748.33 -27.52	2369.00 -29.61	3084.33 -31.31
	16 Free End	28.26 -2.34	146.77 -17.36	336.60 -32.49	561.47 -42.30	1046.33 -35.12	1535.00 -36.37	2263.67 -32.74	2750.00 -38.75
	4 Middle	27.73 -4.16	170.57 -3.96	456.23 -8.50	899.23 -7.60	1535.67 -4.77	1977.67 -18.02	3053.00 -9.29	3785.67 -15.69
	8 Middle	28.13 -2.77	169.00 -4.84	390.87 -21.61	725.80 -25.42	1283.00 -20.44	1846.67 -23.45	2477.00 -26.40	3483.33 -22.42
	12 Middle	27.47 -5.06	161.33 -9.16	366.13 -26.57	635.70 -34.68	1080.67 -32.99	1729.33 -28.31	2377.67 -29.36	2991.00 -33.39
	16 Middle	26.82 -7.30	152.43 -14.17	324.87 -34.85	577.30 -40.68	1024.33 -36.48	1403.33 -41.82	1982.33 -41.10	2820.33 -37.19
	4 Clamped	27.73 -4.16	169.90 -4.34	474.87 -4.76	965.50 -0.79	1387.33 -13.97	2077.33 -13.88	3092.67 -8.11	3946.33 -12.11
	8 Clamped								
	12 Clamped	25.13 -13.14	146.63 -17.44	369.13 -25.97	682.80 -29.84	1039.33 -35.55	1656.33 -31.34	2289.67 -31.97	2949.00 -34.32
	16 Clamped	24.22 -16.29	137.10 -22.81	300.30 -39.77	563.17 -42.13	1026.00 -36.38	1449.00 -39.93	1977.00 -41.26	2755.67 -38.63

Therefore, flexural rigidity decreases by 75% in the regions containing a centerline notch, which by definition reduces the global stiffness of the beam.

Also of interest is the overall trend of frequency reduction from the control specimen as mode number increases. In general, the higher modes deviate much more from the notchless case than do the lower modes, indicating that the higher modes are much more sensitive to damage inclusions than are the lower modes (see Figures 30, 31, and 32), directly in line with the observations made by Tracy and Pardoen (1988).

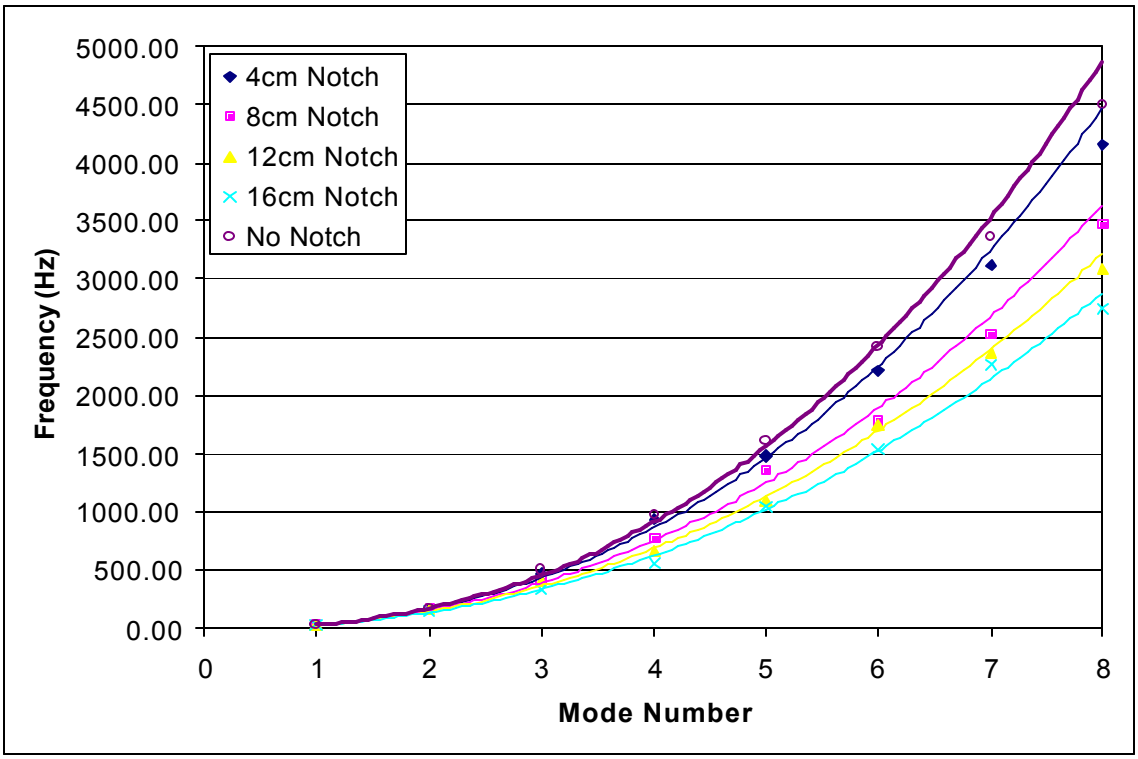

Figure 30. Frequency vs. Mode Number for 2024 T3 Notched Beams--Free End.

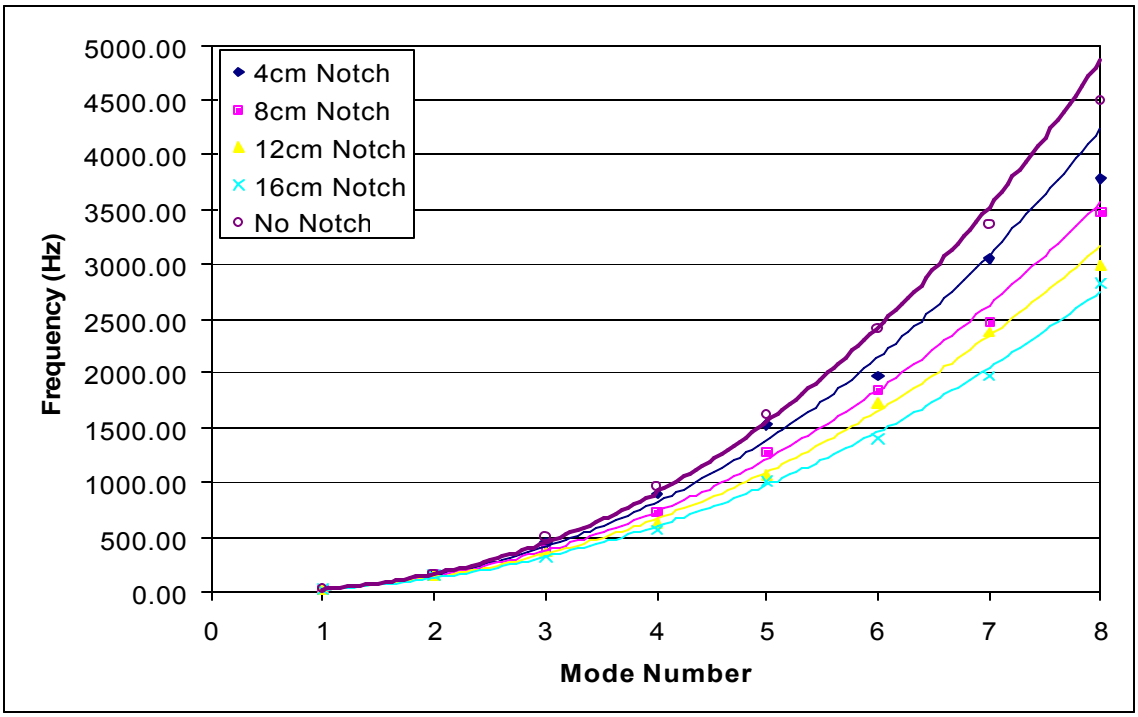

Figure 31. Frequency vs. Mode Number for 2024 T3 Notched Beams--Middle.

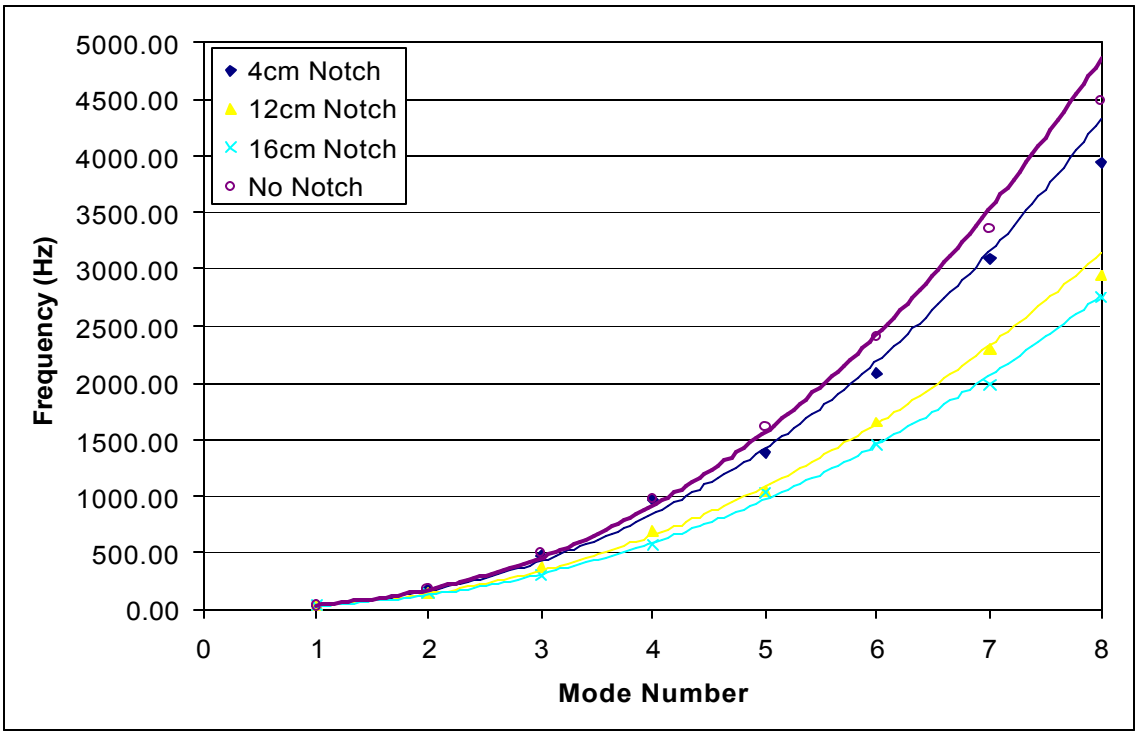

Figure 32. Frequency vs. Mode Number for 2024 T3 Notched Beams--Clamped End (minus the mismanufactured 8cm-notched beam).

Nodal Damage Analysis.

A hypothesis was explored as to whether damage crossing through nodes of modal curvature inflection (i.e. locations where the oscillatory displacements transition from concave-up to concave-down) caused large jumps in modal frequency degradation for a given vibration mode. Since curvature inflection points represent locations of least moment and highest shear, and shear at a free edge must be equal to zero, then a notch crossing through a region of curvature inflection that interrupts the shear flow through the cross-section might have an effect on the dynamics of the beam. Figure 33-a through 33-h show the curvature inflection points and approximate displacements from the cantilevered end for each vibration mode.

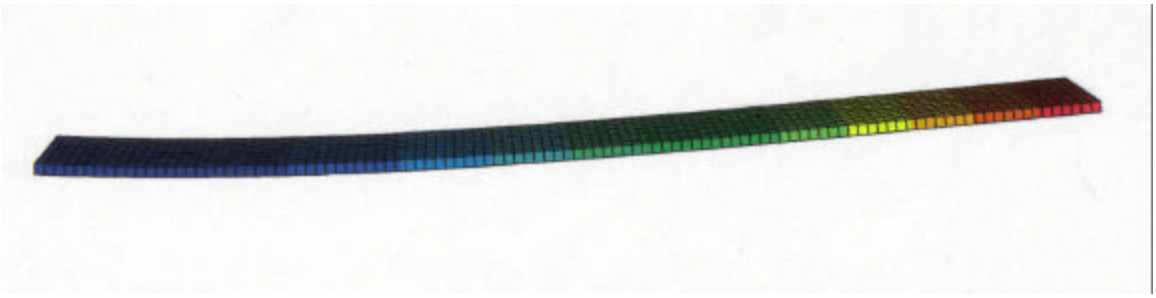

Figure 33-a. 1st Mode of Vibration; No Curvature Inflection Nodes.

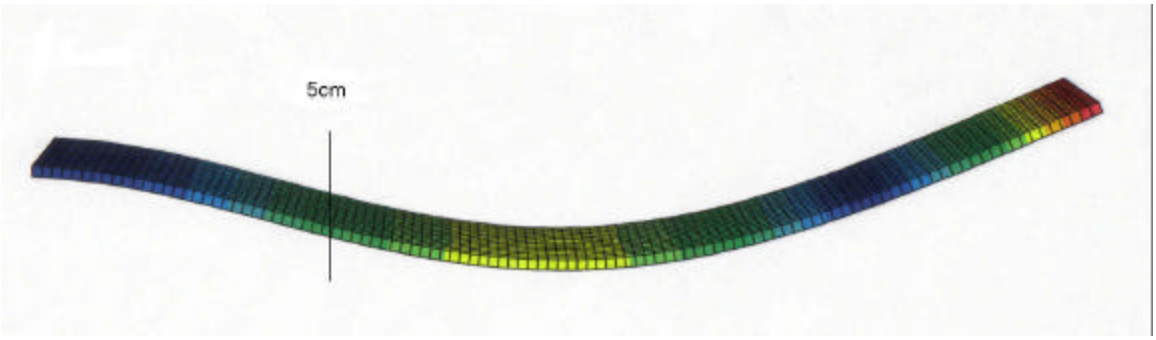

Figure 33-b. 2nd Mode of Vibration; One Curvature Inflection Node.

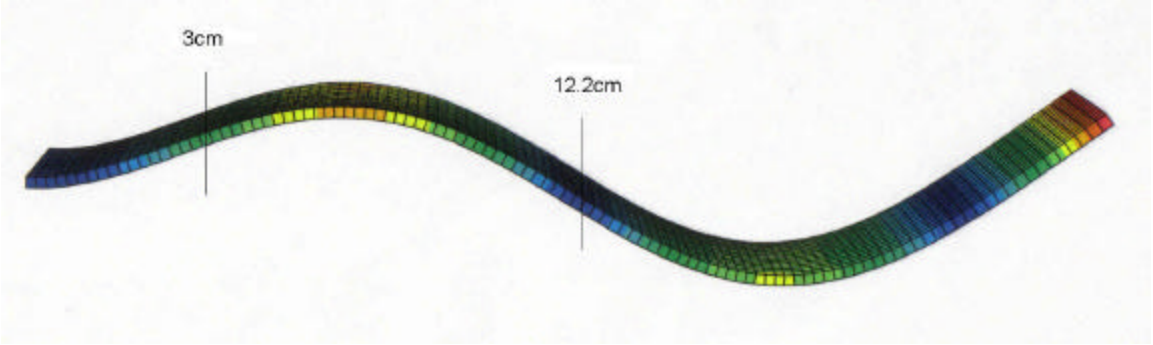

Figure 33-c. 3rd Mode of Vibration; Two Curvature Inflection Nodes.

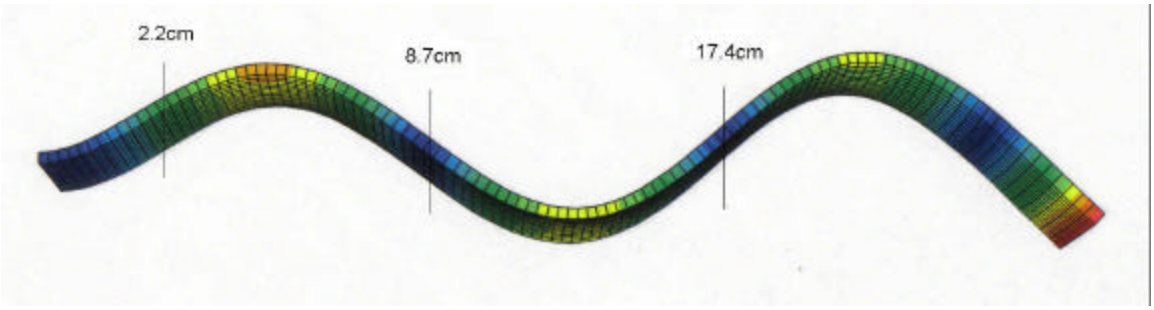

Figure 33-d. 4th Mode of Vibration; Three Curvature Inflection Nodes.

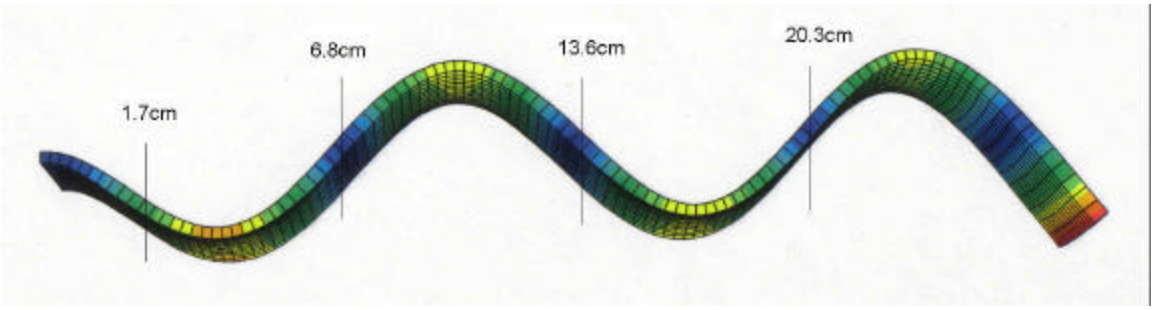

Figure 33-e. 5th Mode of Vibration; Four Curvature Inflection Nodes.

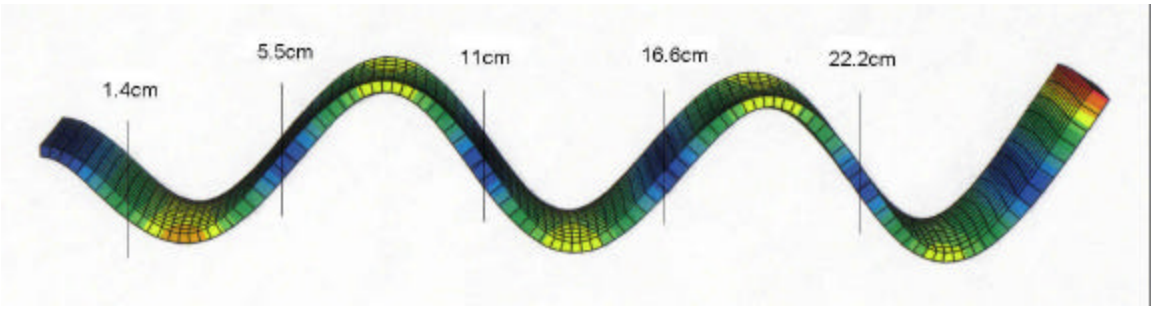

Figure 33-f. 6th Mode of Vibration; Five Curvature Inflection Nodes.

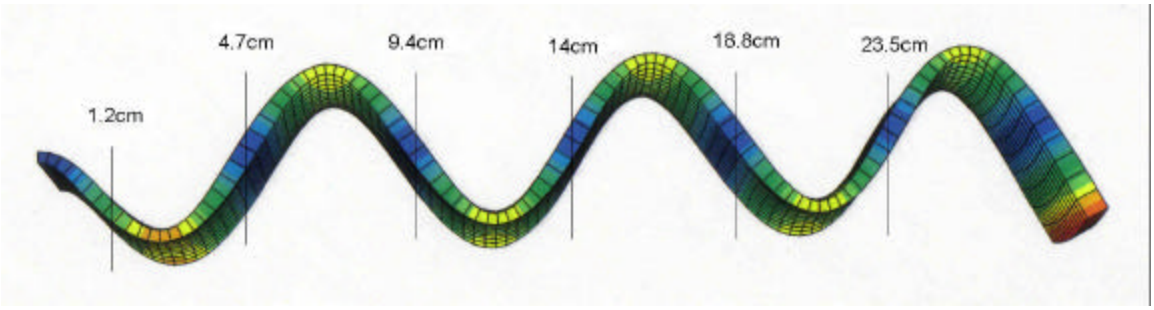

Figure 33-g. 7th Mode of Vibration; Six Curvature Inflection Nodes.

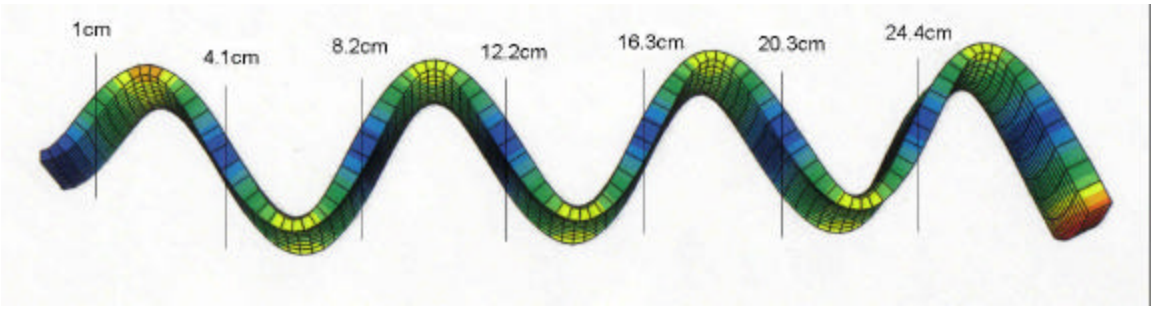

Figure 33-h. 8th Mode of Vibration; Seven Curvature Inflection Nodes.

Table 10 shows modal frequencies for the 2024 T3 notched beams, deviation from the notchless case, and the number of curvature inflection nodes intersected by each notch based on its position and length. For the hypothesis to hold, a large increase in percent deviation from control values should occur for each additional curvature node intersected, and when no additional node is crossed, a minimal frequency drop should be observed. For instance, for the 7th mode, free-end case, as the notch was increased from 4cm to 8cm, one curvature node was crossed and the modal frequency decreased from -7.4% to -24.7%. Similar transitional frequency drops occurred in the 4cm-8cm free-end 8th mode, the 8cm-12cm free-end 5th mode, the 12cm-16cm middle-notch 6th mode, the 12cm-16cm clamped-end 4th mode, etc. Also, a minimal drop in modal frequency is seen in the 12cm-16cm free-end 5th mode case, which does not cross an additional node of curvature even though the shorter notch length before does (and shows the jump in frequency reduction). The same phenomenon is observed across the range of notch lengths for the first and second modes of vibration, as well as various other notch cases throughout the experimental set.

However, several data points disprove the theory as well. The transition from 4cm to 8cm in the middle-notch 4th mode case indicates a large jump of 17.8% in frequency degradation, however no additional curvature node was crossed by the longer notch. This is also the case 12-16cm clamped-end 3rd mode and the 4cm-8cm free-end 4th mode. Similarly, in certain cases an additional curvature node was intersected with no appreciable decline in frequency observed, such as the 8cm-12cm middle-notch 6th mode transition and the 12cm-16cm clamped-end 5th mode transition. Since several areas in the data refute the hypothesis that damage intercepting a region of curvature transition

Table 10. Experimental Modal Frequencies, Deviation from Control Specimen, and Number of Curvature Inflection Nodes Crossed for 2024 T3 Aluminum Beams

NOTCH SIZE (cm) AND LOCATION		MODAL FREQUENCIES (Hz) Deviation from control values (%) Number of curvature nodes crossed							
		1	2	3	4	5	6	7	8
	4 Free end	28.91 -0.08 0	175.27 -1.32 0	471.73 -5.39 0	931.77 -4.25 0	1485.00 -7.91 0	2213.33 -8.25 0	3116.00 -7.42 0	4151.00 -7.55 0
	8 Free End	29.30 1.27 0	166.93 -6.01 0	421.63 -15.44 0	774.33 -20.43 0	1359.67 -15.69 0	1779.33 -26.24 0	2533.33 -24.73 1	3476.67 -22.57 1
	12 Free End	29.04 0.36 0	154.30 -13.12 0	406.27 -18.52 0	658.20 -32.36 0	1090.33 -32.39 1	1748.33 -27.52 1	2369.00 -29.61 2	3084.33 -31.31 2
	16 Free End	28.26 -2.34 0	146.77 -17.36 0	336.60 -32.49 0	561.47 -42.30 1	1046.33 -35.12 1	1535.00 -36.37 2	2263.67 -32.74 2	2750.00 -38.75 3
	4 Middle	27.73 -4.16 0	170.57 -3.96 0	456.23 -8.50 0	899.23 -7.60 1	1535.67 -4.77 1	1977.67 -18.02 1	3053.00 -9.29 1	3785.67 -15.69 1
	8 Middle	28.13 -2.77 0	169.00 -4.84 0	390.87 -21.61 1	725.80 -25.42 1	1283.00 -20.44 1	1846.67 -23.45 1	2477.00 -26.40 2	3483.33 -22.42 2
	12 Middle	27.47 -5.06 0	161.33 -9.16 0	366.13 -26.57 1	635.70 -34.68 1	1080.67 -32.99 2	1729.33 -28.31 2	2377.67 -29.36 3	2991.00 -33.39 3
	16 Middle	26.82 -7.30 0	152.43 -14.17 0	324.87 -34.85 1	577.30 -40.68 2	1024.33 -36.48 2	1403.33 -41.82 3	1982.33 -41.10 3	2820.33 -37.19 4
	4 Clamped End	27.73 -4.16 0	169.90 -4.34 0	474.87 -4.76 0	965.50 -0.79 1	1387.33 -13.97 1	2077.33 -13.88 1	3092.67 -8.11 0	3946.33 -12.11 1
	8 Clamped End								
	12 Clamped End	25.13 -13.14 0	146.63 -17.44 1	369.13 -25.97 1	682.80 -29.84 1	1039.33 -35.55 2	1656.33 -31.34 3	2289.67 -31.97 2	2949.00 -34.32 3
	16 Clamped	24.22 -16.29 0	137.10 -22.81 1	300.30 -39.77 1	563.17 -42.13 2	1026.00 -36.38 3	1449.00 -39.93 3	1977.00 -41.26 3	2755.67 -38.63 4

(and hence changing the shear profile) causes large natural frequency declines, the hypothesis was determined to be incorrect.

Anti-Nodal Damage Analysis.

A similar study was done to determine if damage passing through a region of maximum curvature (and hence maximum normal stress and no shear) had a significant effect on the modal frequencies. Table 11 shows the number of maximum curvature points intersected by each notch of the given length and position. As was the case with the curvature inflection theory, several data points suggested that damage crossing successive regions of maximum curvature reduced resonant frequencies significantly (i.e. the 4cm-8cm free-end 7^{th} mode transition and the 12cm-16cm clamped-end 3^{rd} mode transition), but many other data points disproved the hypothesis (such as the 4cm-8cm middle-notch 4^{th} mode transition where no additional max curvature point was crossed and the 12cm-16cm free-end 5^{th} mode transition where an additional max curvature point was crossed but no appreciable decline in frequency was evident). Therefore, antinodal damage is likewise not shown to be a driving factor behind modal frequency decline. This is quite sensible in that a centerline notch for a region of maximum moment minimally interrupts the normal stress experienced by the cross-section, as the centerline is the neutral axis of the specimen. Should the notch be offset from the centerline, it would more noticeably disrupt the normal stress field of the cross-section and thereby potentially have more of an effect on the frequency response.

Table 11. Experimental Modal Frequencies, Deviation from Control Specimen, and Number of Maximum Deflection Points Crossed for 2024 T3 Aluminum Beams

NOTCH SIZE (cm) AND LOCATION		MODAL FREQUENCIES (Hz) Deviation from control values (%) Number of maximum deflection points crossed							
		1	2	3	4	5	6	7	8
	4 Free end	28.91 -0.08 0	175.27 -1.32 0	471.73 -5.39 0	931.77 -4.25 0	1485.00 -7.91 0	2213.33 -8.25 0	3116.00 -7.42 0	4151.00 -7.55 0
	8 Free End	29.30 1.27 0	166.93 -6.01 0	421.63 -15.44 0	774.33 -20.43 0	1359.67 -15.69 1	1779.33 -26.24 1	2533.33 -24.73 1	3476.67 -22.57 1
	12 Free End	29.04 0.36 0	154.30 -13.12 0	406.27 -18.52 0	658.20 -32.36 1	1090.33 -32.39 1	1748.33 -27.52 2	2369.00 -29.61 2	3084.33 -31.31 2
	16 Free End	28.26 -2.34 0	146.77 -17.36 0	336.60 -32.49 1	561.47 -42.30 1	1046.33 -35.12 2	1535.00 -36.37 2	2263.67 -32.74 3	2750.00 -38.75 3
	4 Middle	27.73 -4.16 0	170.57 -3.96 0	456.23 -8.50 0	899.23 -7.60 1	1535.67 -4.77 1	1977.67 -18.02 1	3053.00 -9.29 1	3785.67 -15.69 1
	8 Middle	28.13 -2.77 0	169.00 -4.84 0	390.87 -21.61 1	725.80 -25.42 1	1283.00 -20.44 1	1846.67 -23.45 2	2477.00 -26.40 2	3483.33 -22.42 2
	12 Middle	27.47 -5.06 0	161.33 -9.16 1	366.13 -26.57 0	635.70 -34.68 1	1080.67 -32.99 2	1729.33 -28.31 2	2377.67 -29.36 3	2991.00 -33.39 3
	16 Middle	26.82 -7.30 0	152.43 -14.17 1	324.87 -34.85 1	577.30 -40.68 2	1024.33 -36.48 2	1403.33 -41.82 3	1982.33 -41.10 3	2820.33 -37.19 4
	4 Clamped End	27.73 -4.16 0	169.90 -4.34 0	474.87 -4.76 1	965.50 -0.79 0	1387.33 -13.97 0	2077.33 -13.88 1	3092.67 -8.11 1	3946.33 -12.11 1
	8 Clamped End								
	12 Clamped End	25.13 -13.14 0	146.63 -17.44 1	369.13 -25.97 1	682.80 -29.84 1	1039.33 -35.55 2	1656.33 -31.34 2	2289.67 -31.97 3	2949.00 -34.32 3
	16 Clamped	24.22 -16.29 0	137.10 -22.81 1	300.30 -39.77 2	563.17 -42.13 1	1026.00 -36.38 2	1449.00 -39.93 3	1977.00 -41.26 4	2755.67 -38.63 4

Damage Magnitude Analysis.

A further study was accomplished to determine whether magnitude, independent of position, could be resolved from the experimental modal frequencies. Table 12 reorganizes the previously displayed modal information by notch length for clarity in this subsection. For longer notch lengths and higher modes, the deviation percentages from the notchless case become quite close despite notch location.

Considering vibration modes 4 through 8, the 16cm notch lengths indicate vibration decreases within only a few percentage points of each other for each mode with the exception of the 7^{th} mode; the 12cm notch cases likewise have modal deviations from the control specimen within a few percentage points of each other, as are the errors associated with the 8cm notches. The 4cm notches show a more varied vibration response over the range of vibration modes, as do the lower modes (1 through 3) for all test specimens.

Approximate damage magnitude is therefore identifiable in the frequency domain for notches of significant size (25% of the total beam length or more), since the notch frequency signature for each of the higher modes will be similar despite damage location. Low vibration modes do not indicate a similar grouping of resonant frequencies for a given notch length at varied locations. Also, the 4cm notches do not demonstrate a tight distribution of frequency errors across the spectrum of vibration modes.

2024 O Test Set

The experimental beams free from residual stresses (2024 O) were likewise tested and the modal frequencies tabulated (see Table 13). Similar trending to that of the 2024 T3 beams is observed regarding frequency reduction as both notch length and mode

Table 12. Experimental Modal Frequencies and Percent Deviation from Control Specimen for 2024 T3 Notched Beams (reorganized based on notch length).

NOTCH SIZE (cm) AND LOCATION		MODAL FREQUENCIES (Hz) Deviation from control values (%)							
		1	2	3	4	5	6	7	8
	4 Free end	28.91 -0.08	175.27 -1.32	471.73 -5.39	931.77 -4.25	1485.00 -7.91	2213.33 -8.25	3116.00 -7.42	4151.00 -7.55
	4 Middle	27.73 -4.16	170.57 -3.96	456.23 -8.50	899.23 -7.60	1535.67 -4.77	1977.67 -18.02	3053.00 -9.29	3785.67 -15.69
	4 Clamped	27.73 -4.16	169.90 -4.34	474.87 -4.76	965.50 -0.79	1387.33 -13.97	2077.33 -13.88	3092.67 -8.11	3946.33 -12.11
	8 Free End	29.30 1.27	166.93 -6.01	421.63 -15.44	774.33 -20.43	1359.67 -15.69	1779.33 -26.24	2533.33 -24.73	3476.67 -22.57
	8 Middle	28.13 -2.77	169.00 -4.84	390.87 -21.61	725.80 -25.42	1283.00 -20.44	1846.67 -23.45	2477.00 -26.40	3483.33 -22.42
	8 Clamped								
	12 Free End	29.04 0.36	154.30 -13.12	406.27 -18.52	658.20 -32.36	1090.33 -32.39	1748.33 -27.52	2369.00 -29.61	3084.33 -31.31
	12 Middle	27.47 -5.06	161.33 -9.16	366.13 -26.57	635.70 -34.68	1080.67 -32.99	1729.33 -28.31	2377.67 -29.36	2991.00 -33.39
	12 Clamped	25.13 -13.14	146.63 -17.44	369.13 -25.97	682.80 -29.84	1039.33 -35.55	1656.33 -31.34	2289.67 -31.97	2949.00 -34.32
	16 Free End	28.26 -2.34	146.77 -17.36	336.60 -32.49	561.47 -42.30	1046.33 -35.12	1535.00 -36.37	2263.67 -32.74	2750.00 -38.75
	16 Middle	26.82 -7.30	152.43 -14.17	324.87 -34.85	577.30 -40.68	1024.33 -36.48	1403.33 -41.82	1982.33 -41.10	2820.33 -37.19
	16 Clamped	24.22 -16.29	137.10 -22.81	300.30 -39.77	563.17 -42.13	1026.00 -36.38	1449.00 -39.93	1977.00 -41.26	2755.67 -38.63

Table 13. Experimental Modal Frequencies and Percent Deviation from Control Specimen for 2024 O Notched Beams.

NOTCH SIZE (cm) AND LOCATION		MODAL FREQUENCIES (Hz) Deviation from control values (%)							
		1	2	3	4	5	6	7	8
	4 Clamped	28.65 -0.98	174.73 -1.62	489.47 -1.84	995.40 2.29	1439.00 -10.77	2136.67 -11.42	3190.67 -5.20	4104.67 -8.58
	8 Clamped	27.73 -4.16	159.40 -10.25	485.53 -2.63	711.70 -26.87	1273.67 -21.02	1817.67 -24.65	2679.67 -20.38	3509.00 -21.85
	12 Clamped	26.17 -9.55	147.57 -16.91	387.40 -22.31	670.20 -31.13	1070.33 -33.63	1695.33 -29.72	2354.67 -30.04	3065.67 -31.72
	16 Clamped	24.61 -14.94	145.43 -18.11	298.97 -40.04	580.73 -40.32	1028.33 -36.23	1495.33 -38.01	2042.00 -39.33	2819.00 -37.22
	20 Middle	24.61 -14.94	142.20 -19.93	267.07 -46.44	539.60 -44.55	811.70 -49.67	1312.00 -45.61	1857.67 -44.81	2392.33 -46.72
	24 Middle	22.79 -21.23	134.80 -24.10	266.93 -46.47	514.33 -47.15	781.27 -51.55	1248.00 -48.26	1762.33 -47.64	2223.00 -50.49

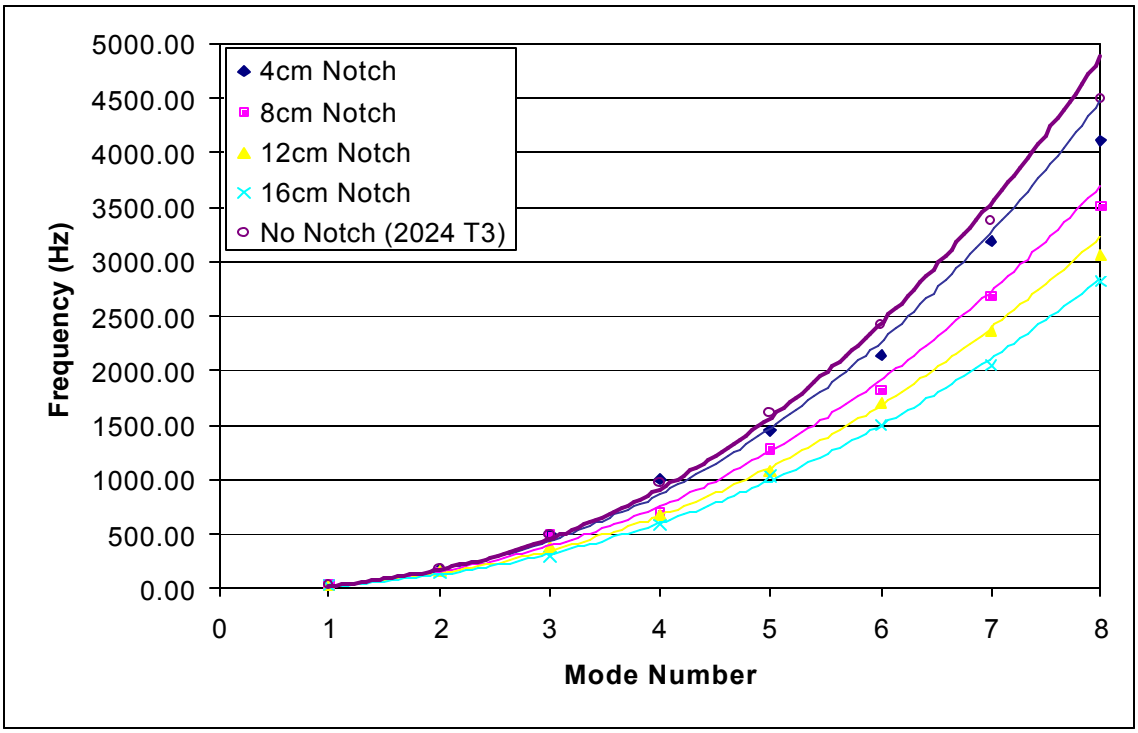

Figure 34. Frequency vs. Mode Number for 2024 O Notched Beams--Clamped End.

number increase. The residual stresses present in the 2024 T3 beams did not adversely affect the dynamic response trends as compared to the 2024 O beams—both indicated a proportional decrease in modal frequencies as notch length increased, and both indicated an increase in frequency reduction experienced by the higher modes versus the lower modes when referenced to the notchless case (see Figures 32 and 34). The residual stress-free results likewise do not support the conjecture that damage at the modal nodes or antinodes constitutes increased degradation of the resonant frequencies.

2024 T3 vs. 2024 O Frequency Comparison

Comparison of the 2024 T3 aluminum specimen modal frequencies with the 2024 O modal frequencies was important to establish whether residual stresses critically damped the former to the point where the results were unusable for analysis.

Experimental results were compared for each of the three specimens created out of both materials: the 4cm, 12cm, and 16cm notched beams with the inclusion located at the clamped end. Table 14 provides a listing of the modal frequencies for each crack length and associated material, as well as the difference relation between the two materials using the stress-free 2024 O aluminum as the fundamental case. The difference between the 2024 O frequencies and the 2024 T3 frequencies averages to be ~3%, with the natural frequencies of the latter lower than the former. This percentage difference was also seen to be the deviation of the 2024 T3 notchless frequency values with theory, as previously shown in Table 5. It is therefore evident that the residual stresses found in the 2024 T3 aluminum induce a relatively insignificant error into the overwhelming reductions in modal frequencies due to longer notch inclusions, as displayed in Tables 9 and 13. The measured results are therefore viable for the conclusions made in determining whether the experimental frequencies of a damaged cantilever aluminum beam can be accurately characterized.

Table 14. Modal Frequency Comparison of 2024 T3 Aluminum with 2024 O Aluminum for 4cm, 12cm, and 16cm Notch Lengths at the Clamped End.

			MODAL FREQUENCIES (Hz)							
			1	2	3	4	5	6	7	8
NOTCH SIZE (cm) AND LOCATION	4 Clamped	2024 O	28.65	174.73	489.47	995.40	1439.00	2136.67	3190.67	4104.67
		2024 T3	27.73	169.90	474.87	965.50	1387.33	2077.33	3092.67	3946.33
		?(%)	-3.21	-2.77	-2.98	-3.00	-3.59	-2.78	-3.07	-3.86
	12 Clamped	2024 O	26.17	147.57	387.40	670.20	1070.33	1695.33	2354.67	3065.67
		2024 T3	25.13	146.63	369.13	682.80	1039.33	1656.33	2289.67	2949.00
		?(%)	-3.97	-0.63	-4.72	1.88	-2.90	-2.30	-2.76	-3.81
	16 Clamped	2024 O	24.61	145.43	298.97	580.73	1028.33	1495.33	2042.00	2819.00
		2024 T3	24.22	137.10	300.30	563.17	1026.00	1449.00	1977.00	2755.67
		?(%)	-1.58	-5.73	0.45	-3.02	-0.23	-3.10	-3.18	-2.25

Usage of the MATLAB Program

A copy of the MATLAB finite element program, which incorporates the theory presented in the 2002 publication by Perel and Palazotto and briefly summarized in Chapter II, was obtained from Dr. Victor Perel for experimental evaluation in February 2003. The innovative purpose of the program was to accurately characterize modal frequencies for a delaminated cantilevered beam while not requiring re-meshing for each included crack length, unlike all current commercial FE analyzers such as ABAQUS, NASTRAN, etc. The MATLAB algorithm was written specifically for the cantilevered beam case (as depicted in Figure 6, Chapt II), requiring several input fields to be filled in by the user regarding specimen characteristics for proper utilization. A copy of the input field for the program is shown and its usage explained in Appendix A.

Once the proper values are entered into the appropriate fields, the program is executed and the output generated. A listing of modal frequencies corresponding to each degree of freedom is generated as well as a plot of a specified eigenvector. Normalized modal amplitude is checked for its order of magnitude and correlated to the appropriate eigenvalue, for all eigensolutions of a given case (ref. Appendix A). These eigenvalue/eigenvector pairs are the predicted modal frequencies and shapes for the instance of interest.

Output Comparison with MATLAB Program

Following the methods described in Appendix A, the MATLAB FE analysis program was configured to characterize all notch lengths and locations representative of the experimental specimens. Considerable effort was taken to ensure accuracy of the input data, as this step required multiple integration calculations for beam parameters as

well as conversions between Standard English units and the SI system. Once all cases had been executed and the appropriate eigenvalues for the considered modes of vibration chosen from the output, the frequency data shown in Table 15 could be compiled. Note that the values entered for the 2024 T3 aluminum include the 3% correction factor for residual stresses, as this modification brings the experimental values closer to the true, stress-free magnitudes.

The data sets shown contain several interesting points that need to be addressed. First, the FE approach developed by Perel and Palazotto accurately characterizes the resonant frequency of an included isotropic beam with small error for short notch lengths. Observing specifically the 4cm notch cases, error from the experimentally obtained frequency values hovers around 5% for the majority of modes considered, though the MATLAB predictions for the first and eighth vibration modes with a crack located at the extrema of the beam provide moderately divergent results, where errors are in the 7% to 14% range. Between these two modes, the results are quite good with the exception of an outlier of 16% for the 6^{th} mode, middle inclusion.

Another observation is that the MATLAB output, as a whole, is relatively more accurate at the lower vibration modes across the range of test results than at the higher modes. Deviation from experiment for modes 1 and 2 is less than 20% for all specimens except the 16cm, clamped end notch. Beyond this point, error increases steadily to 40%, 50%, and in some cases, 60% offset from the experimentally-acquired frequency values. It is therefore evident that the higher the mode being analyzed, the more apt MATLAB is to give largely incorrect results for modal frequency.

Table 15. Modal Frequency Comparison--Experimental Results vs. MATLAB Predictions (20-element model) with Percent Offset from Experimental Values for 2024 T3 Aluminum (with 3% correction for residual stresses).

NOTCH SIZE (cm) AND LOCATION			MODAL FREQUENCIES (Hz)							
			1	2	3	4	5	6	7	8
	4 Free end	Exp.	29.78	180.52	485.88	959.72	1529.55	2279.73	3209.48	4275.53
		MATLAB	26.15	170.66	485.94	963.01	1608.52	2418.87	3382.62	4492.78
		?(%)	-12.17	-5.46	0.01	0.34	5.16	6.10	5.39	5.08
	8 Free End	Exp.	30.18	171.94	434.28	797.56	1400.46	1832.71	2609.33	3580.97
		MATLAB	24.94	172.22	493.05	978.75	1630.34	2431.60	3384.15	4503.56
		?(%)	-17.36	0.16	13.53	22.72	16.42	32.68	29.69	25.76
	12 Free End	Exp.	29.91	158.93	418.45	677.95	1123.04	1800.78	2440.07	3176.86
		MATLAB	24.43	174.02	501.79	983.04	1624.77	2440.46	3390.46	4511.48
		?(%)	-18.31	9.50	19.92	45.00	44.68	35.52	38.95	42.01
	16 Free End	Exp.	29.10	151.17	346.70	578.31	1077.72	1581.05	2331.58	2832.50
		MATLAB	25.25	174.76	504.38	980.58	1630.45	2438.20	3395.01	4514.58
		?(%)	-13.26	15.61	45.48	69.56	51.29	54.21	45.61	59.39
	4 Middle	Exp.	28.56	175.68	469.92	926.21	1581.74	2037.00	3144.59	3899.24
		MATLAB	28.74	169.71	489.01	961.45	1598.53	2376.46	3373.46	4461.30
		?(%)	0.61	-3.40	4.06	3.80	1.06	16.66	7.28	14.41
	8 Middle	Exp.	28.97	174.07	402.59	747.57	1321.49	1902.07	2551.31	3587.83
		MATLAB	28.77	168.18	479.84	958.25	1602.87	2373.17	3314.81	4442.60
		?(%)	-0.71	-3.38	19.19	28.18	21.29	24.77	29.93	23.82
	12 Middle	Exp.	28.29	166.17	377.12	654.77	1113.09	1781.21	2449.00	3080.73
		MATLAB	28.52	170.19	470.30	951.50	1574.97	2394.30	3301.88	4422.16
		?(%)	0.78	2.42	24.71	45.32	41.50	34.42	34.83	43.54
	16 Middle	Exp.	27.62	157.01	334.61	594.62	1055.06	1445.43	2041.80	2904.94
		MATLAB	29.41	173.42	465.19	935.37	1562.18	2341.26	3322.86	4411.72
		?(%)	6.48	10.45	39.02	57.31	48.06	61.98	62.74	51.87
	4 Clamped End	Exp.	28.56	175.00	489.11	994.47	1428.95	2139.65	3185.45	4064.72
		MATLAB	26.50	179.45	497.21	961.40	1589.55	2384.94	3355.43	4461.30
		?(%)	-7.23	2.55	1.66	-3.32	11.24	11.46	5.34	9.76
	8 Clamped End	Exp.								
		MATLAB								
		?(%)								
	12 Clamped End	Exp.	25.88	151.03	380.21	703.28	1070.51	1706.02	2358.36	3037.47
		MATLAB	24.75	181.02	510.59	950.93	1577.61	2386.56	3326.09	4422.16
		?(%)	-4.37	19.85	34.29	35.21	47.37	39.89	41.03	45.59
	16 Clamped End	Exp.	24.95	141.21	309.31	580.06	1056.78	1492.47	2036.31	2838.34
		MATLAB	25.25	180.04	493.63	955.47	1580.49	2363.32	3329.34	4411.72
		?(%)	1.20	27.49	59.59	64.72	49.56	58.35	63.50	55.43

The FE approach also deviates more from experimental observation in cases with long notch length. The 4cm-notch frequency predictions are much less erroneous than the 8cm-notch predictions, which are in turn more accurate than the 12cm-notch predictions, etc. The longer the notch length, the more difficulty the MATLAB program has in producing a reliable estimation of resonant frequencies for each modes.

The same trends were observed in the stress-free 2024 O aluminum, as indicated in Table 16. Error from experiment was still significant for high modes and long notch lengths, indicating that the residual stresses endemic to the 2024 T3 aluminum were not the cause of the significant deviations observed, but rather the deviations were a result of difficulties in the MATLAB solution approach.

Table 16. Modal Frequency Comparison--Experimental Results vs. MATLAB Predictions (20-element model) for 2024 O Aluminum.

			MODAL FREQUENCIES (Hz)							
			1	2	3	4	5	6	7	8
NOTCH SIZE (cm) AND LOCATION	4 Clamped	Exp.	28.65	174.73	489.47	995.40	1439.00	2136.67	3190.67	4104.67
		MATLAB	26.50	179.45	497.21	961.40	1589.55	2384.94	3355.43	4461.30
		?(%)	-7.51	2.70	1.58	-3.42	10.46	11.62	5.16	8.69
	12 Clamped	Exp.	26.17	147.57	387.40	670.20	1070.33	1695.33	2354.67	3065.67
		MATLAB	24.75	181.02	510.59	950.93	1577.61	2386.56	3326.09	4422.16
		?(%)	-5.42	22.67	31.80	41.89	47.39	40.77	41.26	44.25
	16 Clamped	Exp.	24.61	145.43	298.97	580.73	1028.33	1495.33	2042.00	2819.00
		MATLAB	25.25	180.04	493.63	955.47	1580.49	2363.32	3329.34	4411.72
		?(%)	2.58	23.80	65.11	64.53	53.69	58.05	63.04	56.50

The FE mesh in the MATLAB program was refined to investigate whether lengthwise element concentration was the source of the comparative frequency errors. A 40-element mesh (twice the density of the previous analysis) was established and run for all notch length cases. The results (see Table 17) indicate that the overall percentage differences between experiment and FE output decreased over the 20-element model, leading to the conclusion that the mesh refinement lessened the gap between the MATLAB estimation and actual experimental value.

Table 17. Modal Frequency Comparison--Experimental Results vs. MATLAB Predictions (40-element model) with Percent Offset from Experimental Values for 2024 T3 Aluminum (with 3% correction for residual stresses).

NOTCH SIZE (cm) AND LOCATION			MODAL FREQUENCIES (Hz)							
			1	2	3	4	5	6	7	8
	4 Free end	Exp.	29.78	180.52	485.88	959.72	1529.55	2279.73	3209.48	4275.53
		MATLAB	31.75	192.96	510.05	966.54	1569.91	2339.30	3282.82	4390.15
		?(%)	6.62	6.89	4.97	0.71	2.64	2.61	2.29	2.68
	8 Free End	Exp.	30.18	171.94	434.28	797.56	1400.46	1832.71	2609.33	3580.97
		MATLAB	34.30	186.34	481.56	942.76	1571.05	2339.30	3256.91	4390.15
		?(%)	13.66	8.38	10.89	18.20	12.18	27.64	24.82	22.60
	12 Free End	Exp.	29.91	158.93	418.45	677.95	1123.04	1800.78	2440.07	3176.86
		MATLAB	37.68	176.41	479.66	942.21	1545.94	2341.51	3242.89	4354.37
		?(%)	26.00	11.00	14.63	38.98	37.66	30.03	32.90	37.07
	16 Free End	Exp.	29.10	151.17	346.70	578.31	1077.72	1581.05	2331.58	2832.50
		MATLAB	36.64	173.82	481.41	929.83	1553.12	2316.63	3241.23	4334.30
		?(%)	25.88	14.99	38.85	60.78	44.11	46.52	39.01	53.02
	4 Middle	Exp.	28.56	175.68	469.92	926.21	1581.74	2037.00	3144.59	3899.24
		MATLAB	28.62	169.47	489.38	963.91	1599.89	2371.20	3367.46	4411.02
		?(%)	0.19	-3.54	4.14	4.07	1.15	16.41	7.09	13.13
	8 Middle	Exp.	28.97	174.07	402.59	747.57	1321.49	1902.07	2551.31	3587.83
		MATLAB	28.66	168.20	481.05	961.67	1606.27	2373.99	3310.27	4462.28
		?(%)	-1.09	-3.37	19.49	28.64	21.55	24.81	29.75	24.37
	12 Middle	Exp.	28.29	166.17	377.12	654.77	1113.09	1781.21	2449.00	3080.73
		MATLAB	28.41	170.22	471.25	954.38	1577.48	2394.51	3296.39	4462.28
		?(%)	0.42	2.43	24.96	45.76	41.72	34.43	34.60	44.84
	16 Middle	Exp.	27.62	157.01	334.61	594.62	1055.06	1445.43	2041.80	2904.94
		MATLAB	29.30	173.48	466.01	936.18	1562.45	2335.40	3311.90	4428.71
		?(%)	6.08	10.49	39.27	57.44	48.09	61.57	62.20	52.45
	4 Clamped End	Exp.	28.56	175.00	489.11	994.47	1428.95	2139.65	3185.45	4064.72
		MATLAB	25.79	180.00	502.65	973.93	1595.91	2373.13	3344.52	4479.75
		?(%)	-9.72	2.86	2.77	-2.06	11.68	10.91	4.99	10.21
	8 Clamped End	Exp.								
		MATLAB								
		?(%)								
	12 Clamped End	Exp.	25.88	151.03	380.21	703.28	1070.51	1706.02	2358.36	3037.47
		MATLAB	24.20	180.79	519.39	963.11	1577.88	2373.00	3316.20	4440.47
		?(%)	-6.49	19.71	36.61	36.95	47.39	39.10	40.61	46.19
	16 Clamped End	Exp.	24.95	141.21	309.31	580.06	1056.78	1492.47	2036.31	2838.34
		MATLAB	24.71	179.61	500.93	968.18	1579.75	2345.27	3316.45	4421.85
		?(%)	-0.97	27.19	61.95	66.91	49.49	57.14	62.87	55.79

The mesh was further refined to 100 elements lengthwise and the results examined for continued convergence with experiment (data shown in Table 18). Certain modes displayed a small comparative improvement with the new mesh density (e.g. the 6^{th} through 8^{th} modes of the 4cm free-end-notched beam) while others regressed in accuracy (such as all modes for the 16cm middle-notched beam). The 100-element mesh results indicated minimal, if any, improvement in the FE frequency approximations of the

Table 18. Modal Frequency Comparison--Experimental Results vs. MATLAB Predictions (100-element model) with Percent Offset from Experimental Values for 2024 T3 Aluminum (with 3% correction for residual stresses).

NOTCH SIZE (cm) AND LOCATION			MODAL FREQUENCIES (Hz)							
			1	2	3	4	5	6	7	8
	4 Free end	Exp.	29.78	180.52	485.88	959.72	1529.55	2279.73	3209.48	4275.53
		MATLAB	N/A	185.62	511.25	968.45	1560.91	2337.94	3275.90	4375.81
		?(%)		2.82	5.22	0.91	2.05	2.55	2.07	2.35
	8 Free End	Exp.	30.18	171.94	434.28	797.56	1400.46	1832.71	2609.33	3580.97
		MATLAB	N/A	186.37	481.37	941.93	1569.00	2337.94	3253.13	4367.17
		?(%)		8.39	10.84	18.10	12.04	27.57	24.67	21.96
	12 Free End	Exp.	29.91	158.93	418.45	677.95	1123.04	1800.78	2440.07	3176.86
		MATLAB	N/A	173.96	475.94	938.40	1541.83	2336.24	3241.03	4358.75
		?(%)		9.46	13.74	38.42	37.29	29.73	32.83	37.20
	16 Free End	Exp.	29.10	151.17	346.70	578.31	1077.72	1581.05	2331.58	2832.50
		MATLAB	N/A	176.63	487.06	939.64	1570.73	2333.34	3252.97	4345.76
		?(%)		16.84	40.48	62.48	45.75	47.58	39.52	53.42
	4 Middle	Exp.	28.56	175.68	469.92	926.21	1581.74	2037.00	3144.59	3899.24
		MATLAB	N/A	171.98	496.82	977.73	1614.78	2381.86	3378.19	4412.38
		?(%)		-2.11	5.72	5.56	2.09	16.93	7.43	13.16
	8 Middle	Exp.	28.97	174.07	402.59	747.57	1321.49	1902.07	2551.31	3587.83
		MATLAB	N/A	167.80	479.90	959.91	1601.27	2363.48	3287.32	4433.26
		?(%)		-3.60	19.20	28.40	21.17	24.26	28.85	23.56
	12 Middle	Exp.	28.29	166.17	377.12	654.77	1113.09	1781.21	2449.00	3080.73
		MATLAB	N/A	169.49	469.21	952.47	1576.13	2394.12	3317.85	4370.93
		?(%)		2.00	24.42	45.47	41.60	34.41	35.48	41.88
	16 Middle	Exp.	27.62	157.01	334.61	594.62	1055.06	1445.43	2041.80	2904.94
		MATLAB	N/A	175.08	469.98	943.55	1571.70	2341.51	3322.95	4448.36
		?(%)		11.51	40.46	58.68	48.97	61.99	62.75	53.13
	4 Clamped End	Exp.	28.56	175.00	489.11	994.47	1428.95	2139.65	3185.45	4064.72
		MATLAB	N/A	180.67	505.79	980.42	1598.65	2357.36	3300.73	4421.99
		?(%)		3.24	3.41	-1.41	11.88	10.17	3.62	8.79
	8 Clamped End	Exp.								
		MATLAB								
		?(%)								
	12 Clamped End	Exp.	25.88	151.03	380.21	703.28	1070.51	1706.02	2358.36	3037.47
		MATLAB	N/A	181.36	521.91	966.77	1578.62	2362.19	3290.94	4413.13
		?(%)		20.08	37.27	37.47	47.46	38.46	39.54	45.29
	16 Clamped End	Exp.	24.95	141.21	309.31	580.06	1056.78	1492.47	2036.31	2838.34
		MATLAB	N/A	179.88	502.99	973.37	1580.60	2333.39	3286.89	4377.61
		?(%)		27.38	62.62	67.80	49.57	56.34	61.41	54.23

higher modes and overall diminished accuracy of the lower modal frequencies. The first vibration mode became impossible to distinguish from the multiple w_{ij} output as the normalized first-mode eigenvectors showed no relative amplitude deviation, and therefore the correct eigenvalue could not be isolated. The mesh was refined once further to 200 elements, however this resulted in computer lock-up due to overwhelming memory usage for matrix calculations, and hence no results were obtainable.

Both the 40-element and 100-element MATLAB results were likewise tabulated with the 2024 O experimental frequencies to ensure FE accuracy characteristics followed the same trends as previously mentioned, as shown in Tables 19 and 20. Once again, large deviations between MATLAB predictions and experimental results were observed, with errors in excess of 50% in the cases of large crack lengths and high modes. The crack length was increased twice further, to both a 20cm and 24cm notch centered on two 2024 O beams, to note whether the MATLAB solutions for all mesh densities diverged even more from experimental observation for the longer notch cases. Indeed they did, as

Table 19. Modal Frequency Comparison--Experimental Results vs. MATLAB Predictions (40-element model) for 2024 O Aluminum.

			MODAL FREQUENCIES (Hz)							
			1	2	3	4	5	6	7	8
NOTCH SIZE (cm) AND LOCATION	4 Clamped	Exp.	28.65	174.73	489.47	995.40	1439.00	2136.67	3190.67	4104.67
		MATLAB	25.79	180.00	502.65	973.93	1595.91	2373.13	3344.52	4479.75
		?(%)	-10.00	3.01	2.69	-2.16	10.90	11.07	4.82	9.14
	12 Clamped	Exp.	26.17	147.57	387.40	670.20	1070.33	1695.33	2354.67	3065.67
		MATLAB	24.20	180.79	519.39	963.11	1577.88	2373.00	3316.20	4440.47
		?(%)	-7.51	22.52	34.07	43.71	47.42	39.97	40.84	44.85
	16 Clamped	Exp.	24.61	145.43	298.97	580.73	1028.33	1495.33	2042.00	2819.00
		MATLAB	24.71	179.61	500.93	968.18	1579.75	2345.27	3316.45	4421.85
		?(%)	0.39	23.50	67.55	66.72	53.62	56.84	62.41	56.86

Table 20. Modal Frequency Comparison--Experimental Results vs. MATLAB Predictions (100-element model) for 2024 O Aluminum.

			MODAL FREQUENCIES (Hz)							
			1	2	3	4	5	6	7	8
NOTCH SIZE (cm) AND LOCATION	4 Clamped	Exp.	28.65	174.73	489.47	995.40	1439.00	2136.67	3190.67	4104.67
		MATLAB	N/A	180.67	505.79	980.42	1598.65	2357.36	3300.73	4421.99
		?(%)		3.40	3.33	-1.51	11.09	10.33	3.45	7.73
	12 Clamped	Exp.	26.17	147.57	387.40	670.20	1070.33	1695.33	2354.67	3065.67
		MATLAB	N/A	181.36	521.91	966.77	1578.62	2362.19	3290.94	4413.13
		?(%)		22.90	34.72	44.25	47.49	39.33	39.76	43.95
	16 Clamped	Exp.	24.61	145.43	298.97	580.73	1028.33	1495.33	2042.00	2819.00
		MATLAB	N/A	179.88	502.99	973.37	1580.60	2333.39	3286.89	4377.61
		?(%)		23.69	68.24	67.61	53.70	56.04	60.96	55.29

evidenced in Tables 21 through 23. Errors from experimental values reached over 90% in the middle to high vibration modes, once again validating the inaccuracy of the MATLAB solution approach for long notch lengths and high modes. The significant difference in frequency values between experimentation and the MATLAB algorithm indicates the inadequacy of the program to characterize modal frequencies of notched aluminum beams for anything but short notch lengths.

Table 21. Modal Frequency Comparison--Experimental Results vs. MATLAB Predictions (20-element model) for 20cm and 24cm Notches, 2024 O Aluminum.

			MODAL FREQUENCIES (Hz)							
			1	2	3	4	5	6	7	8
NOTCH SIZE (cm) AND LOCATION	20 Middle	Exp.	24.61	142.20	267.07	539.60	811.70	1312.00	1857.67	2392.33
		MATLAB	29.81	176.90	468.04	912.98	1539.59	2321.10	3237.76	4390.04
		?(%)	21.12	24.40	75.25	69.20	89.67	76.91	74.29	83.50
	24 Middle	Exp.	22.79	134.80	266.93	514.33	781.27	1248.00	1762.33	2223.00
		MATLAB	31.27	182.85	481.35	913.11	1515.41	2297.65	3231.27	4289.36
		?(%)	37.20	35.64	80.33	77.53	93.97	84.11	83.35	92.95

Table 22. Modal Frequency Comparison--Experimental Results vs. MATLAB Predictions (40-element model) for 20cm and 24cm Notches, 2024 O Aluminum.

			MODAL FREQUENCIES (Hz)							
			1	2	3	4	5	6	7	8
NOTCH SIZE (cm) AND LOCATION	20 Middle	Exp.	24.61	142.20	267.07	539.60	811.70	1312.00	1857.67	2392.33
		MATLAB	29.72	177.00	470.30	917.19	1542.52	2320.05	3233.53	4321.02
		?(%)	20.77	24.47	76.10	69.98	90.04	76.83	74.06	80.62
	24 Middle	Exp.	22.79	134.80	266.93	514.33	781.27	1248.00	1762.33	2223.00
		MATLAB	30.80	183.01	488.08	924.99	1519.15	2288.75	3223.37	4296.11
		?(%)	35.16	35.76	82.85	79.84	94.45	83.39	82.90	93.26

Table 23. Modal Frequency Comparison--Experimental Results vs. MATLAB Predictions (100-element model) for 20cm and 24cm Notches, 2024 O Aluminum.

			MODAL FREQUENCIES (Hz)							
			1	2	3	4	5	6	7	8
NOTCH SIZE (cm) AND LOCATION	20 Middle	Exp.	24.61	142.20	267.07	539.60	811.70	1312.00	1857.67	2392.33
		MATLAB	N/A	177.30	470.10	915.03	1538.23	2311.55	3207.67	4270.34
		?(%)		24.69	76.02	69.58	89.51	76.19	72.67	78.50
	24 Middle	Exp.	22.79	134.80	266.93	514.33	781.27	1248.00	1762.33	2223.00
		MATLAB	N/A	179.44	481.19	915.04	1501.50	2252.39	3166.86	4240.34
		?(%)		33.12	80.27	77.91	92.19	80.48	79.70	90.75

Comparison of Experiment with ABAQUS

Two notched beam specimens were modeled in the ABAQUS CAE package in an attempt to determine whether the program could accurately replicate the observed dynamic response of the notched cantilever. The 4cm clamped-end notched beam was modeled using just over 14,000 8-noded linear hexahedral brick elements (C3D8R) with a higher concentration of elements near the notched area, as shown in Figure 35. Approximately 60% of the total elements were localized in this region of the modeled beam. The beam was characterized with the same properties as the experimental aluminum, incorporating the modulus of elasticity, Poisson's ratio, and overall

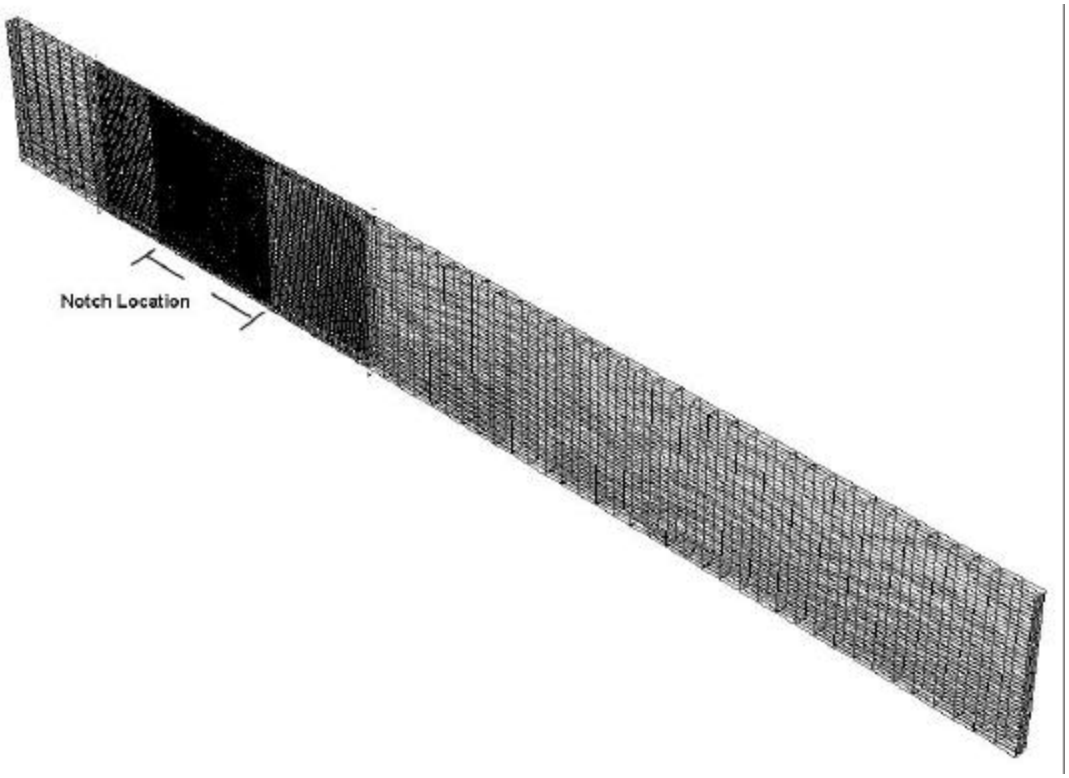

Figure 35. Example of ABAQUS Meshing of 4cm Clamped-End Notched Beam.

dimensionality. The 8cm clamped-end notched beam was likewise modeled in ABAQUS, employing over 24,000 hexahedral brick elements with a large concentration of the elements (also about 60%) near the notched area.

ABAQUS, though quite accurate in the notchless case (as was the MATLAB procedure), could not accurately predict the modal frequencies of a specimen containing a large notch. Though exceptionally good modal frequency predictions for the 4cm notch were obtained, exceptionally bad modal frequency predictions for the 8cm notch resulted (see Table 24). ABAQUS also produced unusual mode shapes for the 8cm notch case. Throughout the course of the experimentation, all eigenvectors (including the notched specimens) resembled the notchless eigenvectors shown in Figures 29-a through h—this is known from the laser vibrometry profiles produced at the time of experimentation. However, ABAQUS returned mode shapes containing excessive bending local to the area of the inclusion, particularly at the higher modes, which was not observed during the experimental process (see Figure 36). ABAQUS also returned local mode shapes which were not observed at all, such as the anomalous mode shown in Figure 37.

Table 24. Modal Frequency Comparison--Experimental Results vs. ABAQUS Predictions for 2024 O Aluminum.

			MODAL FREQUENCIES (Hz)							
			1	2	3	4	5	6	7	8
NOTCH SIZE (cm) AND LOCATION	4 Clamped	Exp.	28.65	174.73	489.47	995.40	1439.00	2136.67	3190.67	4104.67
		ABAQUS	28.60	175.50	498.21	994.97	1502.10	2150.90	3189.30	4310.90
		?(%)	-0.17	0.44	1.79	-0.04	4.38	0.67	-0.04	5.02
	8 Clamped	Exp.	27.73	159.40	485.53	711.70	1273.67	1817.67	2679.67	3509.00
		ABAQUS	10.52	66.57	133.31	321.08	527.30	636.87	897.99	1207.10
		?(%)	-62.06	-58.24	-72.54	-54.89	-58.60	-64.96	-66.49	-65.60

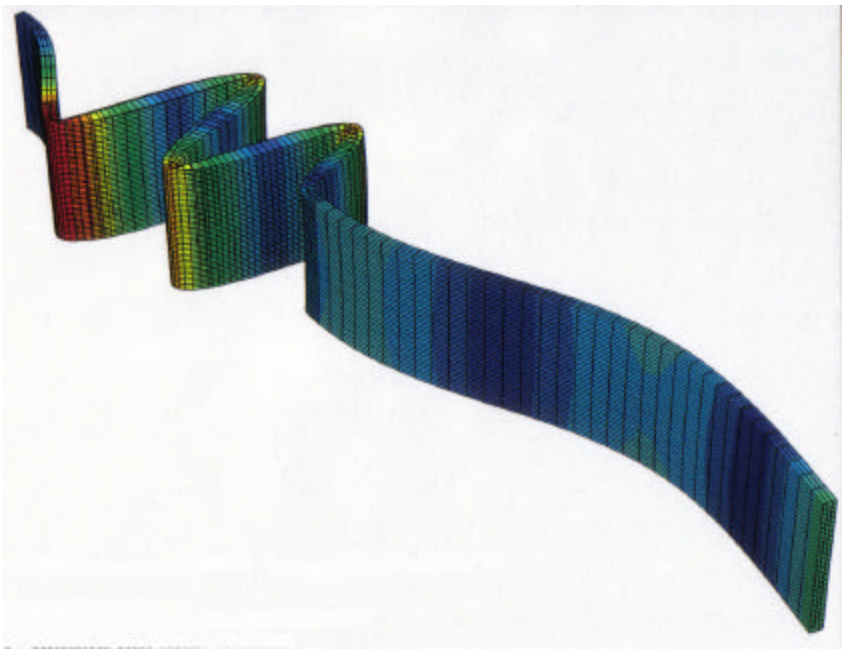

Figure 36. ABAQUS Result for 8cm Clamped-End Notch Displaying Highly Localized Bending (8th translational mode).

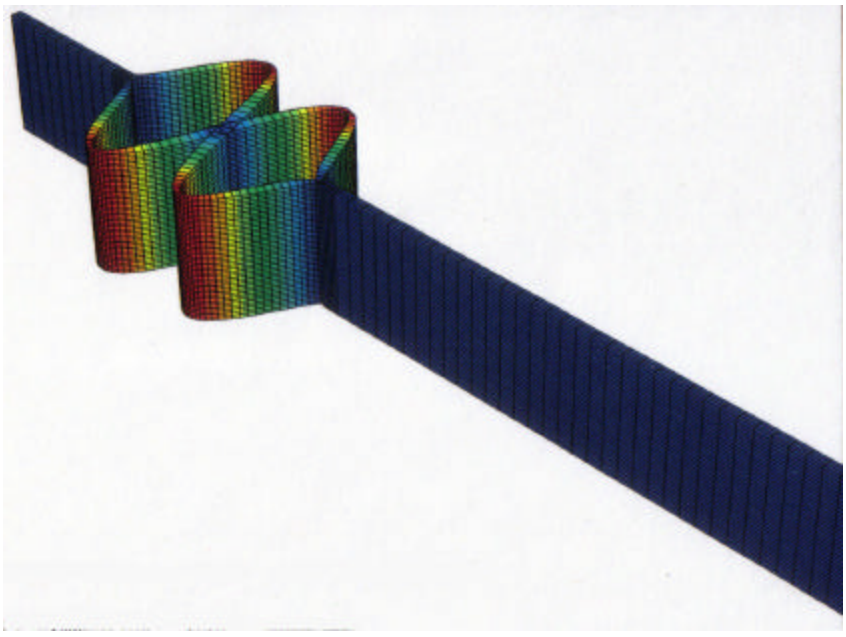

Figure 37. Unobserved Localized Mode Returned by ABAQUS for 8cm Clamped-End Notch.

The modeling method by ABAQUS emphasized the inherent usability of the proposed MATLAB approach in that re-meshing is not necessary for each notch inclusion within MATLAB algorithm, however extensive work was required in ABAQUS to model and mesh each notch case. The results from ABAQUS also re-emphasized the highly non-linear aspects of the vibratory dynamics, which creates a difficult modeling scenario that few, if any, off-the-shelf finite element programs would be able to characterize.

Comparison of MATLAB with Independent Data

As one final additional test, the MATLAB program was compared to previously existing modal frequency data for a delaminated beam as published by Mujumdar and Suryanarayan in 1988. In their experiment, they considered a "laminated" cantilevered beam created by adhering two thin strips of spring steel together, leaving voids in the epoxy where delaminated regions were desired. The experimental setup explanation was incomplete—only beam length and notch location were provided by the authors, leaving out beam width, beam thickness, and all mechanical properties of the material.

A standard materials handbook was referenced to obtain typical mechanical properties of spring steel: $r = 7833$ kg/m^3, $E = 31 \times 10^6$ psi $= 213.74 \times 10^9$ Pa. The thickness of spring steel is usually about 0.02 in $= 5.08 \times 10^{-4}$ m. Since the width of the beam was not specified by the authors, but the delamination was considered to extend through the full width and propagate along the thickness, a width of 1.5 in. = 0.0381m was used for the steel beams considered in this analysis. Thickness was assumed to be two steel strips (t = 0.001016m) since a centerline notch was required. The following inertia values were calculated (using the formulae in Appendix A) for the final spring

steel beam and entered into the MATLAB simulation along with the previous mechanical properties:

$I2 = 0.8982$
$I_{?1} = 0.3925$
$I_{?2} = 7.0728 \times 10^{-8}$

With these values, several representative cases of the Mujumdar and Suryanarayan experimental results were replicated in MATLAB with decent success, as indicated in Table 25. Considering that the first two vibration modes were the only modes studied by the authors, the relatively good MATLAB predictions fall in line with typical percentage errors found beforehand for the first two modes in aluminum beams. As mentioned previously, moderately good results from the MATLAB algorithm are obtained for the low modes, however this is no indication of the MATLAB accuracy at higher modes.

Table 25. Comparison of Existing Published Data with MATLAB Prediction, Various Cases Using Spring Steel (adapted from Mujumdar and Suryanarayan (1988:458)).

			Modal Frequencies (Hz)					
			Mujumdar/Suryanarayan		Perel/Palazotto		Error (%)	
Published Case	Beam Length	Notch Tip Locations	Mode 1	Mode 2	Mode 1	Mode 2	Mode 1	Mode 2
1	0.20m	No Crack	33.7	209.9	32.3	200.9	-4.15	-4.29
3	0.25m	xd1=0.129m xd2=0.173m	21.8	136.4	21.0	120.8	-3.67	-11.44
6	0.20m	xd1=0.075m xd2=0.117m	33.2	208.7	31.1	195.0	-6.33	-6.56
7	0.20m	xd1=0.065m xd2=0.150m	32.0	205.1	31.3	193.2	-2.19	-5.80
19	0.13m	xd1=0.0185m xd2=0.0325m	79.0	496.8	72.0	474.7	-8.86	-4.45

V. Conclusions and Recommendations

Frequency Reductions Due to Damage

As previously found by several authors, a downward shift in modal actuation frequency was observed during experimentation for cantilevered beams with included damage. Specifically, centerline notches of minimal thickness at various locations and lengths significantly reduced the first eight modal frequencies of aluminum cantilevered beam specimens, as would be expected due to the decrease in flexural rigidity EI of the beam. The higher modes experienced a greater reduction in modal frequency than the lower modes for a given notch length. Frequency reductions from the notchless case of 5% for the first mode and 30% for the eighth mode for a given notch length were not uncommon across the spectrum of test sets.

Longer notch lengths reduced frequency more than shorter notch lengths for each vibration mode, as would be expected. For instance, in the case of the first mode for 2024 O aluminum, modal frequency decreases from the notchless case were 1%, 4%, 10%, and 15% (respectively) for the 4cm, 8cm, 12cm, and 16cm clamped-end notches, respectively. The experimental data did not indicate a relation between frequency degradation magnitude and notch length across the spectrum of modes—some modal frequencies decreased in a quadratic fashion for increasing notch length, some in a negative exponential fashion, and some displayed no pattern at all.

Damage passing through regions of curvature inflection (and hence maximum shear) does not have a readily identifiable effect on frequency reduction. The interrupted shear flow through the cross-section at curvature inflection points, though certainly

present, is not the solitary factor in modal frequency reductions. Though several data points from the experimental study seem to support the claim, many other data points do not and therefore the hypothesis is not considered a viable explanation for large-magnitude frequency reductions, though buckling of the .

Damaged regions of maximum curvature (and hence maximum normal stress) within the modal responses of the beam were also explored for patterns associated with the observed frequency reductions, and were likewise found not to be the primary source of frequency degradation.

Damage magnitude is identifiable in the frequency domain for notch lengths at least 25% of the overall beam length (and possibly less, though notches between 4cm and 8cm in length were not considered in this study). The frequency reductions for each notch length for vibration modes 4-8 are approximately the same for each respective mode, independent of notch location. This is a very useful finding for estimation of internal structural crack lengths in a structural health monitoring application.

Residual Stresses

Residual stresses were found to be a significant aftereffect of the cold working process undergone by the 2024 T3 aluminum during fabrication. As the material was cold rolled, a small amount of plastic deformation was induced into the surface of the aluminum, causing a strain profile across the cross-section as described in Chapter III. Without a centerline notch, the stresses associated with these strains are balanced and prevent the material from warping or bending. Upon the inclusion of a notch, two lamina are created, each containing unbalanced residual stresses and therefore buckling of the lamina occurs, causing the notch to collapse or warp.

The presence of residual stresses in the aluminum beams reduced modal frequencies by approximately 3% across the modal spectrum as compared to the frequencies of the 2024 O aluminum beams lacking the residual stresses. Considering the large frequency reductions for increasing notch lengths as compared to the resonant frequencies of the control specimens, the residual stresses played a minor role in the overall modal frequency degradation.

Frequency Profiling Using ABAQUS

The commercial FE program ABAQUS predicted the first eight modal frequencies for the notchless aluminum beam with great precision, with seven out of the eight resonant frequencies accurate to less than 0.3% from experiment. The 4cm clamped-end notch case was accurate as well, with a maximum deviation from experiment of slightly over 1%. The program failed to model the next-longer notch length of 8cm correctly, as the dynamics under consideration became highly nonlinear due to notch face interaction and outside of the scope of the software package. ABAQUS results for the 8cm case yielded deviations from observed experimental values of 50% to over 70% for all modes considered. ABAQUS also generated localized eigenvectors in the sublamina not seen in the laboratory experimentation. ABAQUS was therefore considered inadequate to correctly model the dynamics of cantilever beams with included notches.

Frequency Profiling Using MATLAB

The MATLAB program developed by Perel and Palazotto was designed to overcome the nonlinearity of the vibration response in notched cantilever beams, and also eliminate the need to remesh the specimen for each notch length or location considered

(saving valuable model construction time). Similar to ABAQUS, the program accurately predicted the modal frequencies of the notchless case to within less then 1% for all modes except the first, using a 20-element, a 40-element, and a 100-element mesh. A 200-element mesh was attempted in an effort to further increase output accuracy, however the memory requirements for computation exceeded the computer threshold.

The notched specimens were not as accurately characterized, with the MATLAB program generating frequency predictions increasingly farther from experimental results as notch length increased, as mode number increased, and in some cases as element mesh density increased. For example, in the 20-element model modal frequencies for the 4cm-notched cases were generally 5% off from experimentally observed values, with some outliers in the 11% and 16% range. As notches were allowed to grow, deviation of the MATLAB predictions from experimental results increased dramatically (but in no particular linear, quadratic, or exponential fashion) to over 90% in the 24cm-notched arrangement. Departure from experiment for the short notch lengths reduced slightly in the 40-element model, where the 4cm-notched frequencies were accurate to within 3% in most modes, however there were still outliers in the 11% and 16% range in the same modes as the 20-element model. MATLAB characterization of longer notch lengths exhibited some modes with slightly better accuracy, and some modes with worse accuracy, however deviations from experiment still approached 90% in the longest notches and highest modes. The 100-element model generated output where the first vibration mode was not easily identifiable at all, and though higher modal predictions became better by about 2% to 3%, lower modal predictions became many times worse.

The MATLAB program was also used in an attempt to generate the published frequencies for delaminated, notched beams as reported by Mujumdar and Suryanarayan (1988). Several representative cases were considered, however only the first two vibration modes were studied by the authors. As generally evidenced in the experimental data in Chapter IV, the MATLAB program does a decent job predicting the first two vibration modes for notch lengths extending less than one-half the full length of the test specimen, typically within 10-15% of experimental value. This trend continued in the comparison with Mujumdar and Suryanarayan, where the deviation of the MATLAB program with their results was less than 10% in all cases except one (where the error percentage was 11.4%).

Overall, the MATLAB procedure as it stands now would be a fairly good estimation tool for the modal frequencies of notchless beams or beams with small notches (less than one quarter of the overall beam length for all modes, or up to one half the beam length for modes 1 and 2, to get an accuracy of ~10%), however the program does not work well for beams with longer notches.

Recommendations

Two areas should be investigated in the MATLAB theory in an attempt to generate better accuracy. First, the Heaviside function used in conjunction with the double-sided unit step function to characterize transverse displacement creates a jump discontinuity in adjacent elements, and therefore may not monotonically converge when standard beam-element shape functions are considered in the model (though this is a common practice for delamination modeling according to Reddy [2004:764-766]). Additional research should be accomplished to determine whether the Heaviside solution

approach will converge or diverge with increased elements, or, secondly, whether more robust shape functions (and therefore more robust elements) should be considered for this particular problem. Another consideration is that the Euler-Bernoulli assumptions on which the program is based begin to break down when higher modes are considered, due to the presence of excessive curvature and increasing through-thickness shear. Timoshenko beam theory takes these considerations into account and therefore should be considered.

Further investigation should be accomplished in the realm of internal stress, moment, and shear distributions within the beam cross-section and its effects on the resonant frequencies. A more comprehensive study should be able to relate internal material mechanics to the presence of a notch and to the particular modal response signature.

An interesting follow-on research project would be a vibration analysis of multiple materials containing residual stresses. As discovered in this thesis, residual stresses in aluminum 2024 generate a cross-spectrum frequency reduction for all modes of approximately 3%. The percentage attenuation of modal frequencies is most certainly dependent on the amount of deformation incurred during the cold working process, however the magnitude of cold work done on a material is difficult to estimate without first-hand knowledge of the process from the manufacturer. Zhuang and Halford are quick to point out that "there remains the technical challenge of understanding and accurately quantifying residual stress relaxation and redistribution" after mechanical processes have been undergone, such as the aforementioned cold working (2001:S31). Characterization of residual stress effects on the frequency response of common

structural component materials would greatly benefit the engineering community in their drive for accurate structural health monitoring algorithms.

Appendix A: MATLAB FE Program Interfacing

Proper usage of the MATLAB FE program created by Perel and Palazotto requires understanding of the input parameters necessary for program execution. On a global scale, all values are calculated and need to be entered in the SI unit system. The frequency output listings generated by the program are in units of radians/second (rad/s), and therefore need to be converted to hertz (Hz) via the relation

$$w_{Hz} = \frac{w_{rad/s}}{2p} \tag{A-1}$$

A copy of the input field area used by the program is provided next (taken from the function *BEGIN_RESPONSE_MODAL*.m):

```
format long e
% enter number n of mode shape which is to be plotted
 n=38;

% BEGINNING OF DATA INPUT:
% coordinates of crack tips:
xd1=0.05;
xd2=0.16;
zd=0.0001;

mu=1e0; % a large number used in the penalty function method of applying constraints

BeamLength=0.3048;
height=0.003175;
width=0.0381;
rho=2768;

NumberElements=20;

% Numbers of elements covered with actuator:
El_Num_With_Act=[1,2,3,4];
```

```
bcdof=[1 2 3 4 ]; % a row-vector which contains global numbers of constrained nodal
variables;
dof_plot=41;  % global number of a variable which is to be plotted as a function of time;

TimeIni=0;   % initial time;
dt=0.1;     % time step size;
TimeFin=10;   % final time;
t=[TimeIni:dt:TimeFin]'; % Column-vector of moments of time at which the response
will be evaluated.

I1=-0.001828;
I2=8.61215;  % alternative notation: I2=A0

I_rho_0=0.42413;  % alternative notations: I_rho_0=J0=B0
I_rho_2=5.64633*10^(-7); % alternative notations:= I_rho_2=J2=C0, this is rotary inertia
coefficient

S11=1.368e-11;

V0=200; % amplitude of voltage applied to piezoelectric actuator, it is implied that
voltage varies with time by law V=V0*cos(Omega_V*t+Alpha_V)

% In this program both Amp and V0 can not have non-zero values

Omega_V=600;
Alpha_V=0;

%  All elements are assumed to be of the same length.
ElementLength=BeamLength/NumberElements;

 NumberNodesPerElement=2;
 NumberDofsPerNode=4;
 NumberNodesSystem=(NumberNodesPerElement-1)*NumberElements+1;
 NumberDofsSystem=NumberNodesSystem*NumberDofsPerNode;
 q0=zeros(NumberDofsSystem,1);  % initial displacement vector (initial condition) ;
 dq0=zeros(NumberDofsSystem,1); % initial velocity vector (initial condition) ;

% Simpler notations:
h=height;
b=width;
l=ElementLength;

% END OF DATA INPUT
```

Several of the fields are intrinsic to the operation of the program and therefore were not modified. Others are relatively self-explanatory. Of particular use for the common user were the following:

n: The number of the mode shape which is to be plotted, corresponding to the sequential listing of solution eigenvalues from the program output. [e.g. *n*=38 will plot the eigenvector corresponding to the 38^{th} eigenvalue in the output, not necessarily the 38^{th} mode of vibration.]

xd1: The lateral coordinate of the left end of the included notch from the cantilevered base. Units are entered in meters.

xd2: The lateral coordinate of the right end of the included notch from the cantilevered base. Units are entered in meters.

zd: Vertical distance of notch centerline from beam centerline. This value can be either positive or negative, but must lie within the beam *height* dimension such that it is actually included in the beam. Units are entered in meters. For the purposes of this thesis, the value was 0.0001—small enough to be essentially zero but not exactly zero, which causes singularities in the internal calculations.

BeamLength: Length of beam measured from the cantilevered end to the free end. Units are entered in meters. For the purposes of this thesis, the value was 0.3048 (12”).

height: Thickness of beam in the transverse direction (direction of vibration—along the z-axis according to Figure 6). Units are entered in meters. For the purposes of this thesis, the value was 0.003175 (1/8”).

width: Thickness of beam in the vertical direction (along the y-axis according to Figure 6). Units are entered in meters. For the purposes of this thesis, the value was 0.0381 (1½").

rho: Mass density of the material being used. Units are entered in kg/m^3. For aluminum, this value is 2768.

NumberElement: Number of elements in the mesh. For this program, in accordance with the published theory, the mesh is distributed only in the longitudinal direction. Therefore, a mesh of 20 results in the length of the beam broken into 20 elements of equal length. Meshes of 20, 40, and 100 were used in this thesis. As mesh density increased beyond 100, computation time and inaccuracy greatly increased as well. A 200-element mesh was attempted but the computers used crashed.

El_Num_With_Act: An array of the elements over which the actuator has been affixed. Elements are numbered sequentially from cantilevered end to free end. Calculation by the user is necessary to determine how many of the elements, based on mesh density, are covered by the actuator. For this thesis, the QP10Ni strain actuator was used, which has a length of 2 1/16 inches, or 0.0524 meters. In the 20-element case for the beam of length 0.3048m, elements 1 through 4 are covered.

I2: Second moment of inertia of the beam defined by

$$I2 = b\int_{-t/2}^{t/2} \frac{1}{\overline{S}_{11}^{(0)}} z^2 dz + b\int_{t/2}^{t/2+t} \frac{1}{\overline{S}_{11}^{(p)}} z^2 dz \qquad \text{(A-2)}$$

For this thesis, *I2* = 8.61215.

I_rho_0: Rotational moment of inertia defined by

$$I_{r0} = b\int_{-t/2}^{t/2} r^{0} dz + b\int_{t/2}^{t/2+t} r^{p} dz \qquad \text{(A-3)}$$

where

r^{0} = density of beam material
r^{p} = density of PZT material
all other variables as defined previously

For this thesis, *I_rho_0* = 0.42413.

I_rho_2: Second rotational moment of inertia defined by

$$I_{r0} = b\int_{-t/2}^{t/2} r^{0} z^{2} dz + b\int_{t/2}^{t/2+t} r^{p} z^{2} dz \qquad \text{(A-4)}$$

For this thesis, *I_rho_2* = 5.64633 x 10^{-7}.

S11: Reciprocal of the Young's Modulus for the beam material. For this thesis, *S11* = 1.368 x 10^{-11}.

The remaining parameters are utilized for changing voltage inputs for the PZT, changing the element type and degrees of freedom, setting step times, and creating non-zero initial conditions. For this work, these values remained unchanged.

Once the input arrays are modified as necessary for a given case, the function *BEGIN_RESPONSE_MODAL* can be executed to view modal prediction results. The output is received in two forms. First, a listing of modal frequencies for each degree of freedom is generated, obtained by numerically solving the general eigenproblem

$$\left([K] - w^{2}[M]\right)\{d\} = \{0\} \qquad \text{(A-5)}$$

for all l_i (where [*K*] is the positive semidefinite stiffness matrix, [*M*] is the positive semidefinite mass matrix, and the vector {*d*} represents the degrees of freedom). Due to

the application of constraints to the nodal degrees of freedom, and series of zero-value eigenvalues are produced at the beginning of the output. In the 20-element case, 21 degrees of freedom are restrained—rotation and longitudinal translation at the first node coincident with the cantilever base, and longitudinal translation for all subsequent nodes (since displacement is restrained to transverse motion only), hence 21 zeros are generated at the beginning of the output. Additionally, a plot of the eigenvector associated with degree of freedom *n*, as chosen in the input, is produced.

Since the user is looking for the proper w_{ij}, the decision must be made as to which eigenvalue is correlated to a given vibration mode by comparing eigenvectors. It is important to choose the correct eigenvector for the desired mode as multiple eigenvectors of similar form are generated (incorporating all degrees of freedom), however relative magnitude may be off. Figures A-1 and A-2 show a correct eigenvector versus an incorrect eigenvector for an example mode (in this case, the first bending mode). Note the correct eigenvector in Figure A-1 shows a normalized displacement several orders of magnitude higher than the incorrect eigenvector in Figure A-2. The *n* chosen in the input field to generate the correct eigenvector will correspond to the *n*th modal frequency from the output, which is the desired eigenvalue for the given mode (see following page). The process of checking for proper eigenvectors and eigenvalues is iterative for all modes for a given crack length.

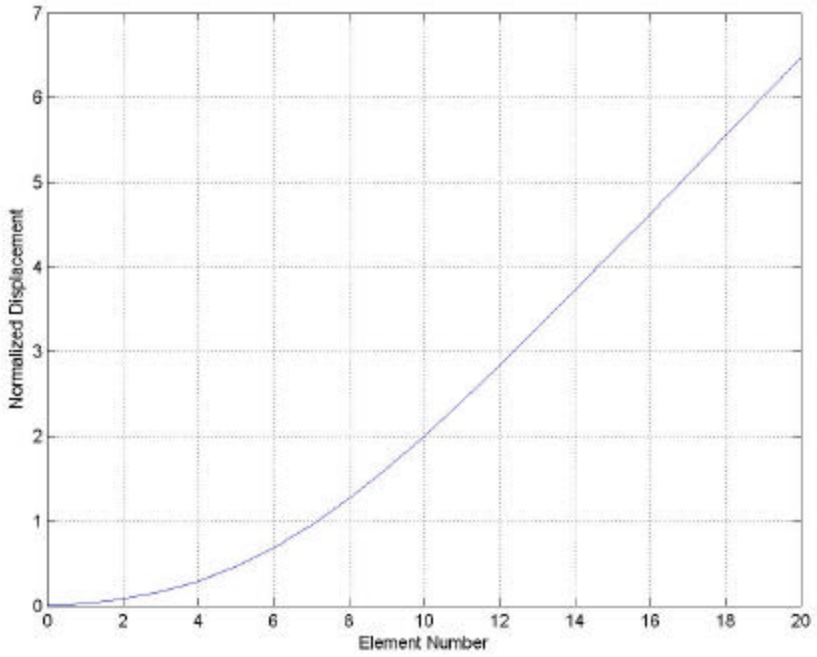

Figure A-1: Correct Eigenvector for First Bending Mode, Displaying Large Normalized Displacement Amplitude (eigenvector *n*).

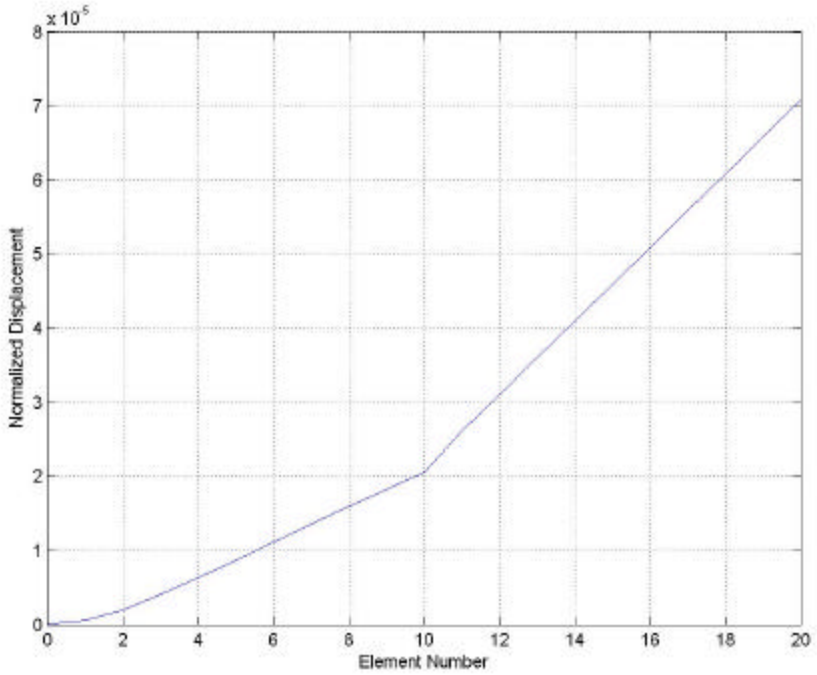

Figure A-2: Incorrect Eigenvector for First Bending Mode, Displaying Small Normalized Displacement Amplitude (eigenvector *n*+1).

Partial Sample Output from Trial Run

```
. . .
. . .
0
0
0
0
0
0
0
0
0
0
0
0
0
4.868081376759656e+000
1.127152812150922e+001
1.165276880735184e+001
1.190093091805270e+001
1.364765533642256e+001
1.471723767297972e+001
2.689233961423111e+001
3.487776530095482e+001
3.725742109050611e+001
3.749889609530827e+001
3.757768315862990e+001
5.973320189630839e+001
7.102339214792067e+001
mode n-1  ?   1.194552099981771e+002
mode n    ?   1.557102896376919e+002
mode n+1  ?   1.698699504505314e+002
2.753268115864362e+002
1.101150177203550e+003
3.023707836243113e+003
6.160291477316835e+003
. . .
. . .
```

Appendix B: Example Test Specimen Design Drawings

(Free-End Notch Set)

4cm Notch, Free End

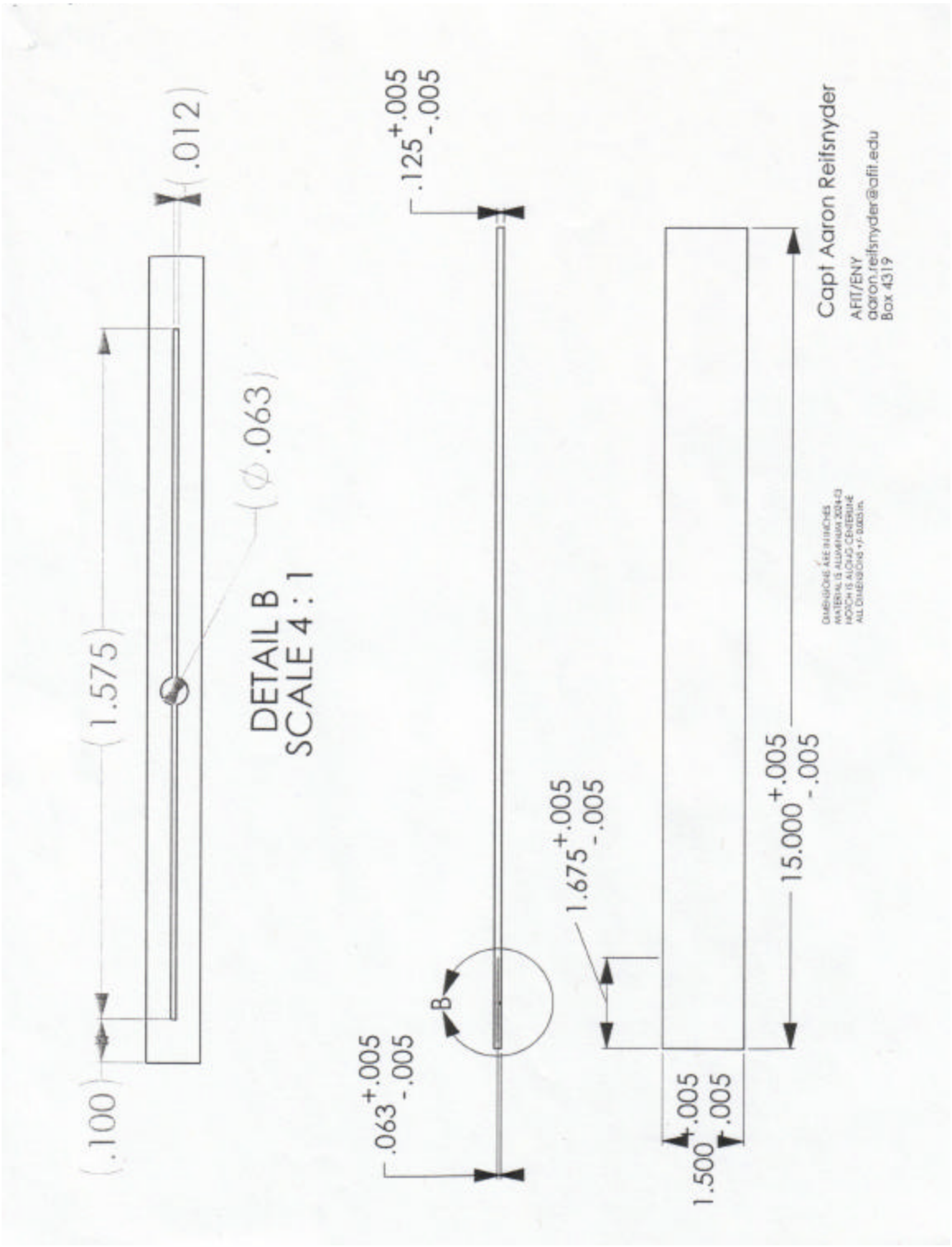

8cm Notch, Free End

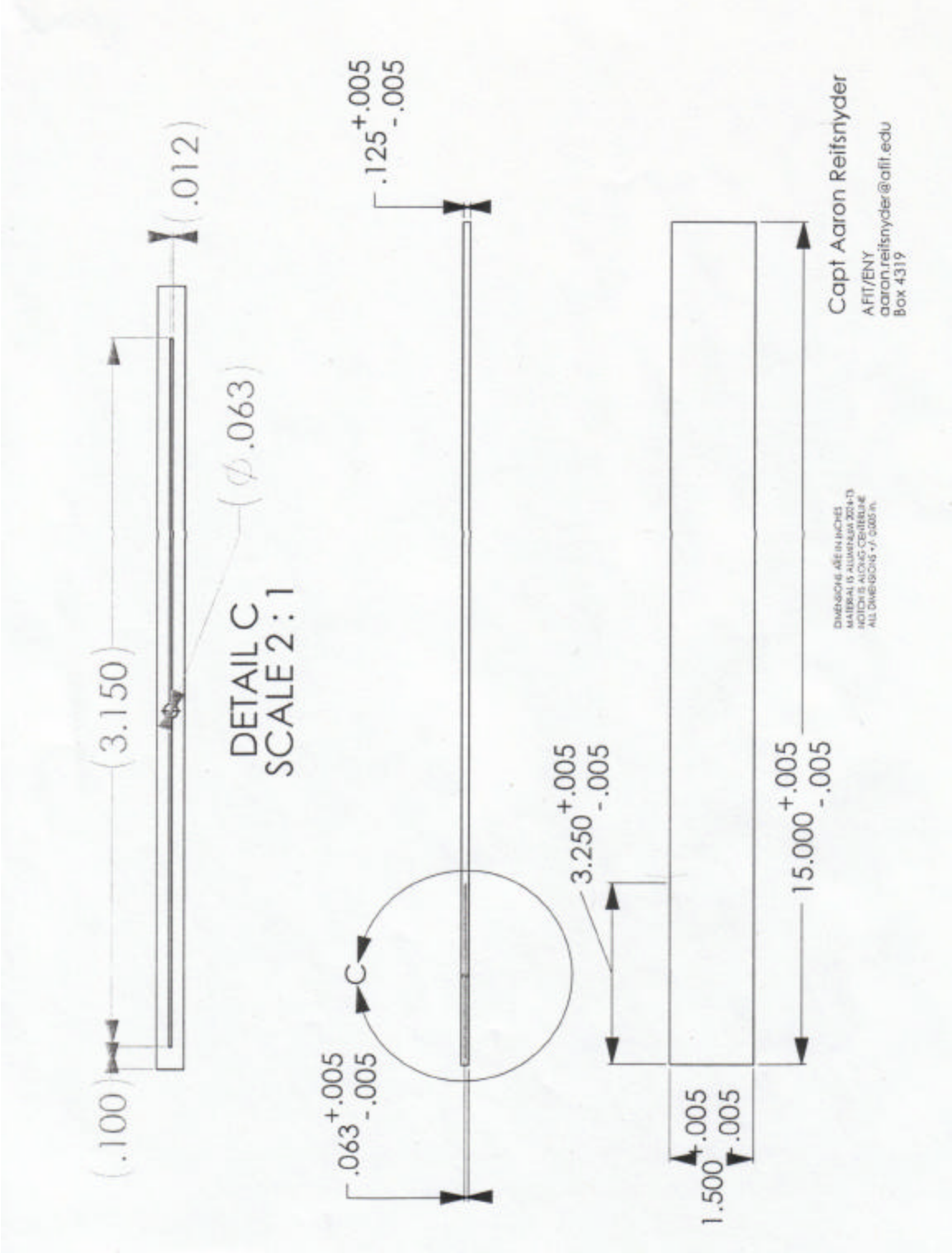

12cm Notch, Free End

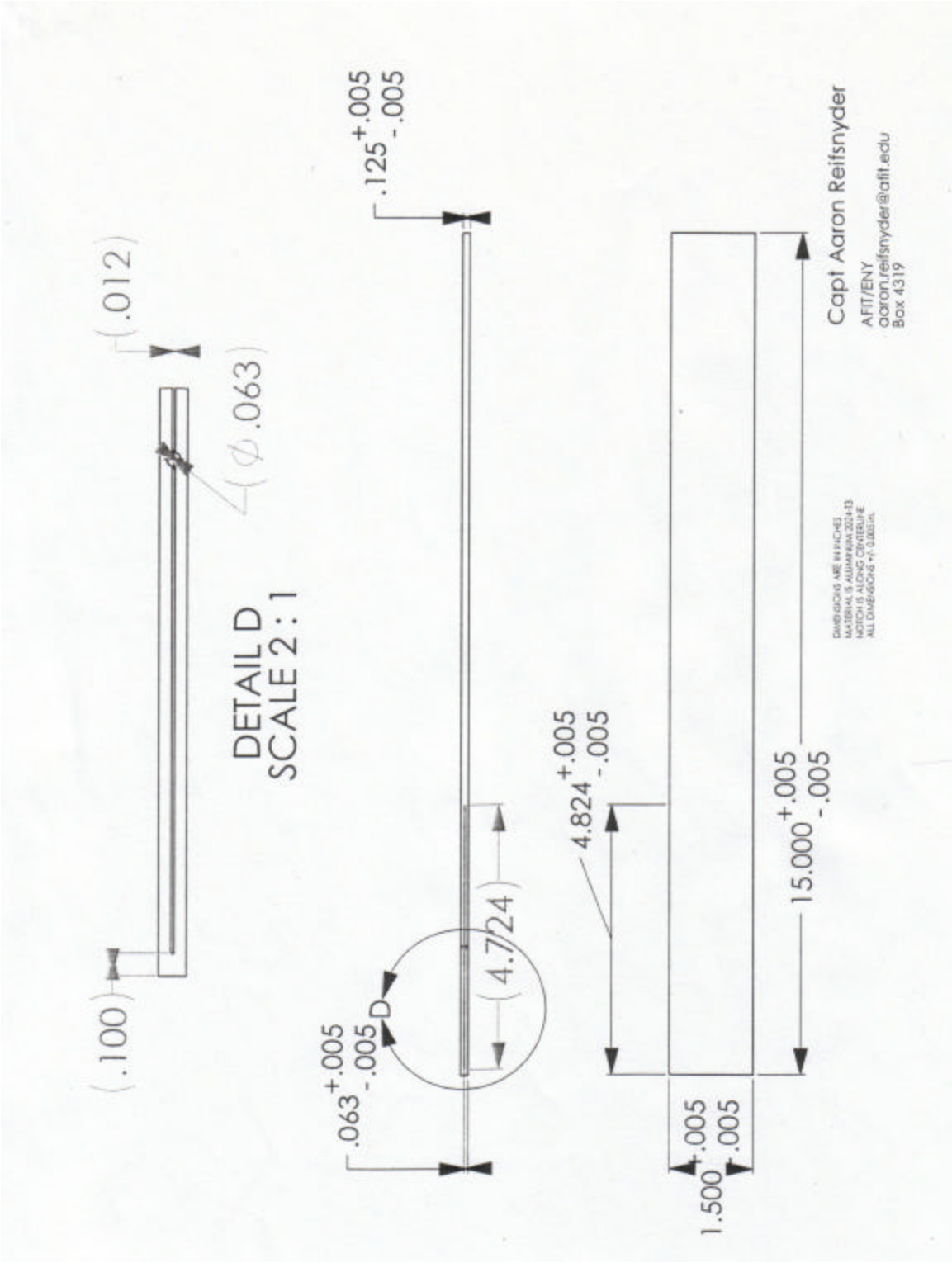

16cm Notch, Free End

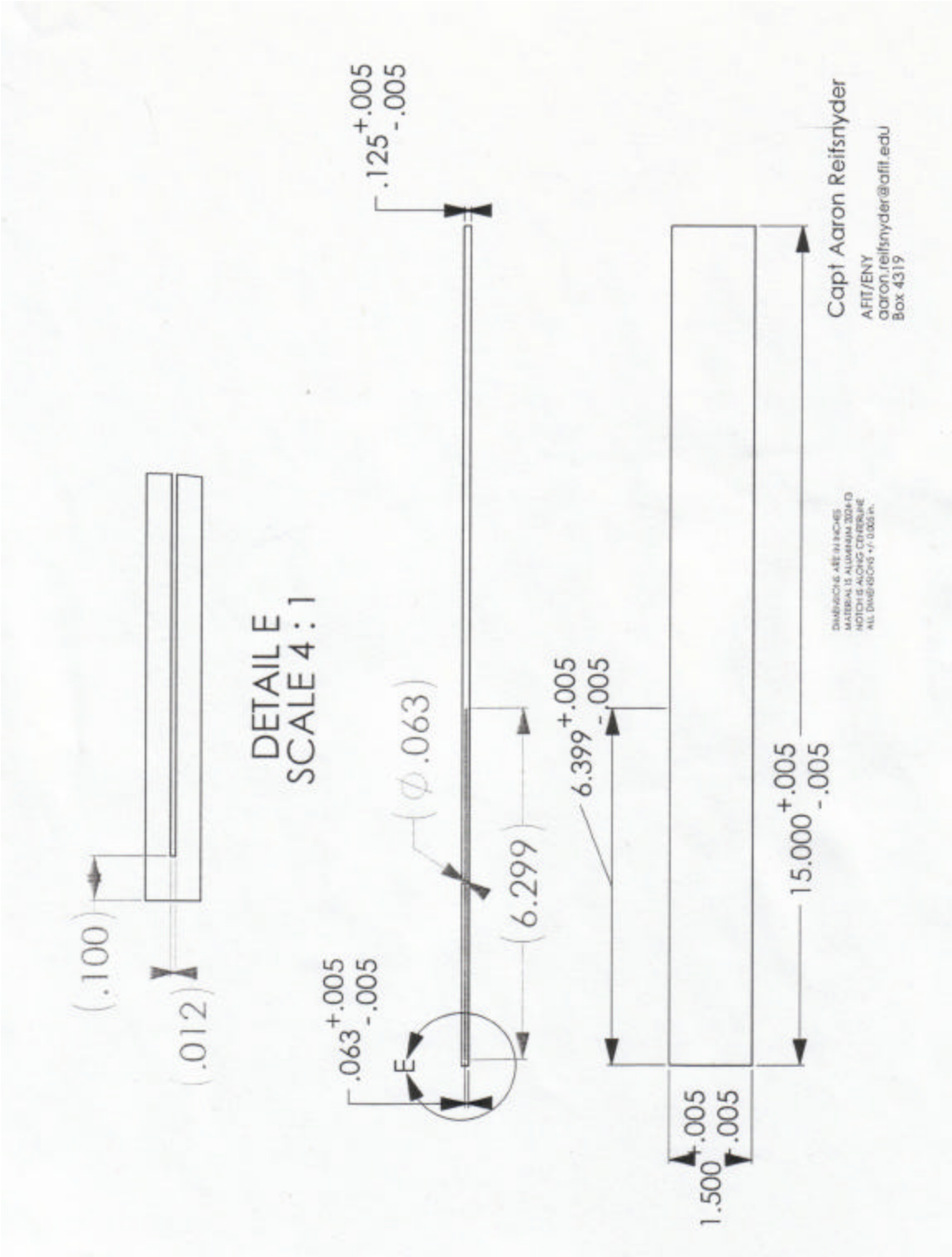

Bibliography

Armao, Frank. "Frequently Asked Questions in Aluminum Welding." Lincoln Electric. http://www.lincolnelectric.com/knowledge/articles/content/alumfaq.asp. Viewed 10 January 2004.

Castellini, P. and G. M. Revel. "Damage Detection by Laser Vibration Measurement." Excerpt from submission, *15th World Conference on Nondestructive Testing, 15-21 October 2000*. n. pag. http://www.ndt.net/article/wcndt00/papers/idn709/idn709.htm.

Cawley, P. and R. D. Adams. "The Location of Defects in Structures from Measurements of Natural Frequencies," *Journal of Strain Analysis*, 14:49-57 (1979).

Cawley, P. and R. Ray. "A Comparison of the Natural Frequency Changes Produced by Cracks and Slots," *Journal of Vibration, Acoustics, Stress, and Reliability in Design*, 110:366-370 (July 1988).

Chondros, T. G. and A. D. Dimarogonas. "Dynamic Sensitivity of Structures to Cracks," *Journal of Vibration, Acoustics, Stress, and Reliability in Design*, 111:251-256 (July 1989).

Cobb, Richard G. *Structural Damage Identification from Limited Measurement Data.* Air Force Institute of Technology (AU), Wright-Patterson AFB OH, March 1996 (ADA304785).

Cook, Robert D. and others. *Concepts and Applications of Finite Element Analysis* (4th Edition). University of Wisconsin-Madison: John Wiley & Sons, 1974.

Dado, Mohammad H. "A Comprehensive Crack Identification Algorithm for Beams Under Different End Conditions," *Applied Acoustics*, 51:381-398 (1997).

Dimaroganas, A. D. and S. A. Paipetis. *Analytical Methods in Rotor Dynamics.* London: Applied Science, 1983.

Doyle, James F. "Determining the Size and Location of Transverse Cracks in Beams," *Experimental Mechanics*, 35:272-280 (September 1995).

*e*funda: Engineering Fundamentals. http://www.efunda.com/materials/alloys/aluminum/temper.cfm. Viewed 30 October 2003.

Gage, Debbie and John McCormick. "Delta's Last Stand," *Baseline Magazine*, 1:17 (1 April 2003).

Gorman, Daniel J. *Free Vibration Analysis of Beams and Shafts.* New York: John Wiley & Sons, 1975.

Halkon, B. J., S. R. Frizzel, and S. J. Rothberg. "Vibration Measurements Using Continuous Scanning Laser Vibrometry: Velocity Sensitivity Model Experimental Validation," *Measurement Science and Technology*, 14:773-783 (2003).

Ismail, F., A. Ibrahim, and H. R. Martin. "Identification of Fatigue Cracks from Vibration Testing," *Journal of Sound and Vibration*, 140:305-317 (1990).

Jian, X. H., H. S. Tzou, C. J. Lissenden, and L. S. Penn. "Damage Detection by Piezoelectric Patches in a Free Vibration Method," *Journal of Composite Materials*, 31:345-359 (1997).

Kam, T. Y. and T. Y. Lee. "Detection of Cracks in Structures Using Modal Test Data," *Engineering Fracture Mechanics*, 42:381-387 (1992).

Kessler, Seth S., S. Mark Spearing, Mauro J. Atalla, Carlos E. S. Cesnik, and Constantinos Soutis. "Damage Detection in Composite Materials Using Frequency Response Methods," *Composites: Part B*, 33:87-95 (2002).

Kim, J. T. and N. Stubbs. "Crack Detection in Beam-Type Structures Using Frequency Data," *Journal of Sound and Vibration*, 259:145-160 (2003).

Man, XiuTing C., Lawrence M. McClure, Zhijing Wang, and Robert D. Finch. "Slot Depth Resolution in Vibration Signature Monitoring of Beams Using Frequency Shift," *Journal of the Acoustical Society of America*, 95:2029-2037 (April 1994).

Meirovitch, Leonard. *Elements of Vibration Analysis*. Boston: McGraw-Hill, 1986.

Mujumdar, P. M. and S. Suryanarayan. "Flexural Vibrations of Beams with Delaminations," *Journal of Sound and Vibration*, 125:441-461 (1988).

Nagy, K., D. A. Dousis, and R. D. Finch. "Detection of Flaws in Railroad Wheels Using Acoustic Signatures," *ASME Journal of Engineering and Industry*, 100:459-467 (1978).

Nicholas, Theodore. Visiting Professor—Aerospace Engineering, Air Force Institute of Technology, WPAFB, OH. Personal Interview. 15 October 2003.

Owolabi, G. M., A. S. J. Swamidas, and R. Sheshadri. "Crack Detection in Beams Using Changes in Frequencies and Amplitudes of Frequency Response Functions," *Journal of Sound and Vibration*, 265:1-22 (2003).

Pandey, A. K., M. Biswas, and M. M. Samman. "Damage Detection from Changes in Curvature Mode Shapes," *Journal of Sound and Vibration*, 145:321-332 (1991).

Patil, D. P. and S. K. Maiti. "Detection of Multiple Cracks Using Frequency Measurements," *Engineering Fracture Mechanics*, 70:1553-1572 (2003).

Perel, V. and A. Palazotto. "Nonlinear Dynamics of Composite Delaminated Beams with Account of Contact Force Between Delaminated Sublaminates," *Archive of Mechanics*, submitted for publication (2003).

Perel, V. Y. and A. N. Palazotto. "Finite Element Formulation for Dynamics of Delaminated Composite Beams with Piezoelectric Actuators," *International Journal of Solids and Structures*, 39:4457-4483 (2002).

Polytec GmbH. "Vibrometer University—Laser Vibrometer Basics." http://www.polytec.de/polytec-com/l_vib/vib_uni_vib.html. Viewed 27 Dec 2003.

Reddy, J. N. *Mechanics of Laminated Composite Plates and Shells*. 2nd Ed. Boca Raton: CRC Press, 2004.

Salawu, O. S. "Detection of Structural Damage through Changes in Frequency: a Review," *Engineering Structures*, 19:718-723 (1997).

Tracy, John J. and Gerard C. Pardoen. "Effect of Delamination on the Natural Frequencies of Composite Laminates," *Journal of Composite Materials*, 23:1200-1215 (December 1989).

Thyagarajan, S. K., M. J. Schulz, and P. F. Pai. "Detecting Structural Damage Using Frequency Response Functions," *Journal of Sound and Vibration*, 210:162-170 (1998).

Waldron, K., A. Ghoshal, M. J. Schulz, M. J. Sundaresan, F. Ferguson, P. F. Pai, and J. H. Chung. "Damage Detection Using Finite Element and Laser Operational Deflection Shapes," *Finite Elements in Analysis and Design*, 38:193-226 (2002).

Wang, J. T. S., Y. Y. Liu, and J. A. Gibby. "Vibrations of Split Beams," *Journal of Sound and Vibration*, 84:491-502 (1982).

Zhuang, Wyman Z. and Gary R. Halford. "Investigation of Residual Stress Relaxation Under Cyclic Load," *International Journal of Fatigue*, 23:S31-S37 (2001).

REPORT DOCUMENTATION PAGE

Form Approved
OMB No. 074-0188

The public reporting burden for this collection of information is estimated to average 1 hour per response, including the time for reviewing instructions, searching existing data sources, gathering and maintaining the data needed, and completing and reviewing the collection of information. Send comments regarding this burden estimate or any other aspect of the collection of information, including suggestions for reducing this burden to Department of Defense, Washington Headquarters Services, Directorate for Information Operations and Reports (0704-0188), 1215 Jefferson Davis Highway, Suite 1204, Arlington, VA 22202-4302. Respondents should be aware that notwithstanding any other provision of law, no person shall be subject to an penalty for failing to comply with a collection of information if it does not display a currently valid OMB control number.
PLEASE DO NOT RETURN YOUR FORM TO THE ABOVE ADDRESS.

1. REPORT DATE *(DD-MM-YYYY)*	**2. REPORT TYPE**	**3. DATES COVERED** *(From – To)*
23 Mar 04	**Master's Thesis**	19 Aug 02 – 18 Jun 04

4. TITLE AND SUBTITLE

VIBROMETRIC DETECTION OF BEAM DAMAGE DUE TO INCLUSIONS

5a. CONTRACT NUMBER

5b. GRANT NUMBER

5c. PROGRAM ELEMENT NUMBER

6. AUTHOR(S)

Reifsnyder, Aaron, J., Captain, USAF

5d. PROJECT NUMBER

5e. TASK NUMBER

5f. WORK UNIT NUMBER

7. PERFORMING ORGANIZATION NAMES(S) AND ADDRESS(S)
Air Force Institute of Technology
Graduate School of Engineering and Management (AFIT/EN)
2950 Hobson Way
WPAFB OH 45433-7765

8. PERFORMING ORGANIZATION REPORT NUMBER

AFIT/GA/ENY/04-J01

9. SPONSORING/MONITORING AGENCY NAME(S) AND ADDRESS(ES)
AFRL/VASM
Attn: Mr. Mark Derriso
2790 D Street
WPAFB OH 45433 DSN: 674-6876

10. SPONSOR/MONITOR'S ACRONYM(S)

11. SPONSOR/MONITOR'S REPORT NUMBER(S)

12. DISTRIBUTION/AVAILABILITY STATEMENT
APPROVED FOR PUBLIC RELEASE; DISTRIBUTION UNLIMITED.

13. SUPPLEMENTARY NOTES

14. ABSTRACT

The Air Force Institute of Technology, in conjunction with the Structural Health Monitoring branch of the Air Force Research Laboratory, is researching methods of determining effects of notch location and size on beam structures using modal frequency analysis. This thesis explores the ability to detect included notches of varying magnitudes and locations within the frequency domain of an isotropic cantilever beam.

A series of experiments employing centerline-notched 2024 T3 and 2024 O aluminum beams was used to determine whether natural frequency measurement in beam structures is a valid mechanism for damage detection. Each specimen was excited by a strain actuator and the dynamic beam response measured using a laser Doppler vibrometer, thereby obtaining eigenvalues and eigenvectors for each case. Results are analyzed for frequency degradation trends based on location, notch length, and vibration mode. Correlation is made between experimentally observed values, ABAQUS modeling, and a series of MATLAB predictions utilizing a finite element solution approach developed by Perel and Palazotto (2002).

It is determined that modal frequency analysis is an adequate global indicator of damage presence and magnitude, which reduces global stiffness. Damage location is not easily identifiable from the data. It is also determined that ABAQUS and the MATLAB solution approach are accurate to within 10% of experimental resonant frequency values for short notch lengths and low vibration modes, but highly deviant from experiment for longer notch lengths and higher modes. Residual stresses contained in the 2024 T3 specimens from cold working are determined to have minimal effect on beam dynamics.

15. SUBJECT TERMS
Structural Analysis, Cantilever Beams, Modal Analysis, Frequency, Frequency Response, Resonant Frequency, Vibration , Laser Velocimeters, Delamination, Finite Element Analysis

16. SECURITY CLASSIFICATION OF:			**17. LIMITATION OF ABSTRACT**	**18. NUMBER OF PAGES**	**19a. NAME OF RESPONSIBLE PERSON**
REPORT	**ABSTRACT**	**c. THIS PAGE**			Dr. Anthony N. Palazotto
U	**U**	**U**	**UU**	130	**19b. TELEPHONE NUMBER** *(Include area code)* DSN 785-3636 x 4599; e-mail: anthony.palazotto@afit.edu

Standard Form 298 (Rev: 8-98)